DEVELOPMENT OF NOVEL APPROACHES FOR THE TREATMENT OF RECURRENT OVARIAN CANCER

By

OBEID MOHAMMADALI POURMALEKSHAH

A dissertation submitted to the

Graduate School-New Brunswick

Rutgers, The State University of New Jersey

In partial fulfillment of the requirements

For the degree of

Doctor of Philosophy

Graduate Program in Pharmaceutical Sciences

Written under the direction of

Arash Hatefi

And approved by

_____

_____

_____

_____

New Brunswick, New Jersey

May, 2020

ABSTRACT OF THE DISSERTATION

DEVELOPMENT OF NOVEL APPROACHES FOR THE TREATMENT OF RECURRENT OVARIAN CANCER

By OBEID MOHAMMADALI POURMALEKSHAH

Dissertation Director:

Arash Hatefi, PhD.

Ovarian cancer is among the five leading types of cancer incidence and has the highest mortality rate of all gynecologic malignancies in the US. The standard of care for this type of cancer is debulking surgery, followed by chemotherapy with a combination of platinum-based anticancer drugs and paclitaxel. Even though most ovarian tumors are sensitive to chemotherapy at the time of diagnosis, approximately 90% of patients after suboptimal resection and 70% of patients after optimal cytoreduction go on to experience relapse within 18–24 months. The main reason for this outcome is the late-stage diagnosis of ovarian cancer, which leads to tumor cell metastasis into the peritoneal cavity and the creation of tumorspheres. These tumorspheres are rich in cancer stem-like cells (CSCs), are resistant to therapy, and are considered a significant source of relapse. Therefore, to tackle these challenges, we aimed at developing treatment methods than can eradicate the peritoneal CSC-rich tumorspheres and inhibit relapse.

The first part of this dissertation describes the development of a safe chemotherapeutic approach for patients who are candidates for debulking surgery. To achieve this goal,

OVASC-1 that is resistant to standard-of-care chemotherapy was obtained from a patient with ovarian carcinoma and recurrent disease. The most effective combination of drugs that could eradicate CSC-rich tumorspheres at nanomolar levels was identified. Luciferase-expressing OVASC-1 cells were used to produce an ovarian cancer xenograft in the peritoneal cavity of nude mice and treated with the selected drug combination. Quantitative imaging was used to study the progression of the disease, and its response to therapy and histopathology was used to study abdominal tissues for any sign of toxicity. Our low-dose intraperitoneal (IP) therapy approach effectively restricted the cytotoxic effects to the tumor cells in the peritoneal cavity, provided a complete response, and eliminated the chance of cancer relapse. These results encourage further investigation into this approach as a potential clinical application either as a first- or second-line therapy in cases of acquired resistance to cisplatin and paclitaxel.

The next part of this dissertation describes a targeted stem cell-based non-surgical treatment strategy in patients who are not candidates for debulking surgery. These patients have unresectable tumors for reasons such as the patient's age and the tumor location. For this purpose, different enzyme/prodrug systems for cancer gene therapy were examined to determine which is the most effective treatment against drug-resistant ovarian cancer cells. Next, the sensitivity of the OVASC-1 cells/spheroids to the metabolites of three enzyme/prodrug systems were assessed, and SN-38 was found to be the most potent drug. Adipose-derived stem cells (ASCs) with inherent tumor tropic properties were genetically engineered to express recombinant secretory human carboxylesterase-2 and nanoluciferase genes for disease therapy and quantitative imaging, respectively. The migration and localization of engineered ASCs in tumor stroma and necrotic regions were showed using

bioluminescent imaging (BLI), magnetic resonance imaging (MRI), and histopathology studies. This migration and homing capacity of ASC provides a unique opportunity to deliver drugs to not only the tumor-supporting cells in the stroma but also the CSCs in the necrotic/hypoxic regions. The statistical analysis showed that the administration of the engineered ASCs in combination with the prodrug (Irinotecan) cured 4/5 mice ($p<0.00004$), inhibited relapse, and provided a survival benefit (80%). The histopathology and hematology data did not show any toxicity to major intraperitoneal organs. Overall, our studies demonstrate the possibility of overcoming drug resistance in ovarian cancer by using the above-mentioned protocols.

ACKNOWLEDGMENT

Completing a doctoral degree was a long journey that I could not have successfully finished without the help, guidance, efforts, and support of many people. Firstly, I would like to express my sincere gratitude toward my mentor, Professor. Arash Hartefi, for his patience, intelligence, encouragement, and insight on different aspects of my research, studies, and providing an opportunity to work in his lab. I believe that my experience in working as a part of his team will help and guide me in my future endeavors in my professional and personal life.

I would also like to acknowledge my gratitude to all of my committee members: professors Tamara Minko, Guofeng You, and Grace Guo for their constructive advice, valuable comments and reviewing my dissertation.

My research projects accomplishment was achieved as the result of a collaborative efforts of the current and past members of Professor Hatefi's lab. Drs Siddik Sarkar, Alireza Nomani, Xuguang Chen and, Shahryar Khoshtinat Nikkhoi, Geng Li and Niket Patel. Also, I would like to thank my collaborators, Drs Parisa Javidian and Marina Chekmareva at Department of Pathology and Laboratory Medicine, Rutgers-Robert Wood Johnson Medical School and Drs Michael Goedken, Marianne Polunas , Pedro Louro at Rutgers Research Pathology Services, Rutgers University. I appreciate their help, efforts and hard work and dedication. I would like to acknowledge and thank members of graduate program in Pharmaceutical Sciences and staff members in department of Pharmaceutics, specially Hui Pung, Fei Han, and Sharana Taylor. Also, I would like to acknowledge the financial support from NIH/NCI, New Jersey Health Foundation and the department of Pharmaceutics during my doctoral studies.

This dissertation is dedicated to my family for their constant love and support. Your encouragement helped me to overcome all of my challenges in my life.

DEDICATION

To My Family

TABLE OF CONTENTS

LIST OF TABLES

LIST OF FIGURES

Chapter 1

Introduction

Among different types of female reproductive cancers, ovarian cancer is the most lethal as it is frequently not diagnosed until it is at an advanced stage, making it hard to treat on a curative basis [1]. Ovarian cancer can be classified based on different stages of development upon diagnosis. In stage I, growth is limited to only the ovaries. In stage II, growth has spread outside the ovaries but not outside the pelvis. In stage III, growth has spread outside the ovaries and either beyond the pelvis or to is to the lymph nodes, and in stage IV, growth has spread to outside organs such as the lungs or liver. This is the most advanced stage of cancer [2].

The standard treatment of ovarian cancer consists of operative tumor debulking, including total abdominal hysterectomy and bilateral salpingo-oophorectomy, and administration of chemotherapy with carboplatin and paclitaxel [3]. Studies focused on the effectiveness of the treatment, and its safety in ovarian cancer patients showed differences based on the stage of cancer. Approximately, 75 percent of ovarian cancer cases are not localized (Stages III and IV) at initial diagnosis. The treatment regimen in these groups after surgery is a combination of platinum-based chemotherapy and paclitaxel. Although more than 80% of these women benefit from first-line therapy, the majority of the patients experience side effects such as bone marrow suppression, neuropathy, and cardiotoxicity. In addition to that, cancer therapy resistance and tumor recurrence occur in almost all of these patients [3]. The main reason for tumor recurrence and treatment failure in these groups are related to cancer drug resistance [4]. The mechanisms underlying chemoresistance in cancer are not clear. One hypothesis is that cancers are driven by a subset of highly tumorigenic cells with stem cell properties within the tumor, cancer stem cells (CSCs). According to this model, the CSCs, but not the remaining cells in the tumor,

can propagate tumorigenesis. CSCs have been implicated in tumor initiation, progression, metastasis, and drug resistance. Therefore, to inhibit relapse and increase patients' survival rate, it is crucial to design a treatment strategy that, during the early stage of treatment, eradicates both primary ovarian cancer cells and CSCs [4, 5]. In the first phase of our research project, we focused on developing a new combination therapy method to be used after debulking surgery in order to target both cancer cells and CSCs and reduce the chance of cancer drug resistance and tumor relapse. After initial in vitro studies, we found a combination of two chemotherapeutic agents (SN-38 and MMAE) that could effectively eradicate cancer cells and CSCs. In the next step, we prepared a xenograft model that represents ovarian cancer after debulking surgery and then tested our combination drugs and showed its effectiveness and fewer side effects compared to cisplatin and paclitaxel treatment.

For patients who are not healthy enough to have full staging and debulking surgery conventional chemotherapy does not have survival benefit. To increase the efficacy of chemotherapy, in these patients, some targeted drugs like bevacizumab (Avastin) might be given along with conventional chemotherapy. Another option is to give intraperitoneal (IP) chemotherapy, along with intravenous (IV) chemotherapy [6]. But all of these treatments are considered as maintenance therapy. The studies so far show that maintenance therapy does not necessarily help a patient live longer and may cause more side effects. Thus numerous studies are focusing on alternative treatment methods in these groups of patients [7]. Our studies in mouse models that represent advanced stages of ovarian cancer that do not receive debulking surgery treatment also showed low efficacy of cisplatin and paclitaxel regimen. To overcome this problem in the next phases of this

project, we focused on developing a stem cell-based system for suicide gene therapy of ovarian cancer that can effectively kill resistant cancer cells and CSCs. For that purpose, we first examined different enzyme prodrug systems and determined the most effective treatment against drug-resistant ovarian cancer cells. Then, different ovarian cancer cell lines (commercial and patient-derived) were screened for their sensitivity to several standard-of-care anticancer drugs in order to find one that is the most resistant. In the next step, adipose-derived mesenchymal stem cell (ASC) was genetically modified to express carboxylesterase enzyme that can convert a less toxic prodrug (Irinotecan, CPT-11) to its active form (SN-38). The ability of the engineered stem cells to kill the chemo-resistant ovarian cancer cells in the presence of a prodrug was evaluated in vitro. In the next step, we used a xenograft animal model of ovarian cancer to evaluate the tumor response to our suicide gene therapy method and prevention of relapse by quantitative live animal imaging. The toxicity of this method of cancer therapy to normal tissues was evaluated by histopathology and hematology studies, and the data did not show any sign of toxicity to major intraperitoneal organs. In general, our studies demonstrate the possibility of reducing the chance of cancer drug resistance and tumor relapse without causing any side effects by using the discussed treatment approaches.

Chapter 2

A novel chemotherapeutic protocol for peritoneal metastasis and inhibition of relapse in drug resistant ovarian cancer[1]

[1] A version of this chapter has been published in Cancer Medicine, PMID: 29926538.

Ovarian cancer is associated with the highest mortality rate of all gynecologic malignancies in the United States and carries an overall 5-year survival rate of 45%. Most patients initially respond to standard treatments combining surgery and chemotherapy; however, the majority acquires multidrug resistance and succumb to their disease because of relapse [8]. It is believed that this clinical course is in line with the cancer stem cell model [8, 9]. According to the cancer stem cell theory, cancer-initiating cells (also termed cancer stem-like cells, or CSCs), play a major role in tumor recurrence and metastatic spread. Therefore, it is crucial to design a strategy that eradicates both differentiating ovarian cancer cells and CSCs during early-stage treatment. The standard of care for an ovarian cancer patient in the early stages consists of debulking surgery followed by six rounds of chemotherapy with platinum-based drugs and paclitaxel. The intent is to rid the patient of all tumors and remaining cancer cells, thereby minimizing the possibility of relapse and metastasis to distant sites. Clinical data show that after tumor debulking, addition of intraperitoneal (IP) chemotherapy to intravenous (IV) therapy significantly improves ovarian cancer outcomes in comparison to IV chemotherapy alone because ovarian cancer cells tend to leak into the abdominal fluid and remain as single or small spheroids [10, 11]. If left untreated, these ascitic cells, which are rich in CSCs, continue to grow and generate new tumors in both local and distant sites. The major deficiency that currently exists is that the ovarian CSCs in the abdominal fluid are usually highly resistant to chemotherapy, and in some cases, high doses of chemotherapeutics are needed for their effective eradication. As a result, IP treatment is associated with significant side effects, which in such cases forces the physicians to halt the chemotherapy. To overcome this deficiency, it was our objective to develop a chemotherapeutic approach that is not toxic

to normal tissues but can effectively kill the CSC-rich tumorspheres in the abdominal fluid and inhibit relapse. As a first step toward achieving our objective, we obtained ascites-derived malignant cells from a patient with recurrent advanced ovarian carcinoma. These ascitic cells overexpress MDR1 and show resistance to chemotherapy with paclitaxel [12]. Using these ascitic cells, termed OVASC-1, we first generated CSC-rich tumorspheres in cell culture under nonadherent conditions. The tumorspheres were then exposed to various anticancer drugs to determine their sensitivity to chemotherapeutics. Using the obtained in vitro data, we created various treatment protocols and examined both the efficacy and toxicity of each approach in nude mice bearing IP xenografts. Ultimately, we identified a low-dose chemotherapeutic approach that could not only kill the xenografted tumorspheres in the peritoneal cavity, but also inhibit relapse. The progression of disease, response to therapy and inhibition of relapse were evaluated by quantitative live-animal imaging. The toxicity of the optimum therapeutic protocol to normal tissues was studied by histopathology.

2.1 Materials and Methods

2.1.1 Chemicals and reagents

Ten percent bovine serum albumin (BSA, Sigma- Aldrich, USA) was prepared in D-PBS (Life Technologies Corporation, NY, USA) and kept at −20°C. Recombinant human epidermal growth factor (EGF) and basic fibroblast growth factor (bFGF) (Life Technologies Corporation) were reconstituted in D-PBS at concentrations of 200 μg/ mL and 100 μg/mL, respectively. A stock solution of 10 mg/ mL (16.23 mmol/L) Hoechst

33342 was prepared in deionized water and stored at −20°C. A stock solution of 1 mg/ mL cisplatin (Sigma-Aldrich) was prepared in 0.9% saline, whereas stock solutions of 5 mg/mL monomethyl auristatin E (MMAE) (MedChemExpress, NJ, USA), 1 mg/mL SN-38 (Cayman Chemical, MI, USA), 50 mg/mL paclitaxel, 30 mg/mL etoposide, 50 mg/mL 6-methylpurine (6-MP), and 50 mg/mL 5-Fluorouracil (5-FU) (Sigma-Aldrich) were prepared in DMSO and stored at −20°C until used.

2.1.2 Cell culture

As a precaution, all cell lines used in this study were first treated with BM-Cyclin (Sigma) to make them mycoplasma- free and then sent in 2016 to the University of Arizona Genetics Core, Cell Authentication Services, for authentica-tion. The A2780 cell line (originally from Sigma) was a kind gift from the laboratory of Dr. T. Minko (Rutgers University) and maintained in RPMI-1640 supplemented with 10% FBS. Malignant ovarian cancer cells (OVASC-1) were originally drawn from the ascitic fluid of an ovarian cancer patient at Rutgers Cancer Institute of New Jersey, deposited into the Biorepository Center (de-identified), and then transferred to our laboratory. OVASC-1 cells were maintained in RPMI- 1640 supplemented with 15% FBS and 2.5 μg/mL insulin [12, 13]. The media was changed every other day to maintain the health of the cells. To obtain OVASC-1 cells with stable expression of the luciferase gene, OVASC-1 cells were transfected with pGL4.5-[CMV/luc2/hygro] (Promega Corporation, WI, USA). Clones were selected under continuous exposure to 400 μg/mL of hygromycin as described

previously [14]. All cell lines were cultured at 37°C in a 5% CO2 95% air-humidified incubator.

2.1.3 Generation, propagation and characterization of tumorspheres

Tumorspheres were generated by transferring 2 × 104 ovar-ian cancer cells (OVASC-1 and A2780) per mL of MEBM supplemented with 0.4% BSA, 20 ng/mL EGF, 10 ng/mL bFGF, 5 μg/mL insulin (Sigma-Aldrich, MO, USA), and 1% antibiotic-antimycotic solution into an ultra-low attachment 6-well plate (Sigma-Aldrich). Cells were allowed to grow until the tumorsphere size reached >100 μm. The tumor-spheres were then dissociated using Accumax (Innovative Cell Technologies, Inc. CA, USA) to make a single cell sus-pension and reseeded in MEBM medium with supplements to create secondary tumorspheres. This process was repeated at least three times to enrich the tumorspheres with CSCs. The live/dead status of cells inside the tumorspheres was studied by staining with calcein-AM (green) and Hoechst 33342 (red) fluorescent dyes for 2-3 hr at 4°C followed by observation under a fluorescence microscope.

To evaluate the expression of stem cell markers, tumor-spheres were dissociated and total RNA from 106 number of the ovarian cancer cells was extracted with a commercially available RNA extraction kit (Qiagen, MD, USA) as per man-ufacturer's instructions. Total RNA (0.5-1 μg) was reverse- transcribed with SuperScript II reverse transcriptase (Life Technologies) using random hexamer priming. Quantitative real-time PCR was performed with an Applied Biosystems 7500 Real-Time PCR system (Applied Biosystems, Life Technologies Corporation) using Taqman Universal qPCR Master Mix

(Life Technologies Corporation) and respective probes as per manufacturer's instructions. Data are presented as mean ± SD (n = 4).

2.1.4 Evaluation of tumorsphere proliferation rate by PKH26 dye

Single cell suspensions of 2 × 106 cells were prepared and labeled with PKH26 dye in diluent C (1:500 dilution, yield-ing a final concentration of 2 μmol/L) as per instructions for PKH26 Red Fluorescent Cell Linker Kits for General Cell Membrane Labeling (Sigma-Aldrich). The cells were washed twice to remove any unbound dye and then suspended in MEBM with supplements at the density of 6 × 104 cells/well in a 6-well low-adherent plate. Tumorspheres were collected at different time (day) intervals, centrifuged, and dissociated into a single cell suspension with Accumax/D-PBS (1:1) prior to analysis with a Gallios flow cytometer (Beckman Coulter, Inc. CA, USA). Proliferation index (PI) and vari-ous other cell tracking parameters were studied and quanti-fied using Modfit LT V4.1.7 software with the cell tracking wizard module.

2.1.5 Dose response curve of various chemotherapeutic drugs

Ovarian cancer cells were transferred into an ultra-low at-tachment plate at the seeding density of 2 × 103 cells/well in 200 μL of MEBM with supplements to generate tum-orspheres as mentioned above. The tumorspheres were treated with increasing doses of MMAE (0.1-10 nmol/L), SN-38 (1-100 nmol/L), etoposide (0.1-10 μmol/L), cispl-atin (1-100 μmol/L), 6-MP (1-100 μmol/L), and 5-FU (1- 100 μmol/L) 3 days post seeding. The

tumorsphere number (N) and radius (R) were analyzed 14 days postseeding. Total cell content (TCC) in each well was calculated by consider-ing the radius of one cell (r) and combining both N and R parameters as shown below:

$$VOLUMEW\ OF\ ONE\ CELL = \frac{4}{3}\pi R^3$$

2.1.6 Determination of combination index value

OVASC-1 cells were seeded in 96-well plates at a density of 5 × 103 cells per well. Twenty-four hours later, cells were treated with SN-38 at concentrations ranging from 0 to 200 nmol/L and MMAE at concentrations ranging from 0 to 20 nmol/L at a 1:10 ratio. After 72 hours, the media was replenished with 100 μL of fresh media containing 10 μL WST-1 reagent (Sigma-Aldrich, PA, USA). After incubation for 2 hours at 37°C, the absorbance was determined with a microplate reader (Tecan, Switzerland). The absorbance of each well was normalized to the negative control (untreated cells) in order to determine the cell viability. To determine the antagonistic, additive, or synergistic effects of combi-nation therapy, we calculated the combination index (CI) using the fractional product method [14, 15]. Then, CI was plotted against the fraction of killed cells, also referred to as fraction affected (Fa).

$$Fa = 1 - \frac{OD_{Treatment}}{OD_{Control}}$$

where ODControl = absorbance of control or untreated cells and ODTreatment = absorbance of cells treated with drug(s).
ACI value of less than 1 indicates synergism, a CI value >1 indicates antagonism, and a CI value of 1 indicates an additive effect.

2.1.7 Evaluation of the therapeutic efficacy and inhibition of relapse in vivo

All in vivo studies described here were performed accord-ing to the guidelines of the Rutgers University Institutional Animal Care and Use Committee (Protocol# 11-001). Outbred homozygous nude J:NU (Foxn1nu/Foxn1nu) female mice (5-6 weeks old) were purchased from The Jackson Laboratory (Bar Harbor, ME). In vivo peritoneal xenografts were generated using OVASC-1-luc cells (OVASC-1 cells stably expressing the luciferase gene). 5×10^6 cells were re-suspended in 500 μL of D-PBS and then injected IP using a 25G needle. Stable expression of luciferase in mouse abdomen was monitored periodically for 7 days before the start of treatment on day 8. Tumorsphere bearing mice were then ran-domized into control and treatment groups. Unless otherwise specified, the chemotherapeutic(s) were administered IP in a total volume of 2 mL vehicle once per week for five doses. The vehicle solution was composed of 1% cremophor:ethanol (50:50) and 99% saline (0.9%).

Bioluminescence imaging (BLI) was conducted as men-tioned previously for monitoring disease progression [14, 16]. Xenografted nude mice were imaged weekly 1 day before the administration of drugs. Data acquisition was conducted using the IVIS Lumina III Imaging System, and images were analyzed using the Living Image 4.5 module. To study treat-ment response, fold change in BLI signal (ie BLI measure-ment at the end of treatment/BLI measurement prior to the first treatment) was calculated for each mouse. To assess re-currence, mice were imaged once every 2 weeks beginning with the final day of the treatment. Observable indicators of health (eg appetite, posture, movement) and weight were con-tinuously monitored to detect any chemotherapeutic-related toxicities or

morbidities resulting from ascitic burden. Loss of more than 10% body weight was considered treatment- related toxicity. When toxicity was observed, either the treat-ment was discontinued or mice were euthanized.

2.1.8 Histopathology study

Organs of all three mice in untreated control group and the group treated with SN-38 1 (mg/kg) and MMAE (100 μg/kg) were collected at the end of the treatment period immediately following euthanasia. Organs were washed in 0.9% saline so-lution, placed inside a Cryomold (Fisher Scientific) filled with Tissue-Plus ™ O.C.T Compound (Fisher Scientific), and then snap frozen in liquid nitrogen. Cryosectioning was performed at the Rutgers Cancer Institute of New Jersey Histopathology Core Facility using a cryostat, followed by fixation and hema-toxylin and eosin (H&E) staining. The slides were interpreted by a histopathologist at the Rutgers Robert Wood Johnson University Hospital. Photomicrography was conducted using a Leica microscope (20× objective).

2.2 Results and Discussion

2.2.1 Ovarian cancer tumorspheres are enriched with CSCs

Subpopulations of ovarian tumor cells in ascitic fluid display cancer stem-like properties including increased resistance to therapies, the ability to spread into distant sites, and the ability to induce cancer recurrence [17, 18]. Since malignant cancer cells in the ascitic fluid are a major source of mortality in ovarian cancer patients, development of a

treatment protocol that can effectively eliminate these cells is of great interest. Suspended cancer cells in the form of spheroids (tumorspheres) represent a suitable in vitro experimental model of ovarian cancer ascites. Therefore, we generated ovarian cancer tumorspheres in low-adherent culture plates using an established A2780 ovarian cancer cell line and OVASC-1 ascitic cells obtained from the IP fluid of an ovarian cancer patient with recurrent disease. We observed that both A2780 and OVASC-1 cells had tumorsphere forming capability even after seven passages under low-adherent conditions (Figure 2.1A). To characterize and better understand the change in the CSC population before and after tumorsphere formation, we measured the expression of classical stem cell markers by real-time PCR. In comparison to the cells cultured under adherent conditions, the A2780 cells inside the tumorspheres showed 35.4 ± 3.2, 32.2 ± 2.4, and 43.3 ± 1.5 fold positive change in mRNA expression levels of NANOG, OCT-3/4 and SOX-2, respectively. Similarly, significant overexpression in mRNA levels of the same genes was ob-served in OVASC-1 cells (Figure 2.1B). The results of this study, as evidenced by the overexpression of major classical stem cell markers, show that the procedure used to generate tumorspheres significantly increases the percentage of the CSC population, resulting in CSC-enriched tumorspheres.

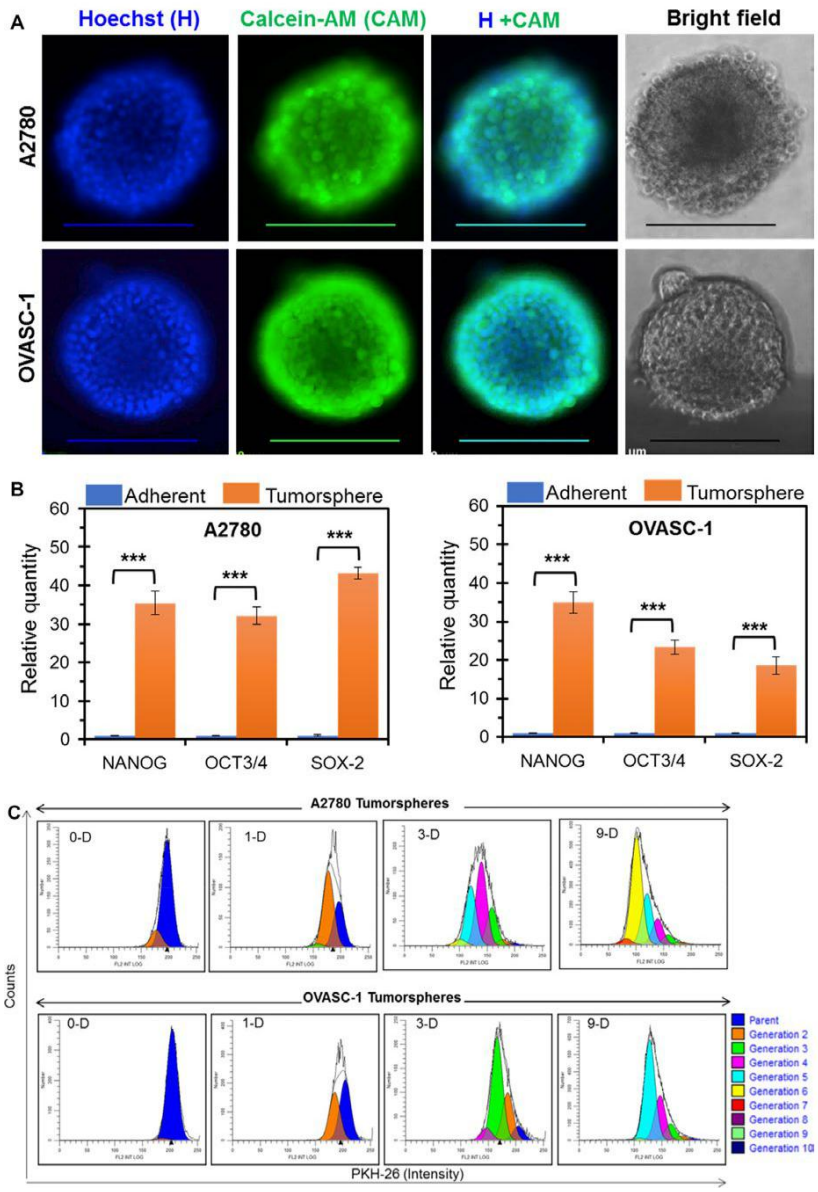

Figure 2.1: Generation and characterization of CSC-enriched tumorspheres of A2780 and OVASC-1 cells. A, Tumorspheres in suspension were stained with Calcein-AM (CAM) and Hoechst 33342 (H) dyes and observed under a fluorescence microscope. Scale bar = 200 µm. B, Relative expression of stem cell markers in ovarian cancer cells under adherent and nonadherent conditions as quantified by real-time PCR. Data are presented as mean ± SD (n = 4). ***Indicates significance (paired t test, P < .001). C, CSC-rich tumorspheres showing heterogeneous population with different proliferation kinetics. Histograms of A2780 and OVASC-1 tumorspheres from day zero (0-D) until day nine (9-D) post seeding, representing progenitors or daughter cells of different generations

To assess whether the cancer cells in the tumorspheres are dormant or have the potential to grow in size under harsh low-adherent conditions, we characterized them further by examining their growth kinetics. For this purpose, we first stained the cells with PKH26 red tracer dye, then reseeded them under nonadherent conditions to form tumorspheres, and finally dissociated them for analysis after predetermined time intervals. The results of this experiment showed that the majority of the cells in tumorspheres were in a proliferation stage by day 3 post seeding. Notably, 1% of A2780 and 7% of OVASC-1 cells were in the parental G1 stage (Figure 2.1 C, and Table 2.1). This result indicates that the tumorspheres are heterogeneous with regard to growth kinetics. By day 9, almost all of the A2780 and OVASC-1 tumorsphere cells were distributed in the G6 (generation 6) or G5 proliferation stage, respectively. The PI, which indicates the average number of cell divisions undergone by the proliferating cells, was calculated to be 15.06 for A2780 and 8.78 for OVASC-1. These data show that the tumorspheres of both cell lines were actively growing under low-adherent conditions. This is an important observation, as it could explain the potential difficulty of effectively killing such tumorspheres in ascitic fluids: the constantly growing suspended tumorspheres could generate substantial resistance to permeation by chemotherapeutics [18]. In addition, the data indirectly suggest that the OVASC-1 tumorspheres, which exhibit a slower growth rate, could show decreased sensitivity to antimitotic chemotherapeutics.

Table 2.1: Tumorsphere proliferation kinetics and analysis: Parent population is represented by Generation-1 (G1), G-max (Generation with maximum % cells), Proliferation index (PI), Non-Proliferating Fraction (NPF), and Precursor Frequency (Pγ).

Cell line	Time (day)	G1 (%)	Gmax	PI	NPF	Pγ
A-2780	0	93	G1	1.04	0.96	0.001
	1	51.69	G1, G2	1.33	0.69	0.004
	3	1.01	G4	6.37	0.06	0.821
	9	0.07	G6	15.06	0.01	0.945
OVASC-1	0	99.81	G1	1	1	0.0003
	1	58.48	G1	1.26	0.74	0.0004
	3	7.86	G3	2.7	0.21	0.411
	9	0.93	G5	8.78	0.08	0.83

2.2.2 Evaluation of the tumorsphere sensitivity to drug treatment

In the next experiment, we investigated the effectiveness of few chemotherapeutic drugs that have been used alone or as antibody-drug conjugates in the past decades to treat ovarian cancer at different disease stages. Tested drugs included MMAE (microtubule-disrupting agent) [19, 20], SN-38 (topoisomerase I inhibitor) [21], etoposide (topoisomerase II inhibitor) [22], cisplatin (DNA crosslinker) [23], 6-MP (nucleotide analogue and inhibitor of RNA and protein synthesis) [24, 25] and 5-FU (pyrimidine analogue and thymidine synthase inhibitor) [25, 26]. As we mentioned above, OVASC-1 cells have been shown to be resistant to paclitaxel; therefore, we did not examine their sensitivity to this drug at the in vitro level to avoid redundancy. Both A2780 and OVASC-1 tumorspheres were first generated and then treated with the aforementioned chemotherapeutic drugs at different concentrations. To examine the effectiveness of each drug, we first measured the change in tumorsphere number and size, and from that we calculated the remaining total cell content in each tumorsphere after treatment. As expected, the results of this experiment showed a significant decrease in the number and diameter of tumorspheres in both cell lines with increasing drug dose (Figure 2.2A,B). We also observed that the effective dose that reduced the number of tumorspheres by 50% was in the nanomolar range for MMAE (1 nmol/L) and SN-38 (10 nmol/L), whereas other drugs were effective in the micromolar range. To analyze the effectiveness of the drugs in a more meaningful way, we used a formula to estimate the total number of cells (total cell content) in each tumorsphere. In essence, the formula takes into account both tumorsphere diameter and number to calculate the total cell content. For example, knowing that the average

diameter of an A2780 cell is 10 μm, the total number of cells in tumor-spheres of the A2780 untreated control group was calculated to be 578 125 (N = 37) (Figure 2.2A). Only MMAE was able to reduce the total cell content in A2780 tumorspheres to approximately 600 cells (<0.1%) at concentrations as low as 1 nmol/L. At a 10 nmol/L concentration, MMAE killed all of the cells in A2780 tumorspheres. By comparison, to achieve the same level of tumorsphere killing efficiency (ie <0.1%), a 100 μmol/L concentration of cisplatin had to be used. Although we observed the same trend in OVASC-1 treated tumorspheres, it was apparent that the OVASC-1 tumorspheres were far more resistant to therapy than the A2780 tumorspheres. For instance, to achieve the same level of tumorsphere killing efficiency (ie <0.1%), at least 10 nmol/L of MMAE was needed, which was ten times more than the needed amount for A2780 tumorspheres (Figure 2.2B).

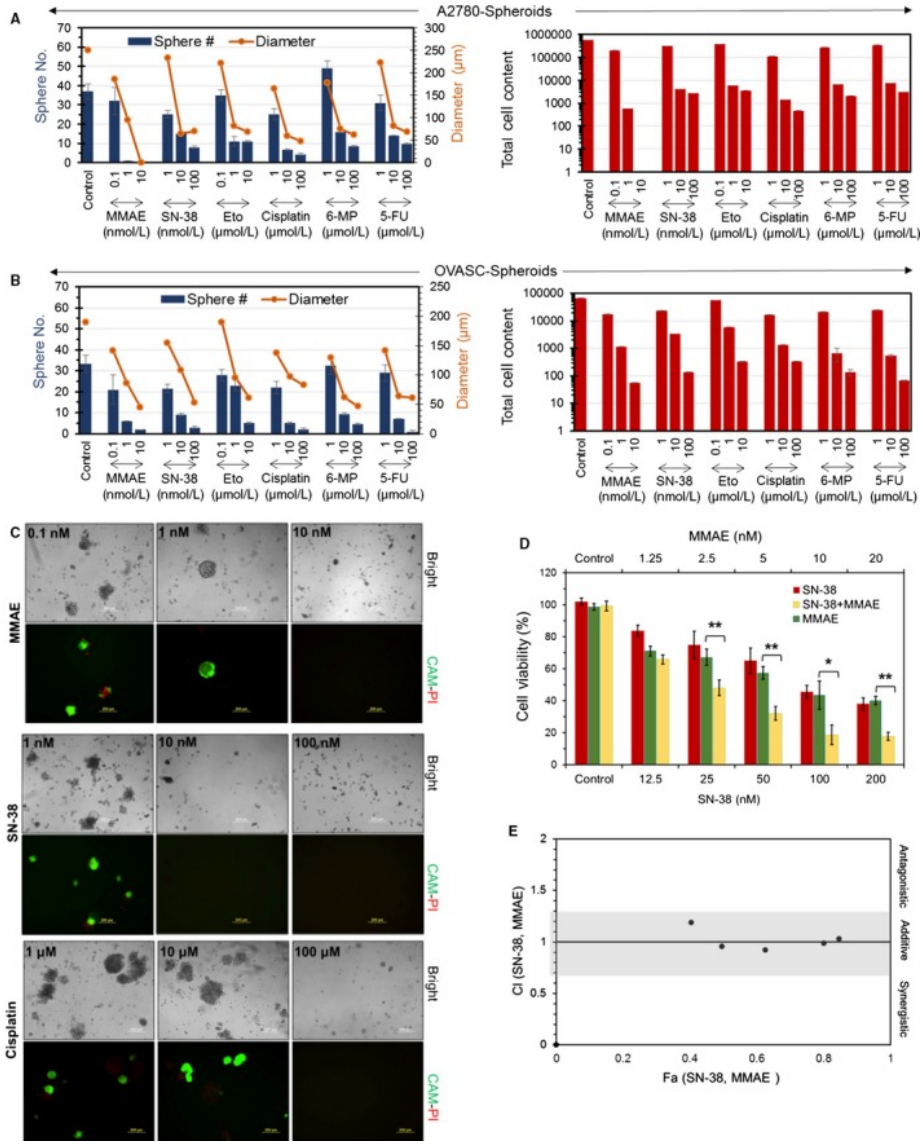

Figure 2.2: Evaluation of the effectiveness of the chemotherapeutic agents in killing CSC-rich tumorspheres: A and B, Measurement of the sphere number, size and total cell content in tumorspheres after treatment with different chemotherapeutics. Data are presented as mean ± SD (n = 4). C, Evaluation of OVASC-1 tumorsphere recurrence 30 d after treatment of primary tumorspheres with MMAE, SN-38 and cisplatin. Tumorspheres were stained with the fluorophores; calcein-AM (CAM) and propidium iodide (PI) to visualize live (green) and dead (red) cells respectively. Scale bar = 200 μm. D, Evaluation of the efficacy of single-agent and combination therapy with MMAE and SN-38 in killing OVASC-1 cells (t test, *P < .05; **P < .01). Data are presented as mean ± SD (n = 4). E, Combination index plot for the determination of antagonistic, additive, or synergistic effects of SN-38 and MMAE combination therapy. The additivity line is at CI = 1; CI < 1 indicates synergism and CI > 1 indicates antagonism. The additivity effect has some level of uncertainty, as depicted by the gray area [27].

Closer investigation of OVASC-1 cells revealed that they exhibit overexpression of the MDR1 gene, which is responsible for mediating multidrug resistance [12]. Therefore, it was very interesting to observe that the OVASC-1 tumorspheres could be effectively killed with MMAE in such low concentrations, despite the findings of a recent report showing that this drug is a substrate for MDR1 [27]. The remarkable anticancer efficacy of MMAE could be attributed to its high potency, which allows this drug to kill cancer cells even at very low concentrations. The sensitivity of the OVASC-1 cells to SN-38 was also interesting. Some older studies have indicated that SN-38 is a substrate for both the MDR1 and the ABCG2 drug efflux pumps [28], whereas recent evidence suggests that the ABCG2 pump is a key mediator of SN-38 resistance [29, 30]. To shed more light on this ambiguity, we measured the expression levels of the ABCG2 transporter in OVASC-1 cells. The results of this experiment showed that more than 90% of OVASC-1 cells expressed ABCG2. However, the expression level was in low intensity meaning that ABCG2 existed in low copy numbers on the cell surfaces (Figure 2.3).

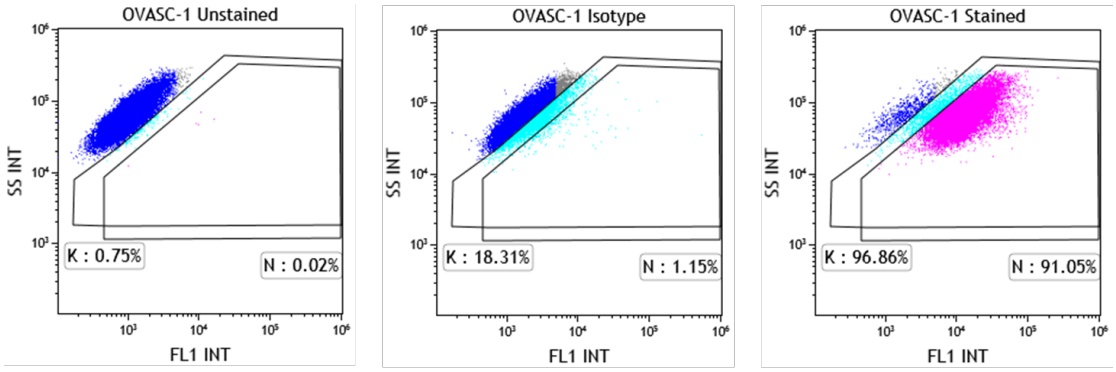

Region	Number	%Total	%Gated	X-Mean	Y-Mean
ALL	25000	82.96	100	1.1	63.6
K	198	0.66	0.75	2.02	42.6
N	5	0.02	0.02	9.07	44.4

Region	Number	%Total	%Gated	X-Mean	Y-Mean
ALL	25000	86.2	100	2.11	64.4
K	4780	16.48	18.31	3.21	57
N	280	0.97	1.15	8.69	51.1

Region	Number	%Total	%Gated	X-Mean	Y-Mean
ALL	25000	85.44	100	13.4	69.3
K	24219	82.77	96.86	13.8	68.7
N	22737	77.71	91.05	14.3	67.2

Figure 2.3: ABCG2 expression level in OVASC-1 cells: Cells were fixed with 4% paraformaldehyde (10 min) followed by permeablization with 0.1% Tween/PBS (20 min). Cells were then incubated with Rabbit Anti-*h*ABCG2 primary antibody (Abcam) overnight at 4 ^{o}C, and then stained with AlexaFluor conjugated secondary Goat Anti-Rabbit IgG antibody (room temperature, 1 h). The isotype was Rabbit IgG monoclonal antibody (Abcam). Data acquisition was carried out using Beckman Coulter Gallios Flow-cytometer and analysis was performed using Kaluza 1.5 module.

Since OVASC-1 cells express MDR1 in high copy numbers but ABCG2 in low copy numbers, our data related to the sensitivity of OVASC-1 to SN-38 at nanomolar (nmol/L) concentrations appears to rule out MDR1 as a prominent mediator of SN-38 resistance, and agree with the more recent studies reported in 2016 [29, 30]. This interesting observation highlights the importance of personalized therapy, in which an IP sample could be taken from each patient and analyzed for ABCG2 expression. If ABCG2 expression exists in low copy numbers, then administration of SN-38 may be more effective than cisplatin, paclitaxel or a combination thereof.

So far, the in vitro data have shown that MMAE and SN-38 have the greatest ability among the tested drugs to significantly reduce the cell content in CSC-rich tumorspheres. This observation prompted us to examine the viability of the cells remaining inside the treated tumorspheres and evaluate their potential to regrow and regenerate the tumorspheres. For this purpose, we characterized the viability of the more resistant OVASC-1 tumorspheres after treatment with one dose of either MMAE or SN-38. Posttreatment, the OVASC-1 tumorspheres were left undisturbed for 30 days in replenishing media to enable the growth of any remaining cancer cells that survived the therapy. After 30 days, the remaining tumorspheres were stained with calcein-AM and propidium iodide to visualize the live/dead cells, respectively. The results of this experiment showed that both MMAE and SN-38 could effectively inhibit tumorsphere regrowth at concentrations as low as 10 nmol/L (Figure 2.2C). This result indicates that at that concentration, all CSCs, as well as mature differentiated cancer cells were killed. In contrast, cisplatin was unable to completely eradicate CSCs even at 10 μmol/L concentration, as evidenced by the presence of live cells in the tumorspheres. When the

concentration of cisplatin was increased to 100 μmol/L, the drug was able to completely kill the tumorspheres and inhibit relapse.

Thus far, the in vitro data highlight the high potency of MMAE and SN-38 and their ability to kill CSC-rich OVASC-1 tumorspheres. However, this high potency could also result in significant toxicity when used in vivo. To investigate treatment options that might maintain high anticancer activity but reduce the potential for toxicity, we examined whether the combined use of MMAE and SN-38 has an additive, synergistic or antagonistic effect. Therefore, OVASC-1 cells were treated with combinations of MMAE and SN-38 at a 1:10 ratio (based on equitoxic dose and IC_{50} values) and different concentrations. The CI was then calculated and plotted against the corresponding Fa. The results of this experiment demonstrated that MMAE and SN-38 have an additive cytotoxic effect, making it possible to use both drugs together at lower concentrations without compromising anticancer activity (Figure 2.2 D,E). This important observation led us to formulate our hypothesis for in vivo studies.

2.2.3 Evaluation of cancer progression, response to therapy, and recurrence in vivo

To determine the biological relevance of these findings, we hypothesized that low dose therapy with MMAE and SN-38 can not only eradicate the CSC-rich IP tumorspheres but also inhibit relapse in mice. To test this hypothesis, we engineered luciferase expressing OVASC-1 cells (OVASC-*luc*) to allow us monitor disease progression over time in live nude mice. Before starting the treatment, we first measured the sensitivity of BLI to identify the minimum number of engineered OVASC-*luc* cells that could be detected in

mice after IP injections. The results of this experiment showed a linear correlation between the number of injected OVASC-*luc* cells and the measured bioluminescence. The results also showed that the minimum number of cells that could be detected by the imaging system after IP injection was 10 000 with a total flux of 1.1×10^6 (P/s) (Figure 2.4 A,B). We also investigated whether the OVASC-*luc* cells could survive the peritoneal environment in nude mice and metastasize to adjacent and distant organs, in a manner similar to its clinical course. Therefore, nude mice were injected with OVASC-*luc* cells, and tumor growth was monitored over a 2 months period. The results of this experiment showed that OVASC-*luc* cells thrived in the mouse abdomens, and quickly metastasized and formed tumor nodules in the lung, liver, pancreas, spleen and reproductive organs (eg ovaries) (Figure 2.4 C). Based on these findings, we set up our in vivo studies, in which OVASC-*luc* cells were injected into the peritoneal cavity of mice and allowed to grow and stabilize for a week. The drug dosing schedule, BLI schedule and other parameters are shown in Figure 2.4 D. In this pilot study, mice were randomly divided into nine groups (n = 3) and received treatments starting 8 days following tumor implantation (Table 1). Since the in vitro studies showed that the tumorspheres are fully formed by day 3, this lag period was provided to ensure their stable establishment.

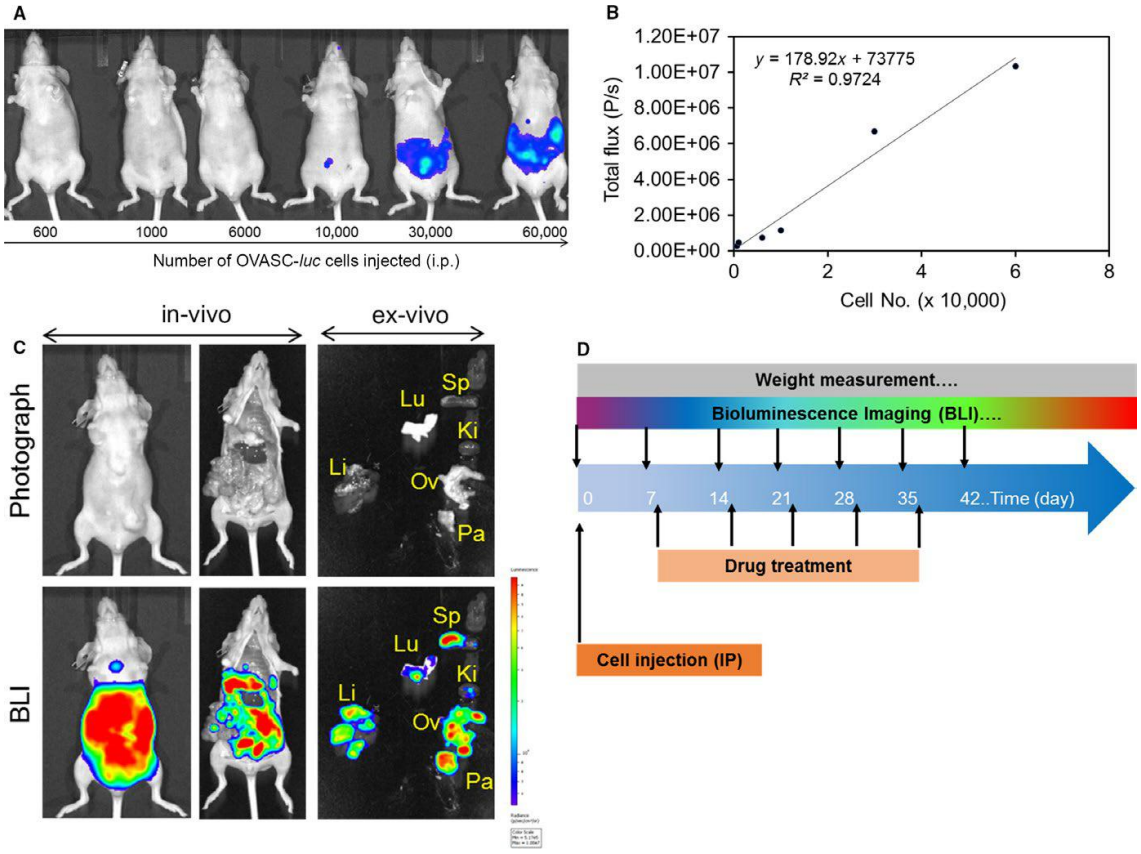

Figure 2.4: Bioluminescence of intraperitoneally injected OVASC-*luc* cells in nude mice. B, Plot of cell number vs total flux and its correlation. C, Brightfield images (up) and BLIs (down) of whole body and individual organs 2 mo post intraperitoneal injection of five million OVASC-*luc* cells. The BLI of mouse shows intact mouse as well as dissected organs such as liver (Li), lung (Lu), spleen (Sp), pancreas (Pa), kidney (Ki), ovary and associated reproductive organs (Ov). D, The drug dosing schedule, BLI schedule and weight measurement studies

Table 2.2: Drug doses and treatment response to various treatment regimens

Group no.	Drug name	Drug dose	Mice (n)	CR	PR	SR	NR	Recurrence
Group 1	Vehicle control	N/A	3				3	
Group 2	Cisplatin + paclitaxel	12+15 (mg/kg)	3		3			
Group 3	SN-38	10 (μg/kg)	3		2		1	
Group 4	SN-38	1 (mg/kg)	3	1	2			
Group 5	MMAE	1 (μg/kg)	3		2		1	
Group 6	MMAE	100 (μg/kg)	3	2	1			
Group 7	SN-38 + MMAE	10+1 (μg/kg)	3		2	1		
Group 8	SN-38 + MMAE	100+10 (μg/kg)	3	3				1 (2nd week)
Group 9	SN-38 + MMAE	1000+100 (μg/kg)	3	3				0

CR: complete response meaning no evidence of the tumor. PR: partial response meaning decrease in tumor volume (≥50%). OR: overall response meaning CR+PR. SR: small response meaning decrease in tumor volume (≤25%); NR: no response meaning significant increase in tumor volume or appearance of new tumor(s). Recurrence: appearance of tumor after complete response.

The untreated control group (Group 1) received vehicle solution only. We also assigned one control mouse group to be treated with cisplatin plus paclitaxel, which are standard-of-care drugs for recurrent ovarian cancer (Group 2). Mice in this group received the maximum tolerable dose of cisplatin (12 mg/kg) and paclitaxel (15 mg/kg), as reported previously [31]. Two groups received ultra-low and low doses of SN-38 (Groups 3 and 4). Two groups received ultra-low and low doses of MMAE (Groups 5 and 6). The final three groups received three different combinations of SN-38 with MMAE (Groups 7-9). The data related to each treatment group were analyzed to understand the disease progression and therapy response. The image analysis of mice in Group 1, which received vehicle solution (no drug), showed a steady-state increase in the bioluminescence signal, indicating an increase in ascitic tumor mass over time (Figures 4and S2). The mice in this group gained weight until they were euthanized due to an impediment of movement resulting from the increase in tumor size. The mice in Group 2, which received cisplatin plus paclitaxel, showed partial response to therapy (Figures 2.5 and 2.7, Table 2.2). The fold change in tumor mass as measured by BLI was 0.062 (0.039-0.006) ([Median] [min-max]) at the end of treatment compared to initial tumor mass prior to treatment (*t* test, $P = .02$). The mice in this group tolerated the treatment for at least 3 weeks but started to show severe signs of toxicity after the fourth dose and lost significant weight. Therefore, these mice were either euthanized when their body weight loss exceeded the 20% threshold, or their treatment was discontinued when other signs of toxicity were observed. Considering that the OVASC-1 cells are samples from a patient with recurrent disease and are resistant to paclitaxel [12], this response rate was expected. Mice in groups 3, 5, and 7 that were treated with the

ultra-low concentration of SN-38 (10 μg/kg) and/or MMAE (1 μg/kg) either as single agents or in combination did not show any response to therapy; the decrease in tumor mass was not statistically significant (*t* test, $P > .05$) (Figures 2.5 and 2.8 – 2.10, Table 2.2). All mice in these three groups gained weight and did not show any visible signs of toxicity.

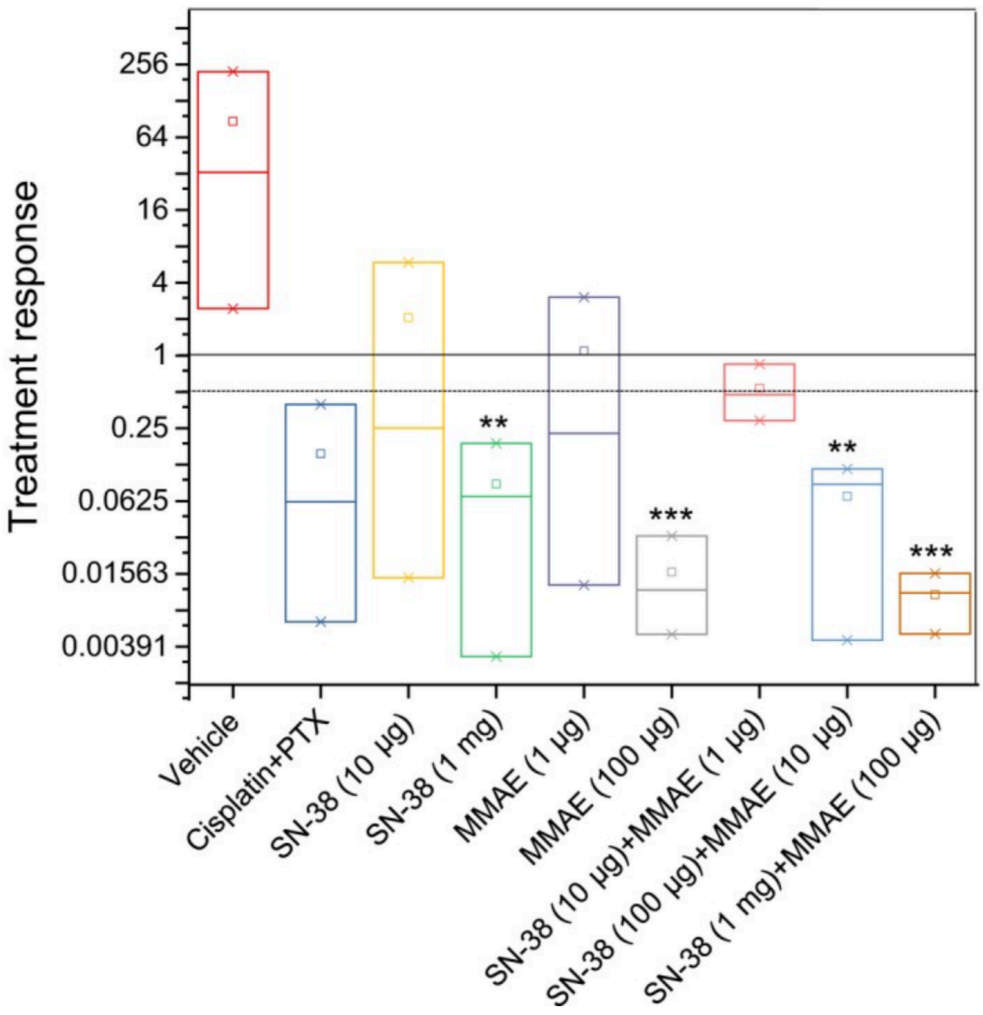

Figure 2.5: Box-and-whisker plot showing median (minimum-maximum) and treatment response (total flux at the end of treatment/total flux before treatment). Data are presented as mean ± SD (n = 3). Statistics were computed by the paired *t* test (prior to vs. last treatment). *, **, and ***indicate *P*-values <.05, <.01 and <.001, respectively.

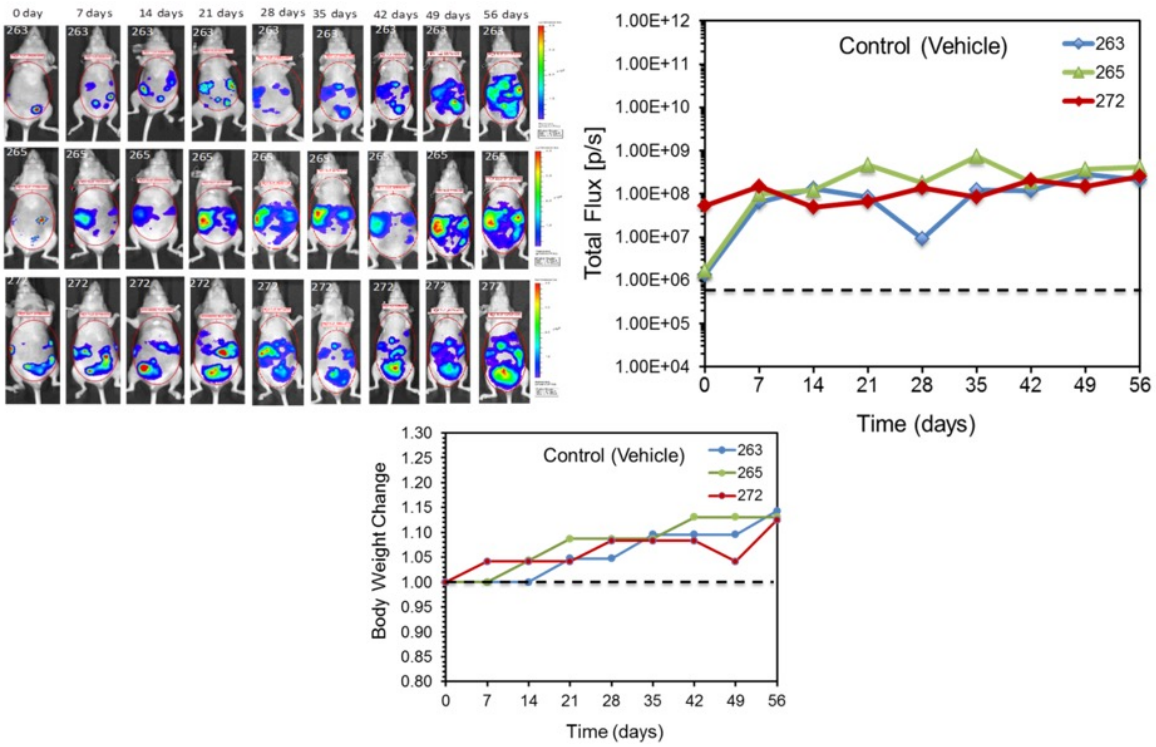

Figure 2.6: Bioluminescence imaging and body weight change measurement of mice in control group treated with vehicle.

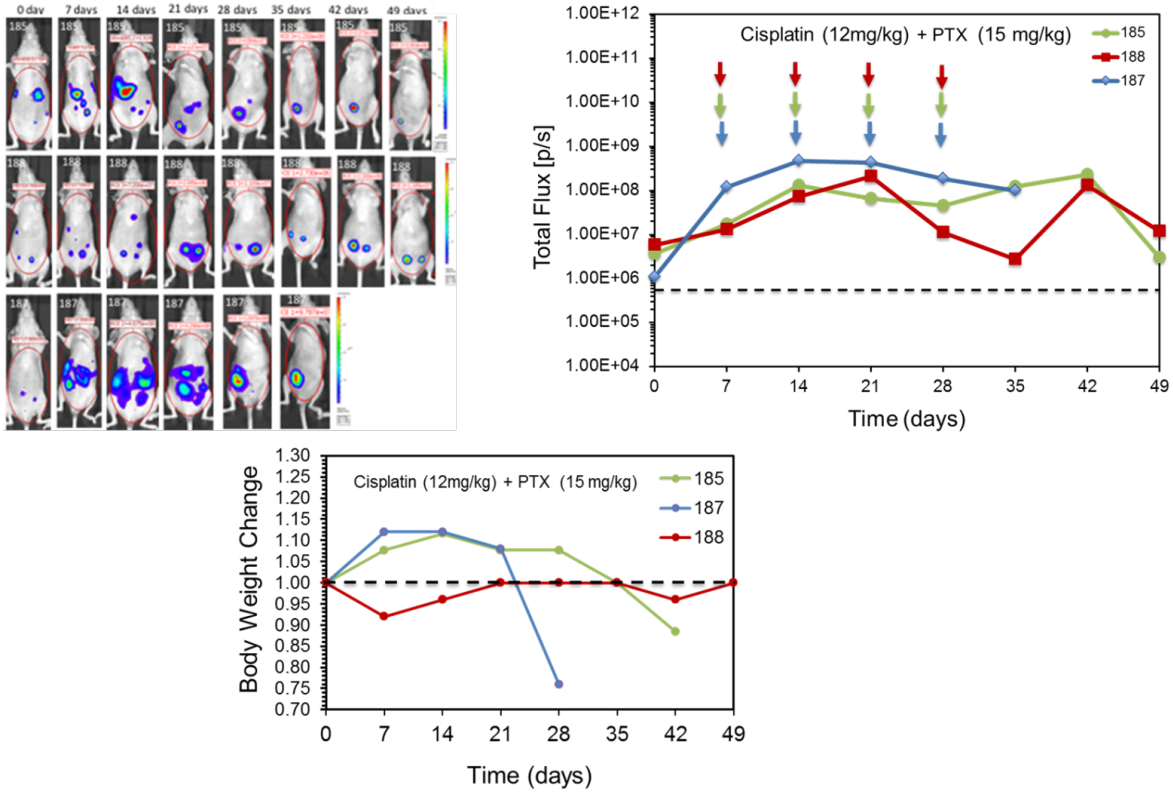

Figure 2.7: Bioluminescence imaging and body weight change measurement of mice in group treated with cisplatin and paclitaxel.

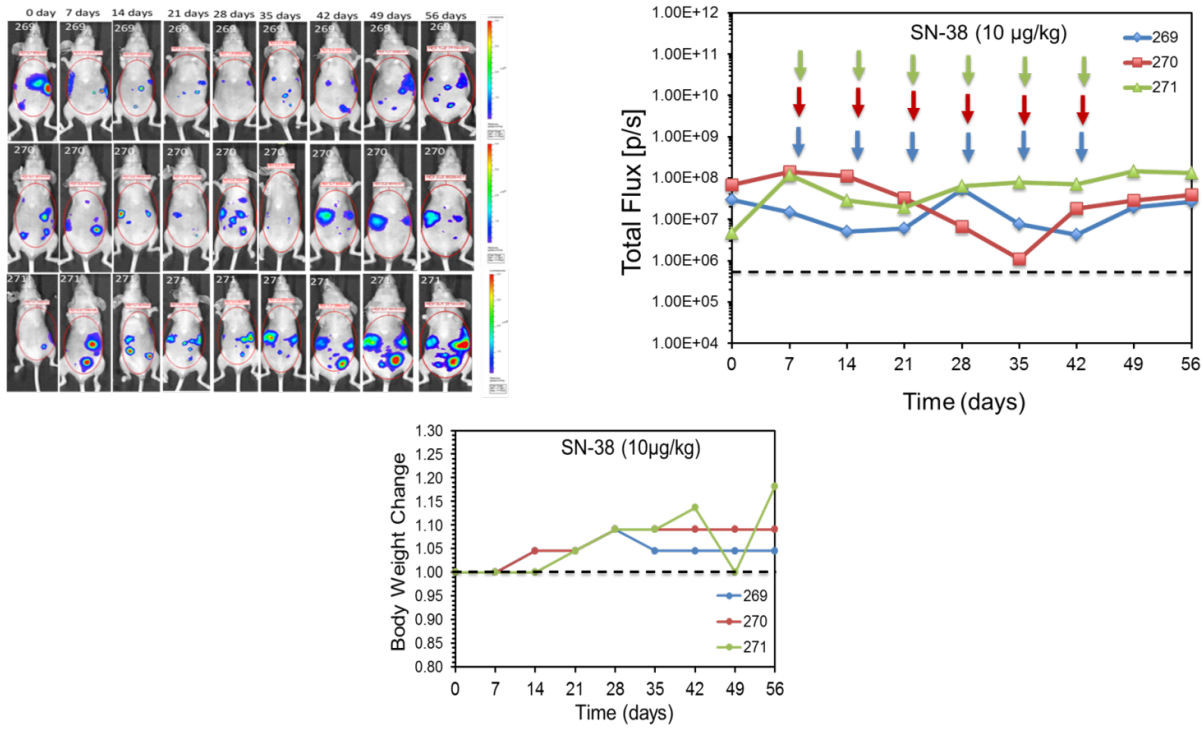

Figure 2.8: Bioluminescence imaging and body weight change measurement of mice in group treated with SN-38 (10 µg/Kg).

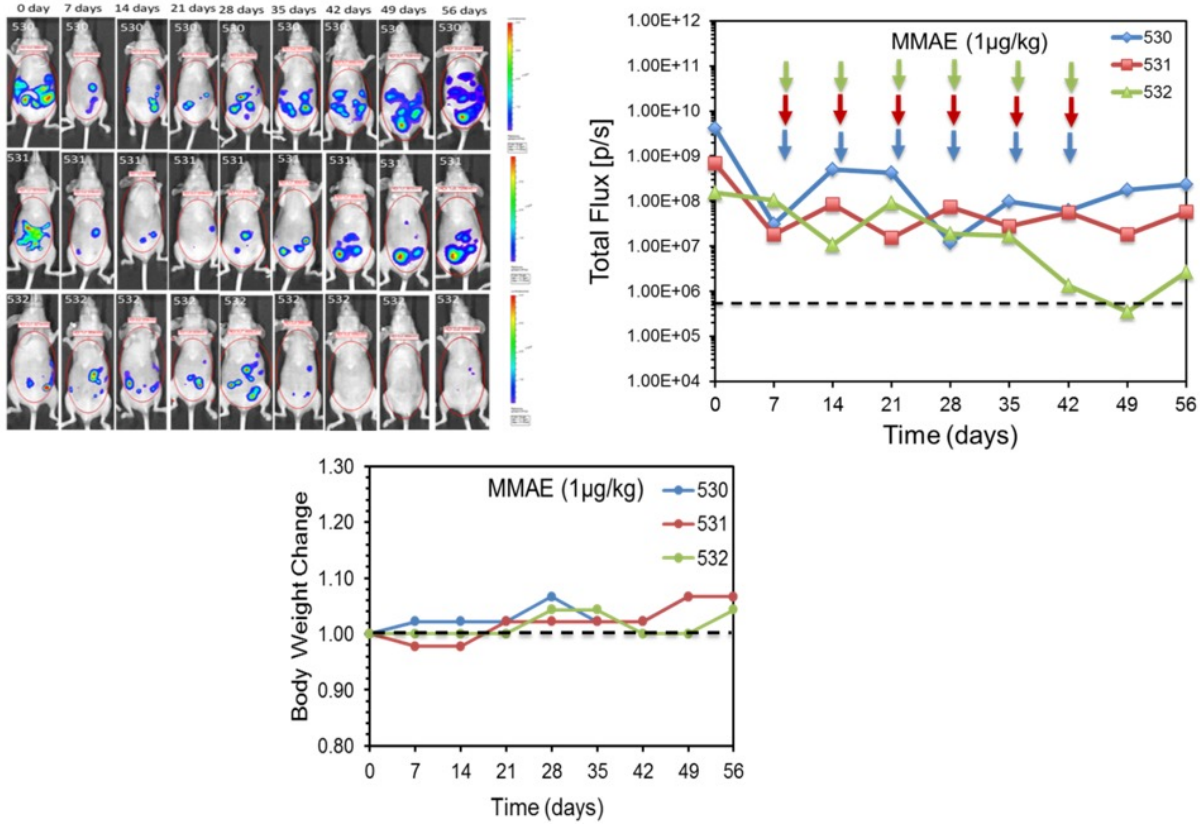

Figure 2.9: Bioluminescence imaging and body weight change measurement of mice in group treated with MMAE (1 μg/Kg).

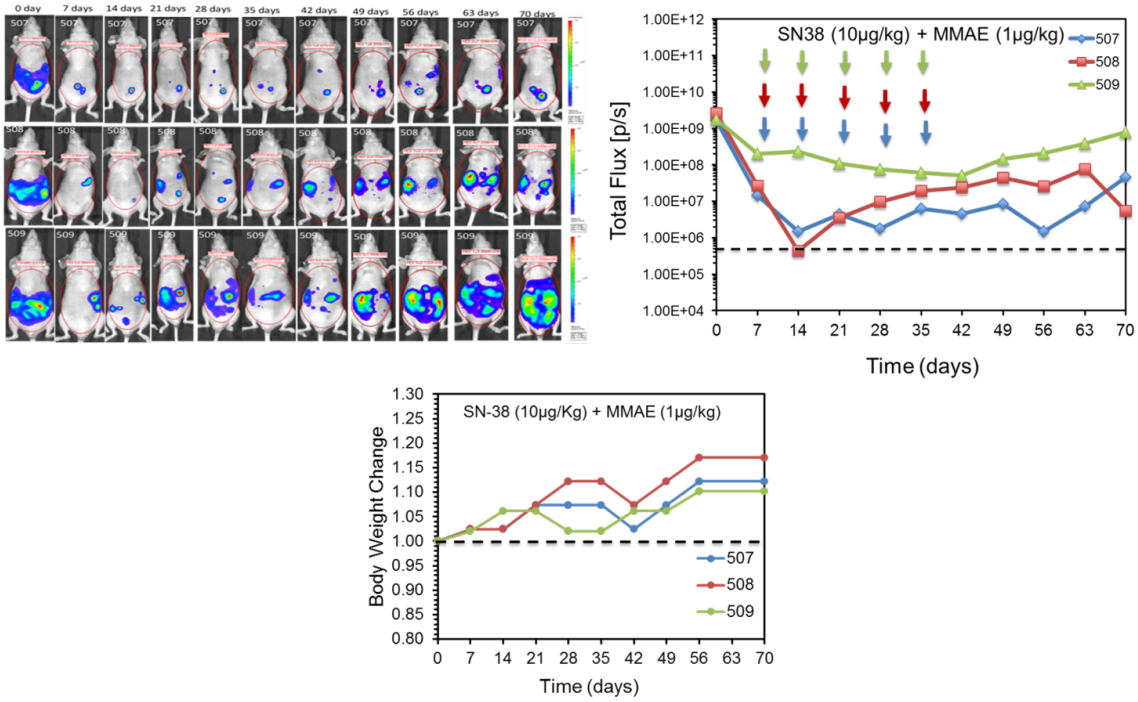

Figure 2.10: Bioluminescence imaging and body weight change measurement of mice in group treated with SN-38 (10 μg/Kg) and MMAE (1 μg/Kg).

Mice in Groups 4 and 6 that were treated with SN-38 (1 mg/kg) or MMAE 100 μg/kg showed a statistically significant response to therapy (*t* test, $P < .01$) (Figure 2.5, Table 2.2). Notably, one mouse in each group completely responded to therapy and remained disease-free for at least 3 months (Figure 5). All mice in these two groups gained weight and did not show any signs of visible toxicity. Mice in group 8, which were treated with a combination of SN-38 (100 μg/kg) and MMAE (10 μg/kg), also showed a significant change in tumor mass (Figure 2.5, Table 2.2). All mice in this group showed a complete response and remained disease-free without any sign of recurrence for at least 90 days (Figure 2.11). However, one mouse showed recurrence after 90 days. Additionally, mice in this group did not show any signs of toxicity. Finally, all mice in Group 9, which were treated with a combination of SN-38 (1 mg/kg) and MMAE (100 μg/kg), showed a complete response to therapy (Figure 2.5, Table 2.2). Remarkably, mice in this group showed a complete response after administration of only four doses of the drug combination. Most importantly, no sign of cancer relapse was observed indicating the complete eradication of both differentiating cancer cells and CSCs; we could not detect a bioluminescence signal even after 105 days (Figure 2.11). Overall, four groups showed a statistically significant response to therapy. These groups included the mice that were treated with SN-38 (1 mg/kg), MMAE (100 μg/kg), SN-38 (100 μg/kg) plus MMAE (10 μg/kg), and SN-38 (1 mg/kg) plus MMAE (100 μg/kg). However, only mice that were treated with a combination of SN-38 (1 mg/kg) and MMAE (100 μg/kg) did not show any signs of recurrence. These data support our hypothesis that low-dose therapy with MMAE and SN-38 can not only eradicate the CSC-rich IP tumorspheres but also inhibit relapse in mice.

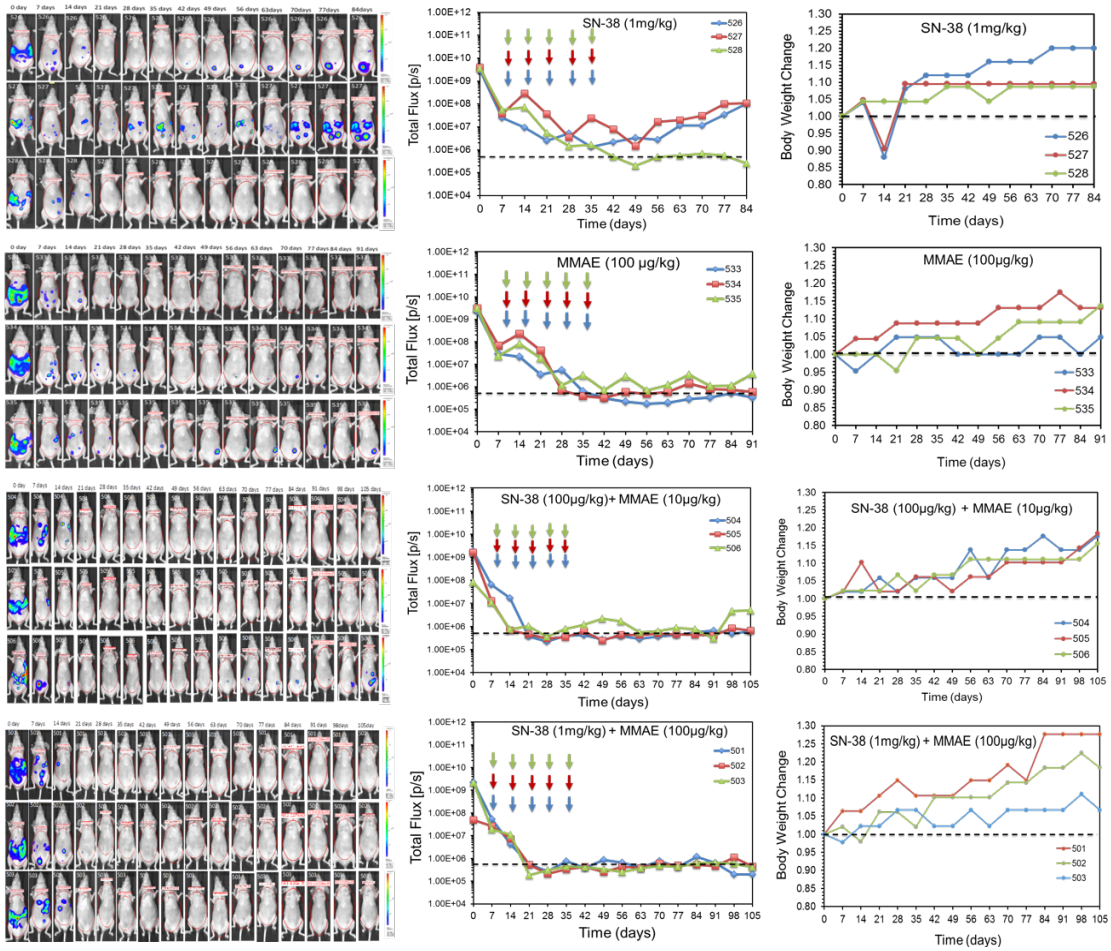

Figure 2.11: Evaluation of disease progression, recurrence and body weight change in the four treatment groups that responded to therapy. The dashed lines indicate the background mouse body bioluminescence which was determined to be 5×10^5. Arrows indicate the days that mice received the drug treatments (ie days 8, 15, 22, 29, and 36)

It is worth noting that the number of animals per group in this proof-of-principle study was set at three to examine merely the effectiveness of IP low-dose combination therapy with the two highly cytotoxic drugs (ie MMAE and SN-38). The exciting outcome of this study encourages further investigation of this approach using larger number of animals.

2.2.4 Evaluation of tissue toxicity

MMAE and SN-38 are both highly potent anticancer drugs that are too toxic for use in an untargeted setting. As a result, they are mainly used as antibody-drug conjugates (ADCs) for the treatment of variety of gynecologic malignancies including ovarian cancer [32, 33]. In fact, for most ADCs currently in clinical development, dose-limiting toxicities appear to be more closely associated with the anticancer drug and not related to the targeted antigen. Since the localized IP therapy with low-dose SN-38 (1 mg/kg) and MMAE (100 μg/kg) was effective and produced no visible signs of toxicity, we used histopathological methods on abdominal organs to investigate whether any toxicity occurred at the cellular level. The histopathological results did not reveal any notable toxicity to the abdominal tissues (Figure 2.12). In addition to evaluating histopathology, we monitored the mice in the MMAE-treated groups for signs of peripheral neuropathy, including extreme sensitivity to touch, lack of coordination and falling, muscle weakness or paralysis, and bowel/bladder problems. Overall, all mice that were treated with either ultra-low or low-dose MMAE did not show any signs of peripheral neuropathy, which is a common MMAE-associated toxicity [34]. These findings indicate that the proposed

regimen is not only effective but also tolerable to mice. The absence of serious toxicity to normal tissues could be attributed to the low-dose, localized administration of the drugs.

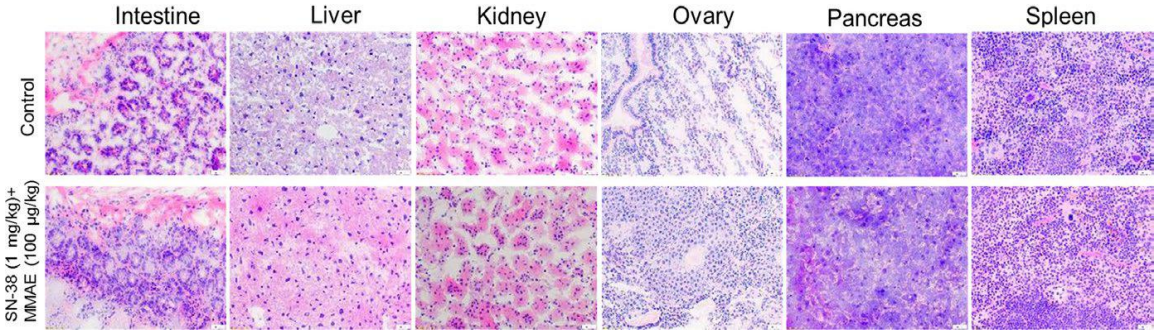

Figure 2.12: Hematoxylin and eosin (H& E) staining of dissected mouse organs. Cryosectioning was performed using a cryostat, followed by fixation and H&E staining. Photomicrography was conducted using a Leica microscope with a 20× objective

2.3 Conclusions

One of the most common causes of death in patients with primary or recurrent ovarian cancer is metastasis to the peritoneal cavity. The standard therapy for metastatic ovarian cancer at this stage is cytoreductive surgery (CRS) of macroscopic disease, followed by IV and IP administration of anticancer drugs such as cisplatin or carboplatin in combination with paclitaxel. The addition of IP chemotherapy to a regimen of CRS and IV chemotherapy could delay cancer relapse in patients with very small residual tumors following surgery. However, IP chemotherapy has not been routinely used, mainly due to increased toxicity and potential complications. Our data show that IP administration of low-dose MMAE and SN-38 could effectively eliminate CSC-rich ascites from the peritoneal cavity without inducing any significant toxicity. While MMAE and SN-38 are not administered as free drugs due to their high potency and potential for systemic toxicity, our low-dose localized therapy approach effectively restricted the cytotoxic effects to the tumor cells in the peritoneal cavity. Consequently, maximum efficacy with minimal adverse effects was achieved. Considering that the OVASC-1 cells showed resistance to therapy with cisplatin and paclitaxel but responded remarkably to combination therapy with MMAE and SN-38, this study could represent a new approach for treating metastatic ovarian cancer without the need for IV chemotherapy. Further investigation into this approach could facilitate translation of this therapeutic regimen into the clinic either as first-line therapy or in cases of acquired resistance to cisplatin and paclitaxel.

Chapter 3

Enzyme/Prodrug Systems and Delivery Methods for Cancer Gene Therapy[2]

[2] A version of this chapter has been published in Current Pharmacology Reports, PMID: 28042530.

In recent years, cancer treatment methods are becoming more focused on targeted approaches in order to maximize treatment efficacy while reducing side effects. One of these targeted approaches is termed suicide gene therapy; also known as, gene directed enzyme prodrug therapy (GDEPT). The success of suicide gene therapy is dependent on its three major functional components; enzyme, prodrug and gene delivery system (vector).

The function of the vector is to carry the gene that encodes an enzyme to the target cancer cells for expression. In general, gene delivery systems can be divided into two major groups including viral (e.g., adenovirus, lentivirus, etc.) and non-viral (e.g., synthetic polymers and lipids, bacteria-based and cell-based) (Table 3.1). Each vector type comes with a series of advantages and disadvantages. For more information related to the use of vectors for cancer gene therapy, we invite the readers refer to excellent recent reviews by Forbes [35], Cattaneo [36], and Mohit et al. [37].

Table 3.1 : Classification of the vectors used in suicide gene therapy of cancer.

Vector Type	Vector Subtype	Advantages	Disadvantages	References
Viral vectors	Retrovirus/Lentivirus	Long-term transgene expression, Integrates the gene into host genome, Low immunogenicity.	Safety concerns (insertional mutagenesis).	[38-40]
	Adenovirus	Effect on dividing and non-dividing cells, Lower risk of host genome integration.	Safety concern (high immunogenicity), Transient transgene expression.	[41-43]
	Adeno-associated virus	Medium to high transgene expression, Effect on dividing and non-dividing cells, No significant immunogenicity.	Low DNA loading capacity, Safety concerns (possibility of insertional mutagenesis).	[39, 44-46]
Non - viral vectors	Synthetic polymers and lipids	Ease of preparation, Lower cost, Lower immunogenicity.	Lower transfection efficiency.	[47-49]
	Amino acid-based vectors	Monodisperse and uniform constructs, ability to fine tune structure.	Lower transfection efficiency.	[50-52]
	Bacteria-based vectors	Large capacity for suicide enzyme loading, Bacterial minicells (BMCs) are non-infectious.	Safety concern (Infection by using live bacteria).	[53-55]
	Cell-based vectors	Tumor tropism, Self-isolated cells without the immunogenicity concerns	Low efficiency of tropism, High costs Safety concern (Unknown fate).	[56-58]

The function of the enzyme which is expressed by the transfected cancer cells is to convert the non-toxic/non-functional prodrug into its toxic (functional) form resulting in the death of the enzyme producing cancer cells as well as neighboring cells through a phenomenon known as bystander effect (Figure 3.1) [59, 60]. It is worth mentioning that the expression of the enzyme in transfected cells can be regulated by tumor-specific promoters. This regulatory element could enhance the enzyme/prodrug system's safety by restricting the enzyme expression only to the tumor cells. By applying the cancer-specific promoters, the suicide gene could get selectively expressed in cancer cells, while sparing normal ones. The promoter of human telomerase reverse transcriptase (hTERT) is one of the most widely used promoters in the field and is the only transcriptional control element that has successfully entered into clinical trials [61]. However, the problem associated with the use of hTERT promoter is its low expression activity. In order to enhance promoter's expression activity and also overcome the potential development of resistance by the tumor cells, several groups have tried to create more specific and efficacious ones. Recently, Rad 51, OPN, RAN, BRMS1 and MCM5 promoters were identified through screening of a large panel of normal and cancer cells and interestingly some of them showed significantly higher activity than hTERT promoter [62-64]. Another means of improving promoter activity is to artificially design a chimeric promoter. For example, a promoter with a stronger activity can be obtained by constructing the chimeric promoters with the fusion of two promoters [65] or various transcriptional regulatory elements [66, 67].

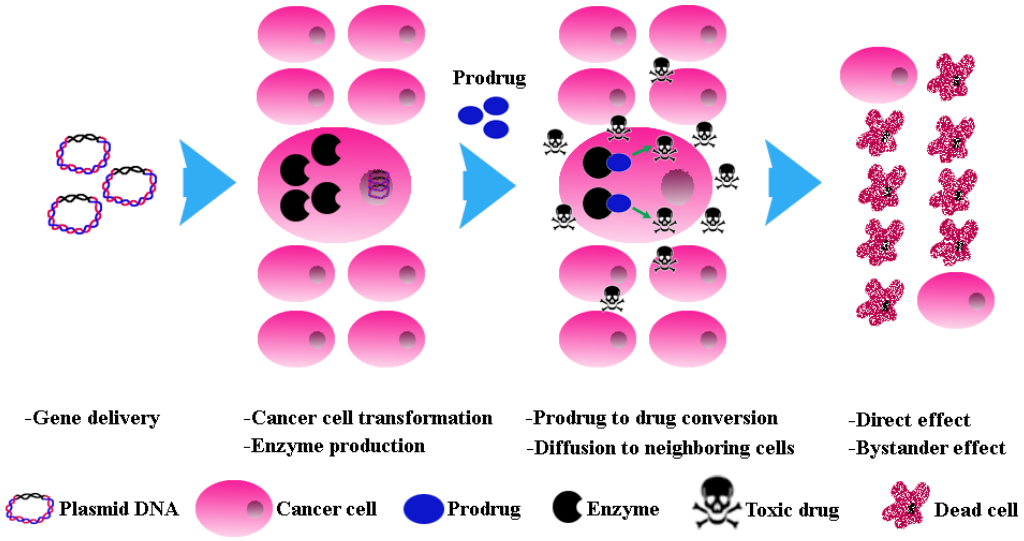

Figure 3.1: Schematic diagram of GDEPT systems: Nontoxic prodrug will be converted to its active form by the enzyme that has been coded with the new delivered DNA construct. The toxic drug will cause its host cell death directly and also will kill other cells through bystander effect.

In the following sections, we provide an overview of the eight most widely investigated enzyme/prodrug systems which are shown to be effective in inducing tumor cell death and inhibiting cancer progression. The purpose of this concise mini-review is to discuss the forte and weaknesses associated with the efficacy and safety of each system. Therefore, the coverage of the literature in this review is not encyclopedic; rather, selected examples have been chosen to highlight certain important points.

3.1 Enzyme/prodrug systems

3.1.1 Herpes simplex virus thymidine kinase (HSV-Tk)/ganciclovir

In this system, gancyclovir (GCV) undergoes a mono phosphorylation step by herpes simplex virus thymidine kinase (HSV-TK) enzyme. After the first phosphorylation step, the triphosphate form of the GCV is produced with the help of endogenous kinase (Figure 2.2 a). In this form, the GCV-triphosphate can cause apoptosis by introducing chain termination and single-strand breaks into DNA [68]. One limitation of using GCV-triphosphate as anticancer agent is that it could only affect the dividing cells [69-72]. The second drawback of this system is that the GCV-triphosphate transportation to surrounding cells is limited by the presence of gap junctional intercellular communications. Recently, Wu et al., showed that the bystander effect of the GCV-triphosphate can be enhanced by the expression of connexin32 (Cx32), that is responsible for producing gap junctions [73]. Furthermore, HSV-TK has a high affinity towards its natural substrate, thymidine, which leads to the need for using a high dose of GCV in order to win the competition [74]. This

higher GCV dose could result in suppression of immune system and damage to bone marrow cells [75]. The enhanced activity of ATP binding cassette (ABC) transporters in cancer resistant cells is one of the main reasons of therapy resistance in cancer [76]. Therefore, ABCG2-mediated efflux of GCV in side population cells can limit the efficiency of this enzyme/prodrug system [77].

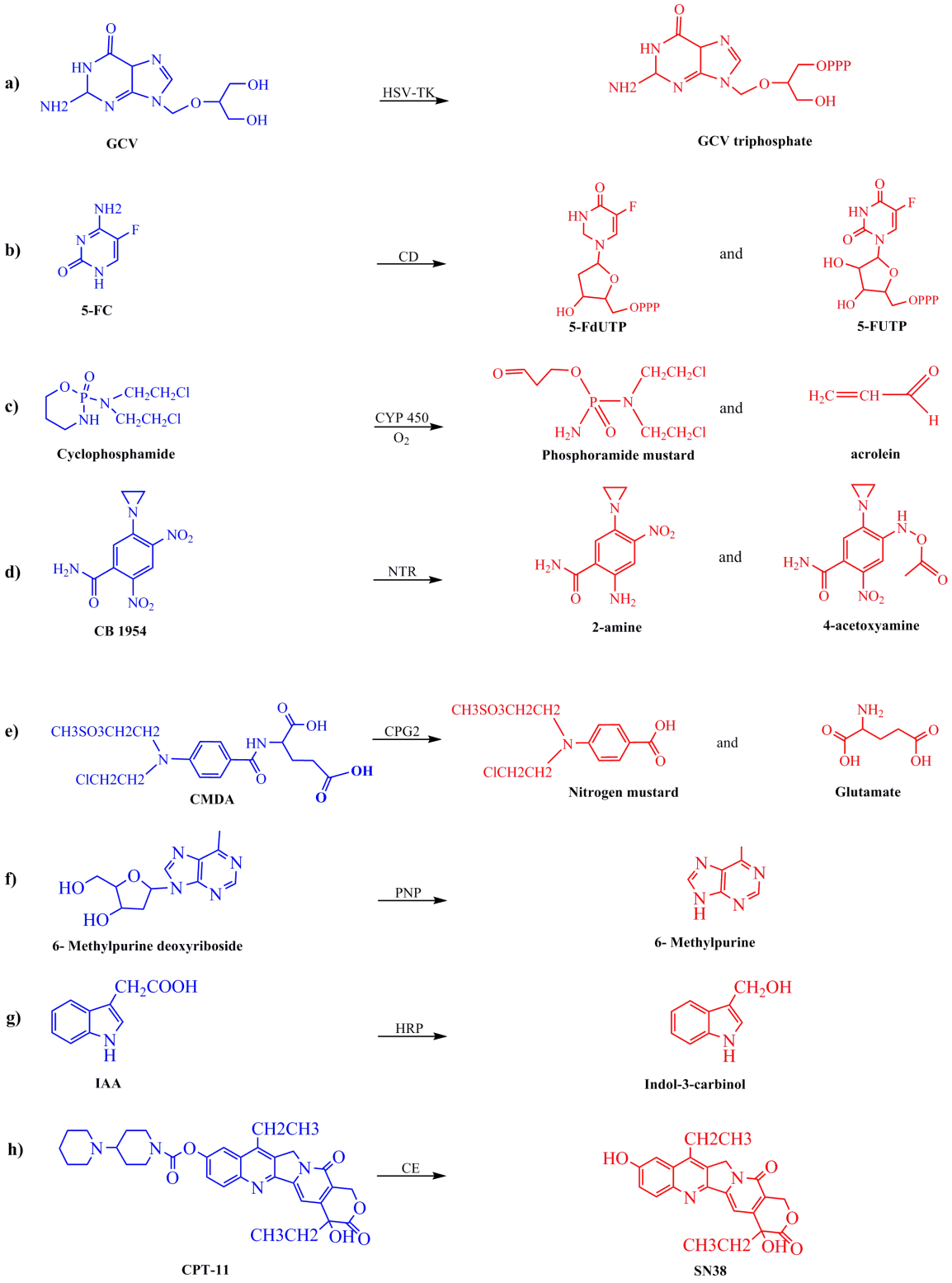

Figure 3.2: Structure of prodrug and drug of eight different GDEPT systems: After activation by enzyme, each prodrug will be converted to its active form which with different mechanisms will cause cell apoptosis and death.

In the past decades several attempts have been made in order to improve the efficiency of TK/GCV system. In one approach, modifications of enzyme active sites have resulted in generation of mutated forms of the enzyme; such as, mutant 30 (L159I/I160L/F161A/A168Y/L169F), SR39 (L159I/I160F/F161L/A168F/L169M) [75, 78], A168H, and a mutated form of A168H (TK007) [79]. All these mutants have shown enhanced enzyme affinity towards GCV in comparison to wild-type. In a different approach, an MDR-1 targeted small hairpin RNA (shRNA) was used to inhibit the ABC transporters which led to the accumulation and increase in drugs effect [80]. Other groups have also examined the use of other drugs such as Acyclovir and Valacyclovir instead of GCV and have observed more efficacy [81, 82].

TK/GCV system has also been used in combination with other therapeutic modalities in order to enhance its anticancer efficacy. For example, TK/Valacyclovir in combination with surgery and accelerated radiation showed an increase in patient survival rates in malignant glioma patients [83]. This approach have also shown to not only increase the efficacy of the treatment but also decrease the toxicity in pancreatic adenocarcinoma [70]. Currently, there are a few clinical trials in progress for patients with high risk acute leukemia (NCT00914628) and in patients with recurrent prostate cancer (NCT01913106) (www.clinicaltrials.gov).

3.1.2 Cytosine deaminases (CD)/ 5-fluorocytosine

In this system, 5-fluorocytosine (5-FC) that is a non-toxic prodrug is converted to its active form, 5-fluorouracil (5-FU), by CD activity (Figure 2.2b) [84]. Although 5-FU

has been used for cancer chemotherapy, but at its therapeutic dose it causes significant side effects such as mucositis, myelosuppression, dermatitis, and cardiac toxicity. Due to these side effects, its application as prodrug in the form of 5-FC and in combination with cytodeaminase enzyme has gained momentum in the past decades. Two forms of cytosine deaminase, bacteria (bCD) and yeast (yCD) have been investigated in the context of cancer therapy. After activation by CD, 5-FU can be further changed into potent pyrimidine antimetabolites by other cellular enzymes. 5-FU can inhibit thymidylate synthase which consequently leads to the cell cycle arrest and apoptosis. Since 5-FU traverse into the neighboring cells independent of gap junctions and even can pass the blood brain barrier by diffusion, it induces a significant bystander effect [85, 86]. Because of its unique properties, CD/5-FC system has been used for the treatment of different types of cancer, such as colon carcinoma, glioma and pancreatic cancer [87-89]. Having been combined with radiotherapy, CD/5-FC has shown quite a promising result due to the radio-sensitizing effect of 5-FU on the treated cells [90]. In comparison to HSV-TK/GCV, CD/5-FC has shown better results in renal and colorectal carcinoma probably due to its more potent bystander effect [91, 92].

Although use of CD/5-FC system has several strengths as mentioned above, but there are some drawbacks that yet need to be addressed. The first drawback is due to the presence of normal flora in the gut which is able to convert 5-FC to 5-FU resulting in side effects. Several groups have worked to create bCD mutants in order to improve its kinetic showing promising results [87, 88, 93]. Yeast cytosine deaminase is another form of the enzyme which provides a few advantages over bCD including high affinity and better prodrug conversion kinetics. In addition, yCD can be fused with E. coli uracil

phosphoribosyl transferase (UPRT) which is absent in mammalian cells. UPRT can directly convert 5-FU to 5-FdUMP [94] resulting in significant improvement of activity and enhanced cancer cell killing efficiency in prostate, ovarian, colon, and breast cancers [95, 96]. Some studies have also shown that yCD:UPRT/5-FC system may not get affected by acquired 5-FU resistance and could potentially kill both proliferating and non-proliferating cancer cells [96, 97].

While past clinical trials with CD/5-FC system alone have reported limited success [25], there are several new clinical trials in progress which could produce interesting outcomes. For instance in one trial, genetically-modified neural stem cells expressing bCD are used in combination with orally administered 5-FC for the treatment of recurrent gliomas (NCT01172964). In another phase I – II study, an investigational drug APS001F is currently being examined in combination with a recombinant bacteria (bifidobacterium longum) which can produce CD (NCT01562626). Finally, there is a phase I study in progress for the treatment of grade III/IV gliomas by using retroviral replicating vector (Toca 511) in combination with 5-FC (NCT01470794). The results of these ongoing trials are not reported yet but can be followed at www.clinicaltrials.gov.

3.1.3 Cytochrome P450 (CYP450) / oxazaphosphorine

Cytochrome P450 (CYP) enzymes are important factors in xenobiotics metabolism as they are responsible for deactivation of the toxic drugs in the liver. It has also been shown that these enzymes play an important role as an activating factor for oxazaphosphorine agents [98]. Oxazaphosphorine is a class of anticancer drugs that

includes cyclophosphamide (CPA) and ifosfamide (IFA). Both of these two akylating agents are the substrates of P450 enzymes which metabolizes these compounds to yield a 4-hydroxy derivative. Then, the resulting metabolites continue their chemical reaction to produce phosphoramide or ifosphoramide mustard and acrolein (Figure 2.2 c). Ultimately, they form DNA cross-links and kill the cells. The resulted active reagents can be transported to the surrounding cells, independent of gap junctions, which gives them potent bystander effect [99]. Another advantage of this system in comparison to the other enzyme/prodrug systems is its less immunogenicity due to the presence of P450 enzymes in human body [57].

One major drawback of this system is the natural metabolism of these prodrugs by the liver P450 enzymes that generates active toxic metabolites in the whole body and eventually causes various side effects, including cardiotoxicity, bone marrow suppression, neurotoxicity and nephrotoxicity. Some of these toxicities can be associated with the chloroacetaldehyde formation from CPA and IFA via N-dechloroethylation [100]. Therefore, the big challenge in this system is the inhibition of P450 enzyme activity in the liver so that the prodrug get activated only in the tumor sites [101].

A few methods have been used to improve the cancer treatment efficacy of P450 GDEPT and to reduce its side effects. In one approach, combined or in parallel with CYP450/oxazaphosphorine treatment, anti-thyroid drugs, such as propylthiouracil and methimazole were used to inhibit hepatic P450 reductase activity and improve the prodrug activation in tumor cells [102]. In another approach, a CYP2B6/RED fusion protein was designed so that it can transfer electrons from NADPH to the heme moiety of the protein.

This modification increases the efficiency of CYP2B6 substrates metabolism into active drugs [103].

In a phase I/II clinical trial, a recombinant retroviral vector that contains human CYP450 type 2B6 genes (CYP2B6), neomycin resistance marker gene and Ecoli *lacZ* has been tested. In this study, gene-based delivery of CYP2B6 to the tumor site led to prodrug activation locally, and produced higher concentrations of the active drug at the target site. The promising results of this study inspired the use of this approach in other cancer treatment studies [40]. However, regardless of the exciting results, there are still serious concerns about using this system for cancer therapy because of normal activity of CYP450 in human cells and difficulty in the delivery of the GDEPT elements to the targeted cancer cells without causing side effects on normal healthy cells [104, 105].

3.1.4 Nitroreductase/CB1954

This enzyme/prodrug system contains group of nitroreductase (NTR) enzymes that can activate prodrugs, such as CB1954 (5-(aziridin-1-yl)-2,4-dinitro-benzamide) (Figure 2.2 d). Two classes of enzymes and four types of prodrugs have been studied in this system. The two classes of enzymes are categorized based on their sensitivity to oxygen. Type I NTR can produce nitroso, hydroxylamine and/or amine terminated products in the presence of molecular oxygen, while type II, on the other hand, can only produce these products when oxygen is absent [106]. The four classes of prodrugs include dinitroaziridinyl benzamides, dinitrobenzamide mustards, 4-nitrobenzyl carbamates, and nitroindolines. CB1954 which is the most widely used prodrug is from dinitrobenzamide group [107]. The

metabolites of this prodrug can freely diffuse to the surrounding cells which induce a strong bystander effect. They can damage DNA by their chelating property leading to p53 and cell cycle independent apoptosis in both dividing and non-dividing cells. This is an important advantage of the system over the ones that can only target the dividing cells [108]. While several studies have reported promising results, but the low activation rate of CB1954 is one major limitation associated with this enzyme/prodrug system. At least two general approaches have been tested to improve the efficacy of this system. One is the engineering and application of alternative CB1954-activating nitroreductases, such as AzoR, NFsA, NemA, and flavin reductase I (FRase I) [109, 110]. The other approach is the synthesis of other nitroreductase prodrugs such as nitro-CBI-DEI and PR-104A [111, 112]. Both approaches have shown promising results *in vitro* and *in vivo*. Effective use of this enzyme/prodrug system has been demonstrated in a few clinical trials for the treatment of prostate and liver cancers [113]. However, the CB1954 low conversion rates, and dose-dependent hepatotoxicity are remained as major challenges for clinical application of this GDEPT method [114, 115]. For additional and more in depth information related to the nitroreductase/CB1954 system, readers are referred to an excellent review by [106].

3.1.5 Carboxypeptidase G2/nitrogen mustard

The enzyme carboxypeptidase G2 (CPG2) is derived from the Pseudomonas strain RS-16 and has no human analogue. This enzyme cleaves glutamic acid from nitrogen mustard-based drugs, such as 4-[(2-chloroethyl)(2-mesyloxyethyl)amino]benzoyl-L-glutamic acid (CMDA) and bis-iodo phenol mustard (ZD2767P), into DNA alkylating

agents, without any further modification (Figure 2.2 e). The resulted active drug can cause inter- and intra-strand DNA cross linking, leading to apoptosis in both dividing and non-dividing cells. It can also freely diffuse through cell membranes independent of gap junctions which offers potent bystander effect. Being independent from host enzymes for prodrug activation, gifts this system an outstanding benefit of a higher prodrug conversion rate, in comparison to the other enzyme/prodrug systems [116]. While different nitrogen mustard reagents have been developed and tested in the past two decades, CMDA (4-[(2-chloroethyl)(2-mesyloxyethyl)amino]benzoyl-l-glutamicacid) is among the first successful ones. Several attempts have been made to increase the potency of CMDA. For example, ZD2767P is 300-times more potent than CMDA [117].

To increase the enzyme efficiency, a mutated form of the CPG2 gene was fused to vascular endothelial growth factor (VEGF). This modification resulted in binding of secreted CPG2 to the VEGF-receptor, which kept CMDA around tumor mass and significantly reduced systemic side effects [118]. This enzyme prodrug system was used in attachment with tumor-specific antibodies in different clinical studies. However, some issues like, immunogenicity against mouse antibodies and CPG2 and also insufficient localization of enzyme\antibody conjugate, limited its success in cancer therapy [117, 119, 120].

3.1.6 Purine nucleoside phosphorylase/6-methylpurine deoxyriboside (PNP/MEP)

In this system, prodrugs such as 6-methylpurine 2-deoxyriboside and fludarabine can be converted to 2-deoxyribose-1-phosphate by the *E. coli* purine nucleoside

phosphorylase (PNP) (Figure 2.2 f). The advantage of using PNP/MEP is its high bystander activity based on gap junction-free transport of activated drugs, its effect on both proliferating and non-proliferating cells and its unique mechanism of action that is independent of DNA synthesis. PNP catalyzes the cleavage in glycoside bond of (deoxy) adenosine-based substrates that produces either (MeP) or 2-fluoroadenine (F-Ade). Then, these substrates are converted to their triphosphate forms by cellular mono- and diphosphate kinases, which can inhibit both RNA and protein syntheses [24, 121]. Three studied prodrugs of this system are 6-methylpurine-2′-deoxyriboside (MeP-dR), 2-F-2′-deoxyadenosine (F-dAdo) and arabinofuranosyl-2-F-adenine monophosphate (F-araAMP). Among them, F-araAMP is clinically approved for chronic lymphocytic leukemia treatment [122]. These (deoxy) adenosine-based analogs are only the substrates of *E. coli* PNP and cannot be recognized by humane PNP. Thus, the prodrugs cannot be converted into toxic metabolites in normal tissues and consequently limits the off-target toxicities. However, the application of bacterial PNP can induce host immune response. A few groups have worked on the development of human PNP that can consume the (deoxy) adenosine-based prodrugs as its substrate [123, 124]. Among the recorded clinical trials, there is only one completed phase I clinical trial using this system. In this trial, the safety of E. coli PNP/fludarabine phosphate in patients with head and neck cancers has been studied. It was shown that localized production of fluoroadenine within tumor tissues, using fludarabine and E. coli PNP system is successful in eradicating tumors without causing any significant toxicity [125].

3.1.7 Horseradish peroxidase/indole-3-acetic acid (HRP/IAA)

This system consists of the horseradish peroxidase (HRP) enzyme and indole-3-acetic acid (IAA) as the prodrug. HRP enzyme oxidizes IAA at neutral pH to its cationic form that produces the carbon centered skatolyl radical. This radical can be changed to peroxyl radical in the presence of oxygen which would turn into byproducts, such as indole-3-carbinol, oxindole-3-carbinol and 3-methylene-2-oxindole (Figure 2.2 g). These reactive byproducts can induce DNA strand breaks, leading to apoptosis and cell death. This system also has a potent bystander effect because of the transportation of the activated drug via diffusion to the untransfected neighboring cells [66]. HRP/IAA system has been tested in several *in vitro and in vivo* models, including bladder, melanoma, and pancreatic cancer [126-128]. However, the major concern of using HRP/IAA system is the low expression level of the enzyme in transfected cells [129, 130]. The second drawback of this system is the origin of the enzyme which comes from plants, because it results in undefined mixture of isoenzyme with different glycosylation patterns which can cause side effect in body. To avoid this problem, different recombinant forms of HRP isoenzymes are produced, which have shown significant effects on breast and bladder carcinoma [131]. Although some promising results have been obtained from HRP/IAA system, there has been no clinical trial with this system by the time of writing this manuscript (www.clinicaltrials.gov).

3.1.8 Carboxylesterase/irinotecan (CE/Irinotecan)

Carboxylesterases are active endogenous enzymes in human body that play roles in hydrolysis of different ester and amide containing chemicals [132]. Because of this property, they can convert Irinotecan (CPT-11), a less cytotoxic agent, into its highly toxic

form, SN-38 (Figure 2.2 h). SN-38 inhibits topoisomerase I and thus alters the DNA relaxation machinery [132, 133]. This enzyme/prodrug system has been used for the treatment of colorectal cancer [134], glioma [135] and various other tumor models [136-138]. While this enzyme has different isoforms, carboxylesterase-1(CE1) which is mostly localized in the liver is the most widely used one. Unfortunately, CE1 suffers from the low catalytic efficiency that limits the conversion rate of CPT-11 to SN-38. To overcome this deficiency, another isoform of this enzyme also known as CE2 has been studied. CE2 isoform is commonly expressed in intestine. CE2 has a higher catalytic efficiency than CE1 [139, 140] and has been used for the treatment of pancreatic and colon cancer [141, 142]. The rabbit analogue of CE1(rCE1) has also been engineered and used for conversion of CPT-11 to SN-38. While this isoform has shown a higher catalytic efficiency in comparison to human CE1 [143], but it can cause immune response in human host. To avoid this problem, mutant CE1 (hCE1m6) was engineered using homology alignment of human and rabbit version of CE1 followed by replacing eight amino acids in human CE1. This change in sequence resulted in higher conversion efficiency [144].

Given that SN-38 has poor water solubility, its bystander activity may get reduced [145]. In an attempt to improve the bystander effect and/or overall anticancer efficacy, secretory form of CE2 has been genetically engineered [141]. This approach has shown promising success in several preclinical models [146, 147]. Currently, there are a few ongoing clinical trials using this enzyme/prodrug system. For instance, there is a phase I clinical trial in progress in which the patients with rrecurrent high-grade gliomas are undergoing treatment. Here, genetically modified neural stem cells which can express carboxylesterase are used in combination with irinotecan hydrochloride (NCT02192359).

3.2 Delivery Systems

The suicide gene could be transported into cells via two major categories of gene delivery systems: viral and non-viral vectors (Table 3.1). However, when those vectors are planning to be systemically administered, the concerns of the off-target and safety could be raised since all cells, including normal and healthy cells, can be transfected. Thus, the gene delivery system has to be carefully designed to assure the suicide gene solely or mainly expressed in the tumor. Furthermore, the gene delivery efficiency, vector cytotoxicity, immunogenicity, time and cost for preparation should also be closely considered when the whole system moves into the clinical practice.

3.2.1 Viral Vector

Multiple types of viral vectors have been evaluated for suicide gene delivery, such as retrovirus [148], adenovirus [149] and adeno-associated virus (AAV) [150]. Among them, the retrovirus [151] and adenovirus [152] that carrying the suicide genes have been pushed forward into the clinical trials. Retrovirus is capable of inserting the gene into the host genome and producing the long-term transgene expression. However, its application is limited by several restraints. For examples, the retroviral vector just can infect the dividing cells. Furthermore, the vector randomly integrates the gene into various sites of host genome, which could potentially induce multiple malignancy and immunodeficiency diseases [153, 154]. The adenoviral vectors allow transient transgene expression on both dividing and non-dividing cells. Meanwhile, this vector has lower risk of host genome

integration. However, the immunogenicity of adenoviral vector is one of their major issues [155]. AAV also can produce transient transgene expression on both dividing and non-dividing cells and there is no significant immunogenicity concern about it. But its DNA loading capacity (about 5000 base pairs) is the major limitation for its further application [45, 153].

Viral vectors can commonly infect a wide range of tissues. To reduce the off-targets effect, one direction under extensive investigation is looking into the naturally occurring viral strains or serotypes to find one with a specific tumor tropism. For examples, oncolytic virus [153, 156, 157], would preferably infect the tumor cells and finally lyse their host. Combining with GDEPT systems, the oncolytic virus are capable to induce more cancer cell killing effect [153, 158-160]. Another method to direct the vector tumor tropism is its conjugation with antibody or other functional tumor specific ligands [161-163], such as chimeric fibers [164, 165] and small peptide [166]. For example, AAV vectors equipping with ankyrin repeat proteins on capsids carrying herpes simplex virus-thymidine kinas and ganciclovir markedly reduced Her-2 positive SKOV-3 tumors model growth without causing lethal toxicity, but in control group, the conventional AAV vectors accumulated in liver tissue and caused death in animals [167].

3.2.2 Non-viral Vector

3.2.2.1 Chemically synthetic Vector

Chemically synthetic compounds, including cationic lipids and polymers and dendrimers, are of major types of non-viral vectors. These chemical vectors, generally,

have lower gene delivery efficiency than viral vectors, due to several barriers present in extra- and intra-cellular delivery pathway [168, 169].However, they are still competitive due to the ease of preparation, lower immunogenicity and minimum risk of infection. Cationic liposomes, as the suicide gene delivery system, have been moved forward into the phase I/II clinical trials [170]. Meanwhile, the cationic polymer polyethylenimine (PEI) have also been extensively studied due to its robust DNA compaction capacity. System coupling the PEI with piggyBac transposon delivering HSV-TK/ganciclovir resulted in 43.07% tumor volume reduction within ovarian cancer tumor xenograft model by only three rounds of gene/prodrug administration [171]. Nevertheless, the cytotoxicity of PEI still limits its clinical application [172, 173]. To reduce the PEI inherent toxicity, several strategies have been developed, including modifying the molecular structure [173], PEGylation [174] and enhancing the material biodegradability [175].

Cationic lipid and polymers attach to cells mainly based on electrostatic interactions between positive charged complex and negative charged cell membrane glycosaminoglycans [168]. Thus, all cells have the possibility to receive the delivered gene. There are two major paths to improve the system specificity. One direction is to enrich the vector concentration within the tumor site through the passive targeting. When the complexes are controllably engineered within a certain size (particularly in submicron size), they will accumulate in tumor site in a much larger amount than other normal tissues because of the blood vessel leakiness within the tumor environment. This property is termed as the enhanced permeability and retention (EPR) effect. Multiple nanomedicine systems were attempting to take advantage of this property to enrich the therapeutic within the tumor site [176].

However, the passive targeting via EPR effect could not reach to the maximum anchoring effect. Thus more and more researches have been focused on the other direction, the active targeting strategies. Similar to viral vectors, the tumor specific ligand or antibody can also be linked into the complex to augment tumor binding ability. Commonly, the binding objectives are various receptors that over-expressed on the tumor cell surfaces, such as the folate receptors [177], the epidermal growth factor receptors [178, 179] and and αβ-integrins [55]. By combining the passive and active targeting strategies, the off-target toxicity concerns could be highly reduced.

3.2.2.2 Biologically synthetic vector

Recombinant protein as a novel bio-synthetic vector seems appealing in the field, since the vector could be engineered to overcome the cell barriers in a single construct with a precise control in the molecular level. For example, our lab has developed a series of recombinant protein based gene delivery vectors and the studies have shown very promising results [51, 52, 179-181]. These biopolymers have only one single peptide, but containing multiple functional units to support systematic gene delivery. These functional unites are the DNA condensing unit to compact DNA into nano complex, the tumor targeted motif with a high affinity affibody to anchor cancer cells, the pH responsive fusogenic peptide to disrupt endosome membranes, and the nuclear localization signal to transport the complex into the nucleus[179]. The vector has shown excellent targeted effect to HER2 positive ovarian cancer cells. Furthermore, the therapeutic efficacy of vector carrying the TK/ganciclovir was extensively evaluated, both *in vitro* and *in vivo* [51]. It has

been shown that 80% of the SKOV-3 cancer cells could be killed with a single dose and significant tumor size reduction was evident by only two rounds of gene/pro-drug administrations.

3.2.2.3 Bacteria or bacteria derived vector

Bacteria or bacteria derived carriers has also been categorized as the non-viral vectors. Bacteria can naturally carry the plasmid and suicide enzyme. Meanwhile, some anaerobic bacteria prefer homing in the tumor site due to the hypoxic tumor environment [182]. Thus, combining both features together, these bacterial vectors have strong potential to serve as the appropriate vectors for GDEPT systems [183]. However, the safety concerns still exist, since these bacteria are alive and can potentially cause serious infection. Thus, another type of carriers, called bacterial minicells (BMCs), have been tried as an alternative strategy to solve the issue. BMCs are nano-sized cells (around 400 nm) and can be synthesized by restricting the polar site of cell fission [54]. The BMCs have all components within bacterial cytosol except chromosomes. Therefore, they cannot divide which makes them as non-infectious carriers. The BMCs can carry various cargos, including plasmids [184], siRNA/shRNAs [185], chemotherapeutics [185], cytotoxins [55] and suicide genes [186]. Meanwhile, they can also be conjugated with tumor-targeting ligands or antibodies [187]. Thus, the BMCs can take the advantage of both passive and active targeting strategies to precisely deliver the suicide gene to the tumor site.

3.2.2.4 Human cell derived vector

The mesenchymal stem cells (MSC) and monocytes/macrophages (Mo-Ma), based on their tumor tropism properties are excellent targeting carriers of genes and proteins to tumors. These cells preferably migrate to the inflammation sites and tumor regions. Moreover, using the patient self-isolated MSC and Mo-Ma avoids the immunogenicity issue. These cells can be engineered to carry suicide genes and then can be administered via intra-tumoral or systemic injection [58]. After migration to the tumor site, the suicide gene can be expressed as the proper enzyme which can convert the prodrug into the toxic drug in the tumor periphery and induce killing of tumor cells. One approach from this category has been approved for the human clinical trial, in which the MSCs or neural stem cells were used to deliver the CD gene to convert 5-FC to 5-FU selectively for treating glioma [188]. A similar approach has been utilized using Mo-Ma as cell-based delivery system for tumor targeting [189].

However, both of these two human cell-based carriers have faced several challenges. For example, the efficacy of tropism is not satisfactory and needs to be further improved. Some researches focused on overcoming the limitations by modification of the tumor microenvironment, or modification of MSC surface molecules for better adhesion and tumor infiltration [190]. Furthermore, enhancement of the MSCs infiltration can be achieved by irradiation of tumor or organ. The radiation could lead to the change of tumor cells in expression profile of chemokines and cytokines, which can help MSCs infiltrate and provide niche for their proliferation [190, 191]. The tropism of MSCs can also be influenced by the route of administration [192-194]. Therapeutic effect could be more obvious when MSCs were intratumorally or intravascularly injected [147, 193]. Moreover,

the infiltration of the engineered MSCs and macrophages to the site can be led by iron nanoparticles and magnetic field [195, 196].

Similar to the viral vectors, the safety concern also exists within cell-based gene delivery systems. Both MSCs and macrophages may have role in tumor growth and self-renewal properties, promoting tumors surviving for an extended time. Meanwhile, MSCs can also potentially be transformed into cancer cells. To solve the safety issues, the specific promoters, such as TetOn® system were applied to regulate the MSCs fate following that they accomplished the curing task at the target site. [189, 197]. When MSCs and macrophages are unnecessary, the promoter could be switched on to express the enzyme which can induce these cells self-destruction.

Overall, the safety and efficacy are the major concerns of GDEPT systems and thus it seems that the enhanced specificity of the gene delivery system can contribute to resolving both factors. Higher specificity can enrich the enzyme concentration within tumor, and therefore, a higher amount of prodrug can be converted on the desire site. Meanwhile, the specificity can reduce the off-target effect and the potential damage to other healthy tissues. Thus, the development and selection of a proper gene delivery system is critical to maximize GDEPT system therapeutic efficacy and safety. The pros and cons of using these gene delivery systems are also eloquently reviewed by several groups [183, 198, 199]and our group [58]. More information and details can be obtained from the above referred review literatures.

3.3 Tumor-specific promoters

Except using the cancer targeted gene delivery systems, the cancer specific expression can also be achieved by transcriptional control. By applying the cancer-specific promoters, the suicide gene will be selectively expressed in cancer cells, while sparing normal cells. The promoter of human telomerase reverse transcriptase (hTERT) is one of the most widely used promoter in the field, and is the only transcriptional control element that has successfully entered into clinical trials [61, 200]. However, the problem of hTERT promoter is that its activity is not yet enough satisfactory. In order to drive a high level of suicide gene expression, stronger promoters are required. Meanwhile, single promoter can easily develop tumor cell gene resistance due to the heterogeneity within cancer cell population. Therefore, plenty of studies were conducted to find out more specific and efficacious inherent promoters to expand the cancer-specific promoter library. Recently, the promoter of Rad 51[64], OPN [63], RAN, BRMS1, and MCM5 [201] were identified through a large panel of normal and cancer cells comparisons and fortunately some of them showed a significantly higher activity than hTERT promoter.

Another way to improve promoter activity is to artificially design a chimeric promoter. For example, a promoter with a stronger activity can be obtained by constructing the chimeric promoters with the fusion of two promoters [65] or various transcriptional regulatory elements [202, 203]. The major limitation of transcriptional targeting is that the suicide gene may be sequestered and silenced within normal cells by non-targeted transfection. However, this combined method with tumor targeting vectors which were mentioned earlier, can favorably mitigate the issue.

3.4 Conclusions

Significant amounts of preclinical work have been performed in the past two decades on gene directed enzyme prodrug therapy of cancer. Based on the preclinical data, numerous clinical trials have been performed. While substantial progress has been made, no cancer suicide gene therapy protocol has been approved for clinical use. Important issues that have yet to be addressed include development of effective vectors for efficient and targeted gene transfer to the tumor cells, design of prodrugs that can be efficiently converted into the active drugs with potent bystander effect and engineering enzymes with low immunogenicity and high affinity towards prodrugs. Overcoming these barriers may open new doors into effective eradication of many of yet incurable and stubborn cancers through GDEPT.

Chapter 4

Bioengineered Adipose-Derived Stem Cells for Targeted Enzyme-Prodrug Therapy of Ovarian Cancer Intraperitoneal Metastasis[3]

[3] A version of this chapter has been published in Journal of Control Release, PMID: 31499084.

The majority of the ovarian cancer patients do not experience symptoms in early stages of the disease and are diagnosed in late stages once cancer cells have leaked into the peritoneal cavity and metastasized into organs outside of the ovaries. The standard-of-care for such patients includes cytoreductive surgery followed by chemotherapy with platinum-based drugs (e.g., cisplatin or carboplatin) and paclitaxel (PTX) [204]. Unfortunately, approximately 90% of patients after suboptimal resection and 70% of patients after optimal cytoreduction go on to experience relapse within 18-24 months [8, 205]. While a standard therapeutic approach for these patients with drug- resistant recurrent disease has not been established, chemotherapy regimens using agents other than cisplatin/PTX such as topotecan [206], CPT-11 (irinotecan) [207], liposomal doxorubicin [208], etoposide [209], gemcitabine [210], and ifosfamide [211] have been employed yielding response rates of between 10% and 30%; however, no survival benefit has been observed [212]. The prognosis is even poorer for patients with recurrent metastatic disease who have unresectable tumors and who are not candidates for surgery. Therefore, the objective of this study was to develop a nonsurgical therapeutic approach that delivers complete response and survival benefits for patients with intraperitoneal metastasis of drug-resistant ovarian cancer.

In the past decades many studies have shown that drug-resistant ovarian cancer cells can be killed under in vitro conditions when exposed to high concentrations of anticancer drugs. Our group has also shown that cisplatin given at 100 μM and SN-38 at 100 nM concentrations can completely eradicate drug-resistant ovarian tumorspheres in the cell culture [213]. However, the main problem faced concerns the fact that such high effective drug doses cannot be easily delivered to tumors due to the resulting dose-limiting toxicity

to healthy tissues. If we could devise a means to simulate in vitro conditions in vivo, it would then be possible to effectively kill drug-sensitive and -resistant cancer cells and cure the disease. To achieve this goal, we took advantage of the inherent tumor tropism of mesenchymal stem cells (MSCs), which is driven by tumor-secreted cytokines [214]. We hypothesized that suicide gene expressing MSCs can actively migrate toward ovarian intraperitoneal tumors and convert prodrugs into their potent metabolites close to the tumor cells, resulting in their complete eradication. In turn, this should inhibit cancer relapse and reduce toxicity to normal tissues. To test the hypothesis, we obtained ascites-derived malignant cells from a patient with recurrent drug-resistant ovarian cancer (OVASC-1). The cells were characterized to identify factors contributing to their drug resistance. To treat OVASC-1 intraperitoneal tumors, ASCs were first genetically modified ex-vivo to express secretory human carboxylesterase-2 (shCE2) enzyme. They were then injected into mice peritoneal cavity to migrate toward OVASC-1 intraperitoneal tumors. Subsequently, CPT-11 (prodrug) was administered to be converted into its cytotoxic form (SN-38) by the secreted CE2. We utilized ASCs as enzyme delivery vehicles because these cells exhibit a high degree of inherent tropism toward ovarian tumors, thus helping us better direct the treatment to the tumors [215, 216]. The ASCs were also engineered to express nanoluciferase for cell tracking and quantitative therapy response analysis. The fate of ASCs after injection into the mice peritoneal cavity (distribution and localization) was studied by bioluminescent imaging (BLI), magnetic resonance imaging (MRI), and histopathology. The responses of tumors to therapy and the inhibition of relapse were studied by quantitative BLI and the survival benefit was measured. Toxicity to normal healthy tissues was studied by histopathology and hematology.

4.1 Materials and Methods

4.1.1 Cell culture

All cancer cell lines were authenticated by the University of Arizona Genetics Core Cell Authentication Services. A2780 (Sigma-Aldrich, MO, USA), cisplatin resistant A2780-Cis (Sigma-Aldrich), SKOV-3 (ATCC, VA, USA), and OVCAR-3 (ATCC) cell lines were purchased (Sigma-Aldrich, MO, USA) and cultured as per vendor's protocol. Ascites-derived epithelial ovarian cancer cells (de-identified) were obtained from the Biorepository Center of Rutgers-Cancer Institute of New Jersey. For simplicity, we named them OVASC-1 since they were originated from ovarian ascites. OVASC-1 cells were maintained in RPMI-1640 supplemented with 15% FBS and 2.5 μg/mL insulin. The media was changed every other day. ASC cell line (ASC52telo, hTERT immortalized adipose-derived mesenchymal stem cells) (ATCC) was cultured in ASC basal medium supplemented with Mesenchymal Stem Cell Growth Kit (ATCC) and 0.2 mg/mL G418 (Sigma-Aldrich). To inhibit bacterial growth, 1% Penicillin- streptomycin solution (Caisson Labs, UT, USA) was added to the culture media of all cell lines.

4.1.2 Measurement of the sensitivity of the ovarian cancer cells to anticancer drugs

To measure the sensitivity of the ovarian cancer cells to the anticancer drugs, they were seeded in 96-well plates at a density of 5×10^3 cells/well. After twenty-four hours, cells were treated with a range of drug concentrations and then incubated at 37°C for 72 hours. Next, WST-1 reagent (Sigma-Aldrich) was added to each well and incubated for 2 hours.

The absorbance of each well was measured at 440 nm. The viability of untreated cells was considered as 100% and from that, the viabilities of other samples were calculated. The data are presented as mean±SD (n=4).

4.1.3 Clonogenic assay

The long-term toxic effects of anticancer drugs were evaluated by clonogenic assay. Briefly, 5×10^2 cells were seeded in 12-well plates and allowed to grow for 3 days. Then, they were treated with anticancer drugs at different concentrations. After incubation for 14 days, cells were washed with PBS and stained with 0.1% crystal violet solution. The number of colonies containing ≥ 50 cells was counted with an inverted light microscope. The data are presented as mean±SD (n=3).

4.1.4 Limiting dilution assay

To determine the frequency of the colony forming cells in each cancer cell population, an in vitro limiting dilution assay (LDA) was performed. Ovarian cancer cells were serially diluted and then seeded in 96-well plates at different cell densities ranging from 1 to 500 cells/well (n=8). After incubation at 37 °C for 21 days, cells were washed twice with PBS and stained with 0.1% crystal violet solution (Sigma-Aldrich). The number of colonies containing ≥ 50 cells was counted with an inverted light microscope. Using the data, the frequency of the cancer initiating cells (CICs) in each ovarian cancer cell line was estimated

by ELDA online software (http://bioinf.wehi.edu.au/software/elda/index.html) as previously described [217].

4.1.5 ALDH activity assay

The activity of aldehyde dehydrogenase enzyme (ALDH) in ovarian cancer cells was evaluated by using ALDEFLUOR™ kit and protocol (Stem Cell Technologies, BC, Canada). Ovarian cancer cells were grown in T-75 flasks and one million cells were counted. Half a million cells were transferred into a microfuge tube and treated with diethylaminobenzaldehyde (DEAB) and ALDEFLUOR substrate. The same number of cells was counted and treated with ALDEFLUOR substrate only. Cells were incubated for 45 min at 37°C in the dark and then analyzed by Gallios Beckman Coulter Cytometer (Beckman Coulter, Inc., CA, USA). Gating was established using propidium iodide (PI) to exclude non-viable cells. ALDEFLUOR plus DEAB was used to determine the negative gates. Data analysis was conducted by using Kaluza® Flow Analysis software (Beckman Coulter, Inc.). The data are reported as mean±SD (n=3).

To measure the activity of ALDH enzyme in OVASC-1 and OVACR-3 cells that were treated with SN-38 and cisplatin, 1×10^6 cells were seeded in 6-well plates. After 24 hours, cells were treated with 1-100 μM of cisplatin or 1-100 nM of SN-38. After 72 hours of treatment, the ALDH enzymatic activity in the abovementioned cell lines was measured by ALDEFLUOR kit as explained.

4.1.6 Measurement of MDR1 and ABCG2 cell surface transporters

To determine the cell surface expression levels of MDR-1 and ABCG2 transporters, cells were seeded in 6-well plates and then incubated either with anti-MDR-1 primary (abcam, Cambridge, MA) (ab10333) and corresponding secondary antibody (ab150117), or anti-ABCG2 primary (ab207732) and secondary antibodies (ab150077). Flow cytometry analyses were performed on cells by using the Beckman Coulter Gallios flow cytometer. As negative controls, the staining procedure was performed by using IgG isotype controls (ab18413) and (ab172730) for MDR-1 and ABCG2, respectively. The duration of antibody treatment and concentration were based on the vendor's protocol. Data are reported as the percentage of cells expressing each protein. X-mean denotes the fold change in the fluorescent intensity of the test group in comparison to the corresponding IgG isotype. Data analysis was performed using Kaluza® Flow analysis software (Beckman Coulter, Inc).

4.1.7 Ovarian tumorsphere formation and characterization

OVASC-1 tumorspheres were generated and the stem cell biomarkers expressions (NANOG, SOX-2 and OCT-4) were measured by Real-Time PCR as described previously (11). Primer probe numbers were catalog# Hs02758991_g1 for human GAPDH; catalog# Hs04399610_g1 for NANOG; catalog# Hs04234836_s1 for SOX2 and catalog# AIKAMMD PN4331348 for OCT-4 (TaqMan® Gene Expression, Thermofischer scientific, MA, USA). All quantitative real-time PCR reactions were performed and analyzed using the StepOne Plus Real-Time PCR System (Applied Biosystems) with the

comparative ΔCt method. The relative expression of genes with respect to the housekeeping gene human GAPDH are presented as mean±SD (n=4).

4.1.8 Measurement of tumorsphere diameter and viability

To evaluate the effects of anticancer drug treatment on tumorspheres, OVASC-1 tumorspheres were generated, treated once either with 1-100 μM of cisplatin or 1-100 nM of SN-38, and then incubated for 14 days. The diameters of the tumorspheres were measured under an Olympus light microscope by using Infinity Analysis software. Data are presented as mean±s.d. (n=4). The viability of the cells in tumorspheres was determined by fluorescence microscopy after staining with 2.5 μM of Calcein AM (live cells) and 30 μM propidium iodide (dead cells) (Sigma-Aldrich) for 2 hours at 4°C.

4.1.9 Genetic engineering of ASCs

The genes encoding human carboxylesterase-2 (hCE2) and nanoluciferase (NanoLuc®, Promega, Madison, WI) were designed and then synthesized by VectorBuilder Inc. (Santa Clara, CA, USA) for mammalian cell expression using PiggyBac transposon system. The secretory form of human carboxylesterase-2 (shCE2) was generated by removing the ER retention signal (HTEL) from the non-secretory form (hCE2). This signal is encoded as 12 nucleotides (4 amino acids) located at the peptide's C-terminal. The ASCs were seeded in 6-well plates at the density of 3×10^5 cells/well and then cotransfected with the constructed transposon plasmid vectors along with helper plasmid encoding hyperactive PiggyBac

transposase system by using XFECT™ reagent (Takara Bio, Inc., CA, USA) following the manufacturer's protocol. Transfected ASCs were maintained in full media supplemented with 400 µg/ml Hygromycin B (Clontech, CA, USA) for 3-4 weeks to obtain the stable clones expressing carboxylesterase and nanoluciferase. The stable clones ASC-shCE2:nLuc (secretory) and ASC-hCE2:nLuc (non-secretory) were generated, expanded and stored under liquid nitrogen for further use.

4.1.10 Evaluation of the activity of the expressed human carboxylesterase-2

ASC-shCE2:nLuc cells were seeded in 24-well plates at the density of 2.5×10^4 cells/well in 500 µl of complete culture media. After 24 hours, 100 µL of the media was collected and incubated with 100 µl of fluorescein diacetate (FDA) (12 µM). The fluorescent signal of by-product (fluorescein) was measured for 30 min at 5 min intervals by using Tecan plate reader instrument (Tecan, Männedorf, Switzerland), excitation/emission set at 485/525. Culture media taken from ASC-hCE2:nLuc cells (non-secretory), culture media alone, and PBS were used as controls.

The ability of the secreted carboxylesterase from ASC-shCE2:nLuc cells to convert CPT-11 to SN-38 was examined by Liquid Chromatography-Mass Spectroscopy (LC/MS). For this purpose, ASC-shCE2:nLuc cells were seeded at the density of 2.5×10^4 cells/well in a 24-well plate with 500 µl of complete media. The next day, the culture media was removed from each well and treated once with 7.5 µM of CPT-11 and then incubated for 72 hours at 37^{o}C. Next, 100 µl of the treated media was mixed with 200 µl acetonitrile (Sigma-Aldrich) and analyzed by LC/MS at Biological Mass spectrometry core facility of

the Rutgers-Robert Wood Johnson Medical school.

4.1.11 In vitro evaluation of the cancer cell killing efficiency of suicide gene expressing ASCs

ASC-shCE2:nLuc cells were co-cultured with OVASC-1 cells at the density of 1000 and 2500 cells/well. After 24 hours, CPT-11 (1 μM) was added to the media and incubated for an additional 72 hours. A cell viability assay was performed by using WST-1 reagent as described above. OVASC-1 cells and ASC-shCE2:nLuc cells seeded separately were used as controls. The viability of ASC-shCE2:nLuc cells co-cultured with OVASC-1 cells but without any CPT-11 treatment was considered as 100% viable. The data are presented as mean±SD (n=4).

4.1.12 Evaluation of the ASC tropism toward peritoneal tumors by BLI, MRI, and histopathology

All animal studies were performed according to the guidelines of the Rutgers University Institutional Animal Care and Use Committee (IACUC) and all experiments conformed to all relevant regulatory standards. Outbred homozygous nude J:NU (Foxn1nu/Foxn1nu) female mice (5-6 weeks old) were purchased from the Jackson Laboratory (Bar Harbor, ME). OVASC-1 cells that stably expressed firefly luciferase gene (OVASC-1-fLuc) were created as described previously [213]. Five million OVASC-1-fLuc cells were suspended in 500 μL of D-PBS and injected intraperitoneally (IP) into nude mice

using a 25-gauge needle. The cancer cells were left to grow for three weeks to form peritoneal tumors. At this point, ten million ASC-shCE2:nLuc cells were injected IP. After 24 hours, mice were anesthetized by isoflurane and injected IP with 0.1 mg/kg of furimazine (Nano-Glo substrate) (Promega, WI, USA) and 150mg/kg of D-luciferin (GoldBio, MO, USA) dissolved in 100 µL sterile PBS. Mice were imaged to detect and measure bioluminescence signal intensity within 30 seconds of furimazine and five minutes of D-luciferin injections with acquisition times of 60 seconds. Bioluminescent images were captured using In Vivo MS FX PRO (Carestream Health, NY, USA) with 535nm filter (Acquisition time: 60 seconds) to eliminate spectral overlap. The fLuc substrate (D-luciferin) and nLuc substrate (furimazine) are enzyme specific and do not cross react. The results were analyzed using Bruker MI molecular imaging software, version 7.1.3.20550.

To examine the colocalization of the ASCs with the peritoneal tumors, magnetic resonance imaging (MRI) in conjunction with histopathology was used. OVASC-1 peritoneal tumors were implanted as mentioned above. Then, ASC-shCE2:nLuc cells were transfected with FluidMAG-D (150nm size) (Chemicell GmbH, Berlin, Germany) superparamagnetic iron oxide nanoparticles (SPION) to make ASC-shCE2:nLuc:SP cells. For that, 2×10^6 ASC-shCE2:nLuc cells were seeded in a 150 cm^2 tissue culture flask and treated with 162.5 µg/ml of FluidMAG-D for 24 hours. The ASC-shCE2:nLuc:SP cells were washed several times by PBS, harvested, and then injected (1×10^7 cells) into the peritoneal cavity of tumor-bearing mice. The tropism of ASC-shCE2:nLuc:SP cells toward the OVASC-1-fLuc peritoneal tumors was evaluated by 1Tesla ASPECT M2 MRI seven days post-injection at the Rutgers University Molecular Imaging Center. To determine the locations of the ASC-shCE2:nLuc:SP cells within the tumors, the mice were euthanized,

the intraperitoneal tumors extracted, washed with 0.9% saline solution, placed inside a Cryomold (Fisher Scientific) filled with Tissue-Plus™ O.C.T compound (Fisher Scientific), and then snap frozen by liquid nitrogen. The tumors were sliced and then stained by using Gomori Iron Prussian Blue Stain (Newcomer Supply, WI). Photomicrography was conducted using a Leica microscope (20X objective) and the slides were studied by a histopathologist at Biorepository and Histopathology Core Facility at Rutgers-CINJ.

4.1.13 Evaluation of therapy response, ovarian cancer relapse and survival rate in nude mice

Female nude mice were injected with five million of OVASC-1-fLuc cells to form intraperitoneal tumors as described above. Cancer cells were left to grow for 3 weeks to form tumors and the bioluminescence signal intensity reaches in the range of 1.0×10^8 to 1.0×10^9 (p/s) indicating presence of well-established tumors. Mice were then randomly divided into five groups of five and received treatments. Group 1 (G1) received vehicle only twice per week. The vehicle solution was composed of 1% cremophor:ethanol (50:50) and 99% saline (0.9%). Group 2 (G2) received cisplatin (5 mg/kg) and paclitaxel (15 mg/kg) dissolved in vehicle once per week. Group 3 (G3) received CPT-11 (40 mg/kg) twice per week (Thursdays and Saturdays) for ten weeks. Group 4 (G4) received CPT-11 (80 mg/kg) twice per week (Thursdays and Saturdays) for ten weeks. Group 5 (G5) received ten million ASC-shCE2:nLuc cells once a week (Mondays) and CPT-11 (40 mg/kg) twice per week (Thursdays and Saturdays) for ten weeks. In this protocol, the first

drug dose was administered 72 hours post ASC injection and there was a 48 hours lag in between the first and second CPT-11 injections. All drug and cell administrations were IP. To monitor disease progression and treatment effects, bioluminescence signal intensity was measured by using an IVIS Lumina III Imaging System (PerkinElmer, MA, USA) as previously described [213]. The acquired images were analyzed by the Living Image 4.5 module. To eliminate spectral overlap, the BLI of fLuc and nLuc were performed on different days (two days apart).

Observable indicators of health (i.e, diarrhea, appetite, posture, movement) and body weight were continuously monitored to detect any treatment-related toxicities or disease-related morbidities resulting from the ascitic burden. Loss of more than 10% body weight in one week or more than 20% at any time period was considered as the study end-point. When significant toxicity was observed, either the treatment was discontinued or mice were euthanized.

4.1.14 Tissue toxicity studies by hematology and histopathology

To evaluate the effects of treatment on mice blood factors, 50 µl blood samples were collected postmortem from mice in each group by cardiac puncture blood collection method and tested for hematologic parameters at the In Vivo Research Services of Rutgers University.

To determine the toxicity to normal tissues inside the peritoneal cavity after treatment, major intraperitoneal organs were removed immediately after the last treatment point. Cryosectioning was performed at the Biospecimen Repository and Histopathology Service

Core Facility at Rutgers-Cancer Institute of New Jersey followed by fixation and hematoxylin and eosin (H&E) staining. The slides were interpreted by a histopathologist at the Rutgers-Robert Wood Johnson University Hospital. Photomicrography was conducted using a Leica microscope (20X objective).

4.1.15 Statistical analysis

For in vitro studies, the experiments were repeated at least three times unless otherwise stated. Data are presented as mean ± SD (standard deviation). When two groups were compared, the statistical significance was determined by using Two-tailed Student's t-test. One-way analysis of variance (ANOVA) was used for multiple comparisons and Tukey's post hoc test was used for pairwise comparisons. Differences were considered statistically significant when p value was < 0.05.

4.2 Results

4.2.1 Assessment of the drug sensitivity and resistance of ovarian cancer cells

To assess the sensitivity of the OVASC-1 ovarian cancer cells to the prodrug metabolites, a cell viability assay and clonogenic assay were performed. While the cell viability assay measures acute toxicity, clonogenic assay measures the long-term effects of anti-cancer drugs (chronic toxicity) and evaluates all potential forms of cell death. In this experiment, 5-FU, 6-MP and SN-38 which are the toxic metabolites of prodrugs 5-FC, 6-

MPd, and CPT-11 were used [21, 25]. Cisplatin was also used as a point of reference since it is standard-of-care for ovarian cancer. For comparison purposes, established ovarian cancer cell lines OVCAR-3, SKOV-3, A2780, A2780-Cis were also investigated. The results of the cell viability assay showed that OVASC-1 cells were the most drug-resistant and SN-38 was the most potent cytotoxic drug of the ones tested (Table 4.1, Figure 4.1A-4.1D). The IC_{50} of SN-38 was in low nanomolar range whereas the IC_{50} of all other drugs fell within the micromolar range. Of the established cell lines, OVCAR-3 and A2780-Cis showed more resistance to the drugs than the others. The IC_{50} values of cisplatin for OVASC-1 and A2780-Cis were 19.75 μM and 15.69 μM, respectively. This shows that OVASC-1 was more resistant to cisplatin than A2780-Cis. The results of the colony formation assay also show that SN-38 best prevented the formation of new colonies within low nanomolar range (< 20 nM) (Figure 4.2). All other drugs (i.e., 5-FU, 6-MP and cisplatin) were able to prevent the formation of colonies at micromolar levels (> 10 μM).

To better understand the cause of the OVASC-1 cells' drug resistance, they were characterized with an Aldehyde dehydrogenase (ALDH) enzyme activity assay and limiting dilution assay (LDA). ALDH plays a vital role in cellular detoxification and is upregulated in drug-resistant cells [218]. Therefore, its measurement provides an insight into resistance to therapy. The results of this experiment showed that OVASC-1 cells had the highest percentage of $ALDH^+$ cells followed by OVCAR-3 (Figure 4.3A, Figure 4.4A) (*ANOVA, $p < .05$). In addition, an LDA was performed to determine the frequency of CICs, also known as CSCs, which are able to initiate new colonies [8, 9]. The LDA shows that OVASC-1 presented the highest number of CICs in its population (~5%, 1 in 20) followed by OVCAR-3 cells (~3%, 1 in 32) (Figure 4.3B, Figure 4.4B).

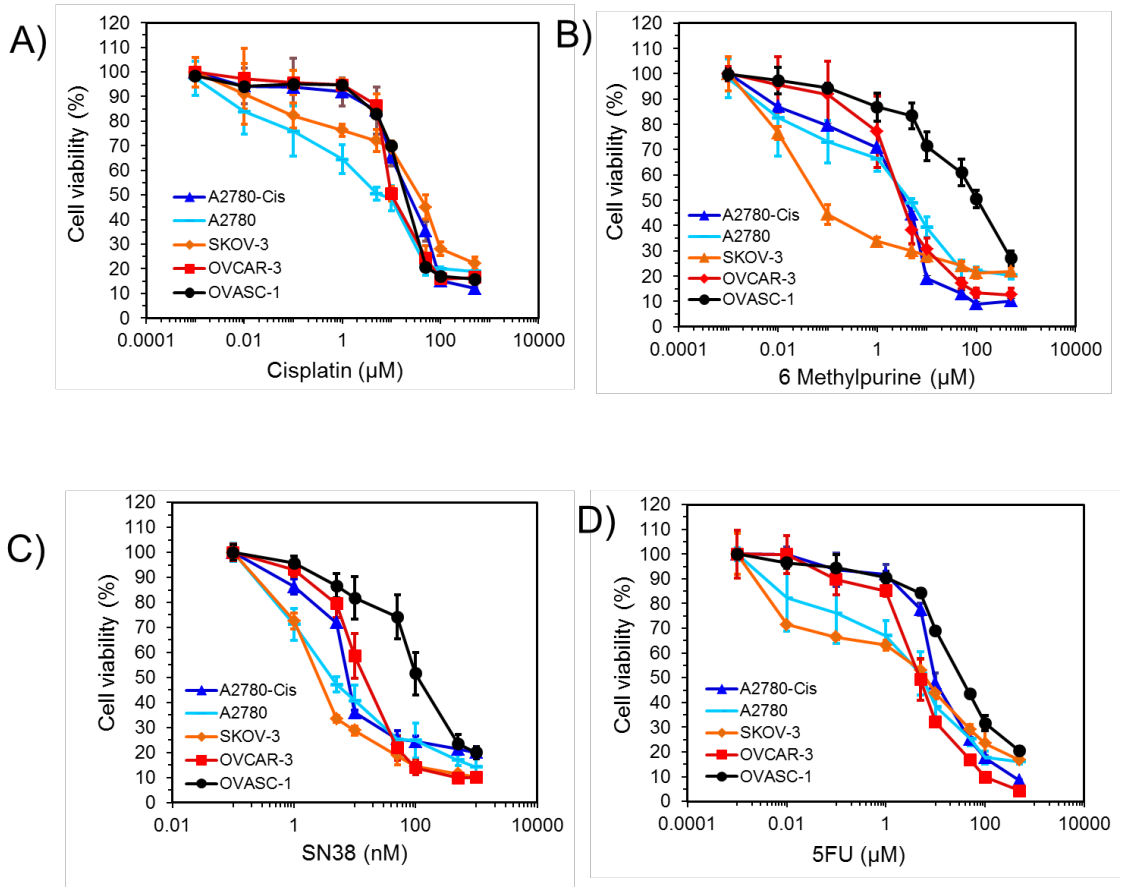

Figure 4.1: Evaluation of the cell viability by WST-1 cell toxicity assay. (Panels A-D) Ovarian cancer cells were exposed to different concentrations of the drugs and the viability of the cells was measured. The X-axis is plotted in Log scale. The data are reported as mean±SD (n=4).

Table 4.1: Determination of IC50 of anticancer drugs in different ovarian cancer cell lines based on the cell viability curves (Figure. 4.1). The data show that OVASC-1 is the most drug-resistant cell line and SN-38 the most potent anticancer drug among the ones tested.

Drug/Cell line	A2780	A2780-Cis	SKOV-3	OVCAR-3	OVASC-1
Cisplatin (μM)	1.1	15.69	9.1	11.78	19.75
6 Methylpurine (μM)	2.51	4.7	0.12	5.46	39.74
5 Fluorouracil (μM)	2.46	4.45	2.88	2.4	35.8
SN-38 (nM)	6.21	17.98	3.59	22.1	48.73

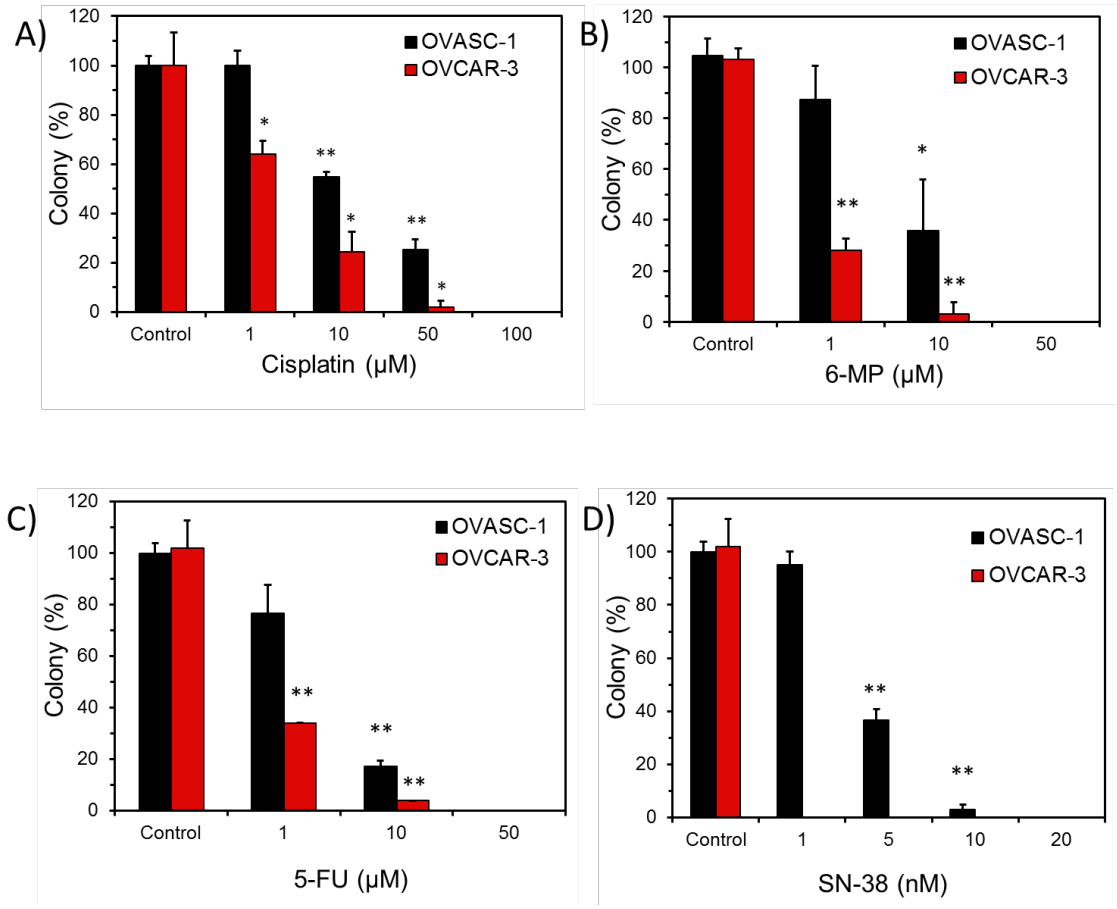

Figure 4.2: The measurement of drugs' chronic toxicities to OVCAR-3 and OVASC-1 cells by clonogenic assay. Ovarian cancer cells were exposed to different concentrations of the drugs and the number of colonies in each well was counted after 14 days. This figure shows that the OVASC-1 cells are the most drug-resistant cells and SN-38 is the most potent anticancer drug. The data are presented as mean±SD (n=3).*Statistical significance, t-test (p<0.05).

A)

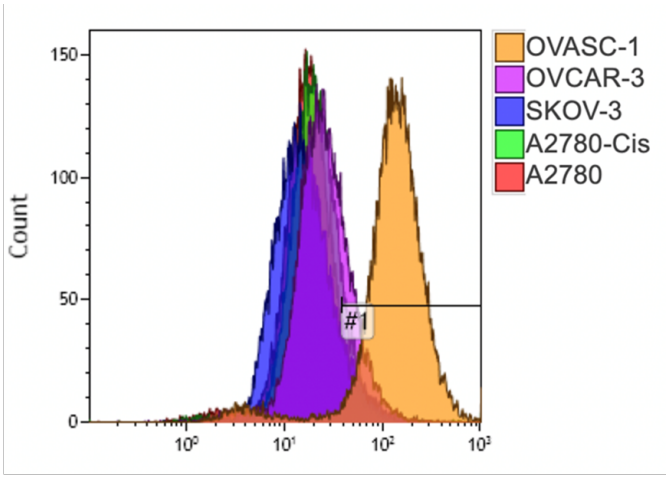

B)

0.95 Confidence interval
(1/colony forming cells frequency)

Cell line	Lower	Estimate	Upper
OVASC-1	31.7	20.3	13.1
OVCAR-3	49.4	31.7	20.3
A2780-CIS	73.4	47	30.2
SKOV-3	74.8	47.9	30.7
A2780	108	69.2	44.3

Figure 4.3: Flow cytometry histograms of the ALDH+ ovarian cancer cells and Estimation of the frequency of CICs in different ovarian cancer cell populations: A) Cells were treated with ALDHFLUOR substrate and the intensity of the fluorescent signal was detected by flow cytometry. This figure shows that OVASC-1 cells have the highest population of ALDH+ cells. B) The frequency of CICs in different ovarian cancer cell populations (0.95 Confidence Interval) was estimated by limiting dilution assay using ELDA online software (http://bioinf.wehi.edu.au/software/elda/index.html).

To examine whether SN-38 can kill the drug-resistant SP cells, we treated them with SN-38 and then measured the resulting change in the ALDH enzyme activity. We used cisplatin as a control drug for comparative purposes. The results of this study show that at low concentrations, both SN-38 and cisplatin first killed the sensitive cell population resulting in the enrichment of ALDH+ cells in the remaining population. Once the drug concentration surpassed a certain threshold (i.e., 10 nM for SN-38 and 10 μM for cisplatin), the drug started to kill the drug-resistant cells (Figure 4.4C-1D) (*t-test, $p<0.05$).

Since OVASC-1 cells showed resistance to all four drugs tested in this study, we looked at the expression of multi-drug resistance gene 1 (MDR-1) and ABCG2 transporters which are the common players in cancer cell adaptation to chemotherapy with cisplatin, SN-38, 5-FU and 6-MP [30, 213, 219]. The results of this experiment showed that ~48% of the OVASC-1 cells had an overexpression of MDR-1 and more than 93% of the population had overexpression of ABCG2 transporters (Figure 4.4E-4.4F, Figure 4.5-4.6).

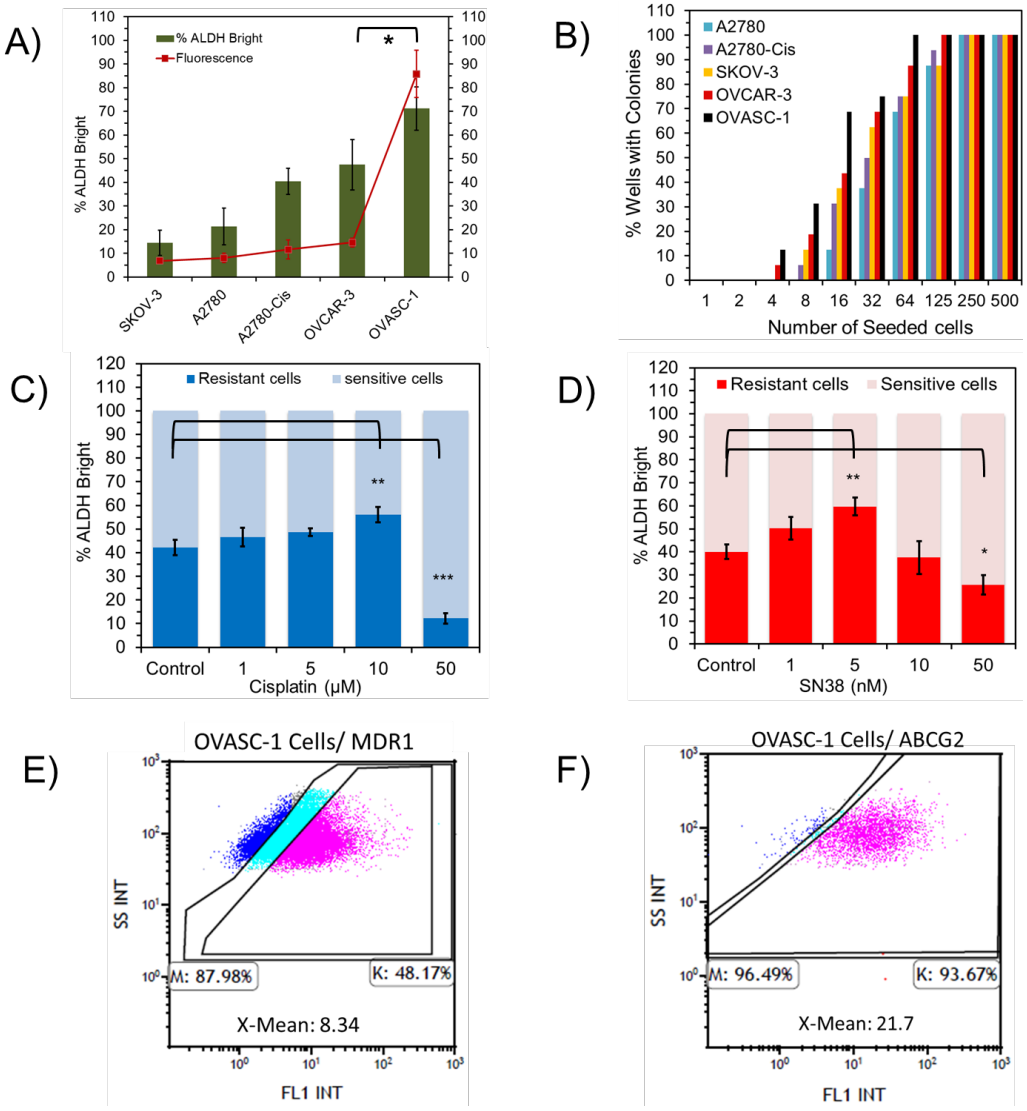

Figure 4.4: Assessment of the percentages of drug-resistant cells and CICs. A) Determination of the percentage of ALDH+ (bright) cells in the general population of ovarian cancer cells by ALDH assay. B) Measurement of the percentage of the CICs in each ovarian cancer cell population by Limiting Dilution Assay. For details of data analysis, please see Figure S3B. C-D) Change in the percentage of ALDH+ cells in OVASC-1 cells after treatment with cisplatin (1-50 μM) and SN-38 (1-50 nM). The total number of cells (sensitive and resistant) as measured by flow cytometry is normalized to 100%. E-F) The percentages of OVASC-1 cells that express MDR1 and ABCG2 transporters. X-mean denotes the fold difference in between the expression of the transporters on the surface of OVASC-1 cells stained by the anti-MDR1/anti-ABCG2 antibodies and by the IgG isotype control. This fold difference in X-Mean indicates the transporter density.

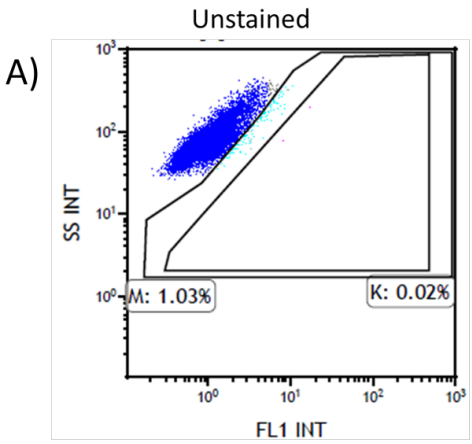

Gate	Number	%Total	%Gated	X-Mean	Y-Mean
All	11,832	93.3	100	1.24	87.06
M	122	0.96	1.03	4.43	132.36
K	2	0.02	0.02	12.82	133.77

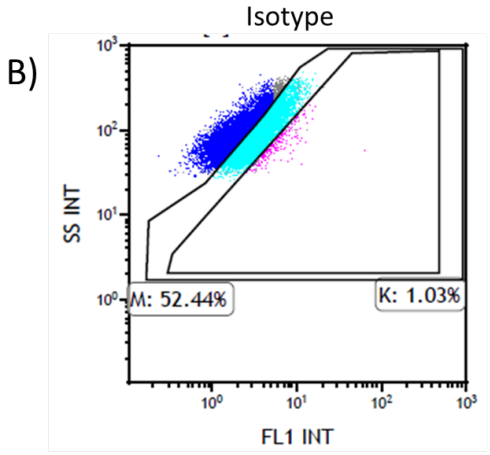

Gate	Number	%Total	%Gated	X-Mean	Y-Mean
All	26,703	93.39	100	2.97	92.87
M	14,003	48.97	52.44	3.72	88.72
K	274	0.96	1.03	6.65	74.68

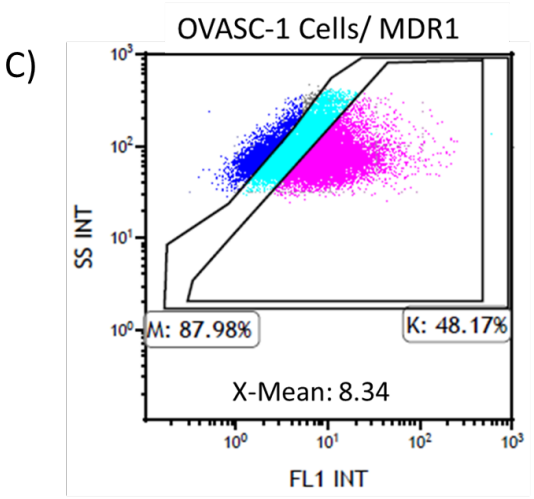

Gate	Number	%Total	%Gated	X-Mean	Y-Mean
All	26,717	93.27	100	8.34	92.05
M	23,506	82.06	87.98	9.11	90.55
K	12,870	44.93	48.17	12.42	76.51

Figure 4.5: Evaluation of the expression of MDR1 transporters on the surface of OVASC-1 cells. A-B) Unstained OVASC-1 cells and cells labeled with fluorescent IgG1 isotype (controls). C) OVASC-1 cells were labeled with fluorescent anti-MDR1 primary antibody and analyzed by flow cytometry. X-mean denotes the fold difference in between the expression of the transporter on the surface of OVASC-1 cells stained with the anti-MDR1 antibody and the IgG isotype control indicating the transporter density.

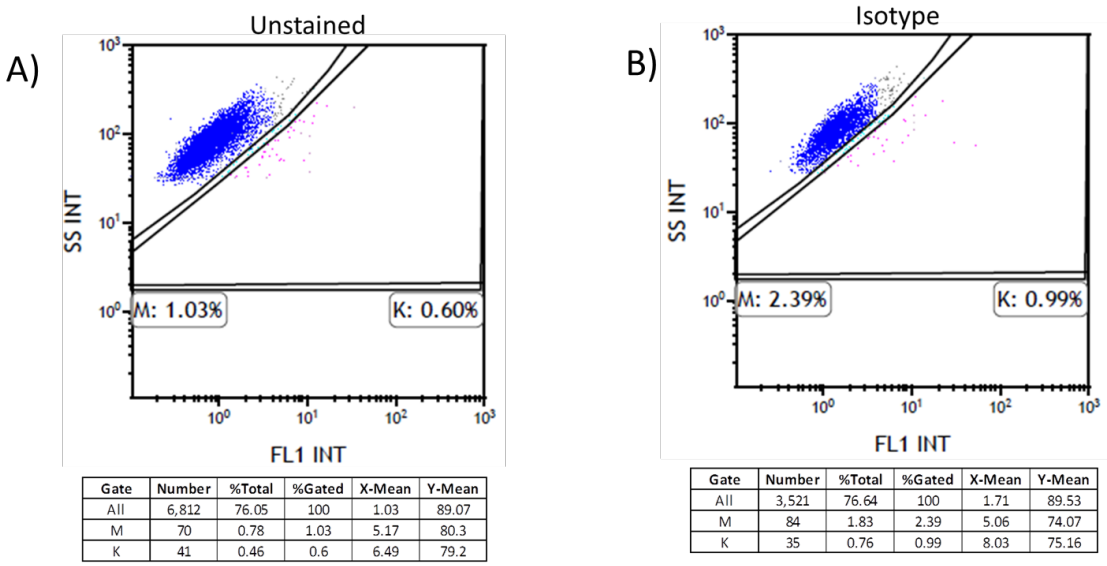

Gate	Number	%Total	%Gated	X-Mean	Y-Mean
All	6,812	76.05	100	1.03	89.07
M	70	0.78	1.03	5.17	80.3
K	41	0.46	0.6	6.49	79.2

Gate	Number	%Total	%Gated	X-Mean	Y-Mean
All	3,521	76.64	100	1.71	89.53
M	84	1.83	2.39	5.06	74.07
K	35	0.76	0.99	8.03	75.16

Gate	Number	%Total	%Gated	X-Mean	Y-Mean
All	3,302	73.69	100	21.7	89.14
M	3,186	71.1	96.49	22.38	88.74
K	3,093	69.02	93.67	22.93	88.43

Figure 4.6: Evaluation of the expression of ABCG2 transporters on the surface of OVASC-1 cells. A-B) Unstained OVASC-1 cells and cells labeled with fluorescent IgG1 isotype were used as controls. C) OVASC-1 cells were labeled with fluorescent anti-ABCG2 primary antibody and analyzed by flow cytometry. X-mean denotes the fold difference in between the expression of the transporter on the surface of OVASC-1 cells stained with the anti-ABCG2 antibody and the IgG isotype control indicating the transporter density.

4.2.2 Evaluation of the sensitivity of CSC-rich OVASC-1 tumorspheres to SN-38

To examine the effectiveness of the SN-38 in killing the CSCs in the OVASC-1 cell population, we cultured the cells under low-adherent conditions and generated CSC-rich tumorspheres (Figure 4.7A). To validate CSC-enrichment, we measured the expression of typical stem cell biomarkers such as NANOG, SOX-2 and OCT-4 in OVASC-1 cells grown under both adherent and non-adherent conditions. The results of the experiment showed a significant increase of stem cell biomarker expression in tumorspheres indicating CSC-enrichment (Figure 4.7B) (*t-test, $p<0.05$). We also examined the expression levels of ABCG2 transporters in tumorspheres because ABCG2 is a biomarker for ovarian CSCs [220-222]. The results of the experiment showed a significant increase in density of ABCG2 transporters on the surface of OVASC-1 cells in the tumorspheres as compared to the OVASC-1 cells grown under adherent conditions. While percentage of cells that expressed ABCG2 remained the same for OVASC-1 cells grown under adherent and non-adherent conditions, the X-mean for ABCG2 expression on the surface of OVASC-1 tumorspheres (i.e., X-Mean: 44.04) showed 2-fold increase in comparison to the cells grown under adherent conditions (i.e., X-Mean: 21.7) (Figure 4.7C vs 4.4F, and Figure 4.6 vs 4.8). Since MDR-1 is not a biomarker for ovarian CSCs, we also measured its expression in OVASC-1 tumorspheres as a control. The results of this experiment showed that the density of MDR1 expression on the surface of OVASC-1 tumorspheres was similar to OVASC-1 cells grown under adherent conditions (Figure 4.7D vs Figure 4.4E, and Figure 4.5 vs Figure 4.9). Next, we treated the tumorspheres with different concentrations of SN-38 to determine the ability of SN-38 in killing the CSC-rich tumorspheres. The results

showed that the drug had the ability to diffuse into the tumorspheres and kill the drug-resistant cancer cells. As a result, the diameter of the tumorspheres significantly decreased as the concentration of the drug increased (Figure 4.7E) (*t-test, $p<0.05$). While SN-38 at concentration of 100 nM could completely kill the OVASC-1 tumorspheres, cisplatin could achieve approximately the same level of tumorsphere killing efficiency at concentration of 100 μM. To examine whether remaining cells in the treated tumorspheres were alive or dead, we stained them with calcein AM (C-AM) and propidium iodide (PI) to visualize the live and dead cells, respectively. The results show that remaining cells in the SN-38- (100 nM) and cisplatin-treated (100 μM) groups were in fact clumps of cell debris (Figure 4.7F). Tumorspheres treated with lower concentrations of drugs included a mixture of live and dead cells (Figure 4.10).

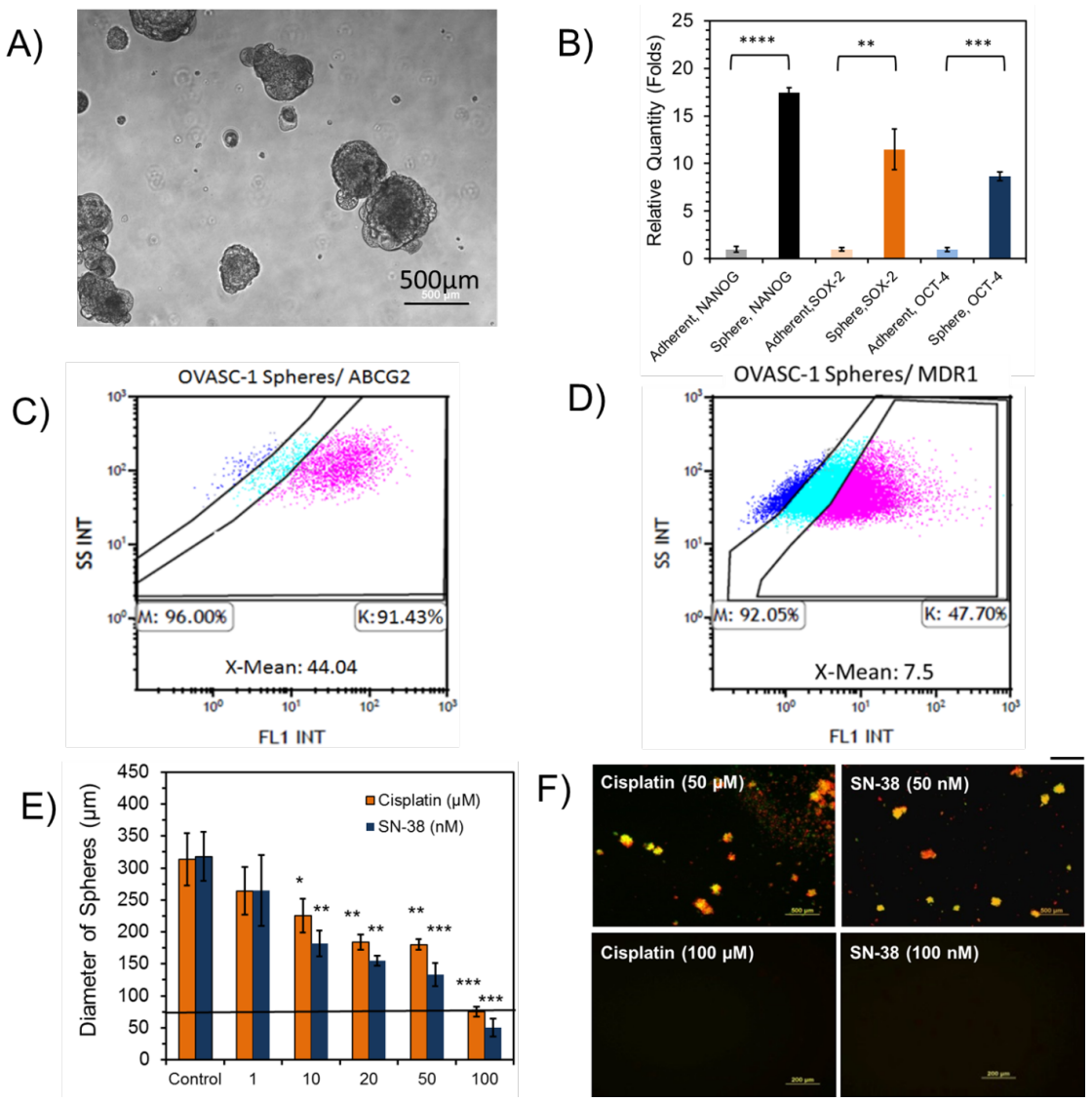

Figure 4.7: Characterization and evaluation of the sensitivity of OVASC-1 tumorspheres to drugs. A) Formation of OVASC-1 tumorspheres in low-adherent plates. B) Measurement of typical stem cell biomarkers in OVASC-1 tumorspheres generated under non-adherent conditions and in comparison to cells cultured under adherent conditions. *Statistical significance, t-test (p<0.05). C-D) The percentages of cells that express ABCG2 and MDR1 transporters in OVASC-1 tumorspheres. X-mean denotes the fold difference in expression of the transporter on the surface of OVASC-1 cells stained by the anti-MDR1/anti-ABCG2 antibodies in comparison to the IgG isotype control indicating the transporter density. E) Measurement of the tumorspheres' sizes after treatment with SN-38 and cisplatin. Data are presented as mean±s.d. (n=4). F) Tumorspheres were stained with the fluorophores calcein-AM (CAM) and propidium iodide (PI) to visualize live (green) and dead (red) cells, respectively. Scale bar= 500 µm.

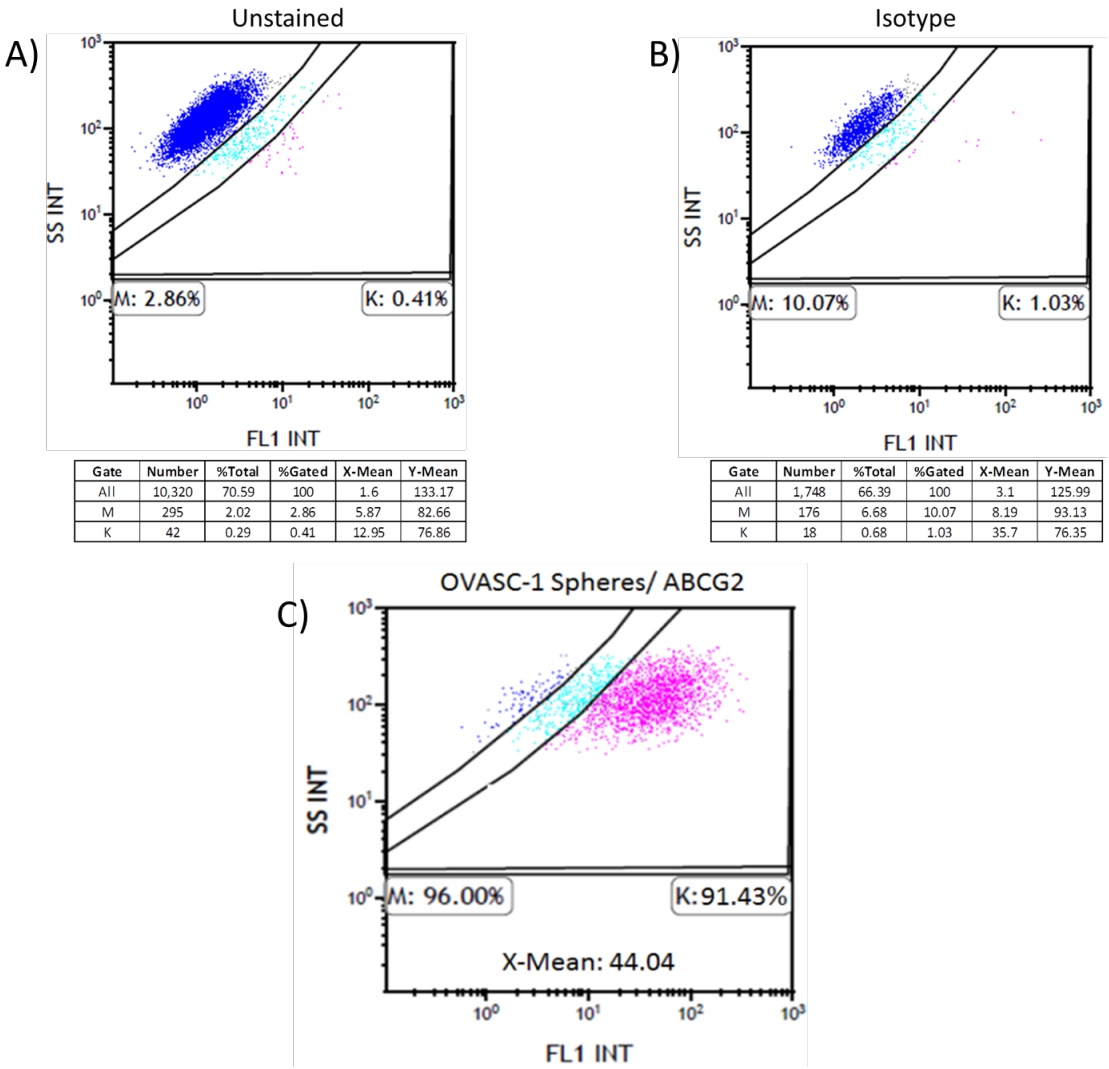

Gate	Number	%Total	%Gated	X-Mean	Y-Mean
All	10,320	70.59	100	1.6	133.17
M	295	2.02	2.86	5.87	82.66
K	42	0.29	0.41	12.95	76.86

Gate	Number	%Total	%Gated	X-Mean	Y-Mean
All	1,748	66.39	100	3.1	125.99
M	176	6.68	10.07	8.19	93.13
K	18	0.68	1.03	35.7	76.35

Gate	Number	%Total	%Gated	X-Mean	Y-Mean
All	2,448	68.36	100	44.04	125.09
M	2,350	65.62	96	45.74	124.81
K	1,969	54.98	91.43	52.81	124.48

Figure 4.8: Evaluation of the expression of ABCG2 transporters on the surface of OVASC-1 cells in tumorspheres. A-B) Unstained OVASC-1 cells and cells labeled with fluorescent IgG1 isotype were used as controls. C) OVASC-1 cells from tumorspheres were labeled with fluorescent anti-ABCG2 primary antibody and analyzed by flow cytometry. X-mean denotes the fold difference in between the expression of the transporter on the surface of OVASC-1 cells stained with the anti-ABCG2 antibody and the IgG isotype control indicating the transporter density.

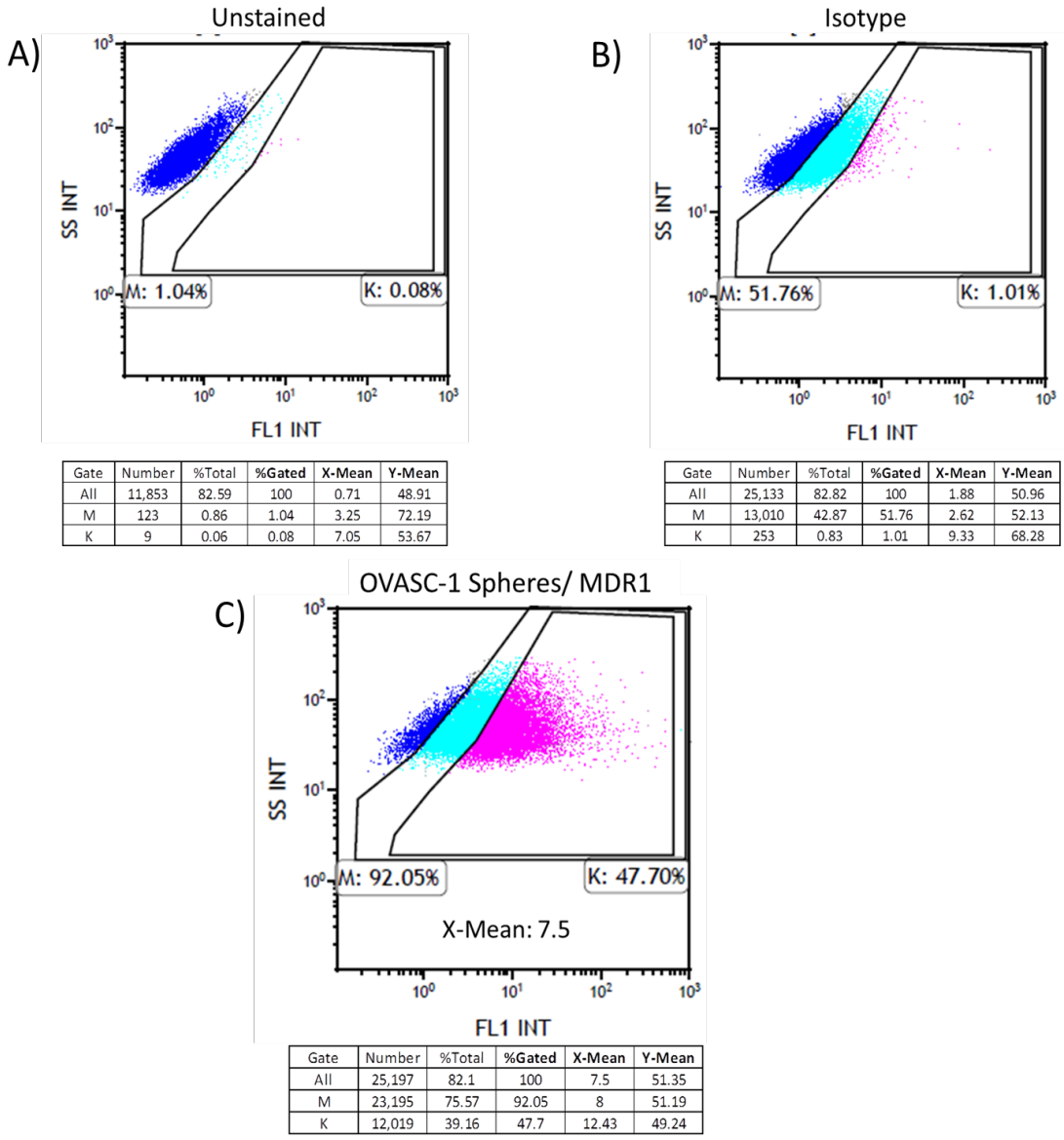

Gate	Number	%Total	%Gated	X-Mean	Y-Mean
All	11,853	82.59	100	0.71	48.91
M	123	0.86	1.04	3.25	72.19
K	9	0.06	0.08	7.05	53.67

Gate	Number	%Total	%Gated	X-Mean	Y-Mean
All	25,133	82.82	100	1.88	50.96
M	13,010	42.87	51.76	2.62	52.13
K	253	0.83	1.01	9.33	68.28

Gate	Number	%Total	%Gated	X-Mean	Y-Mean
All	25,197	82.1	100	7.5	51.35
M	23,195	75.57	92.05	8	51.19
K	12,019	39.16	47.7	12.43	49.24

Figure 4.9: Evaluation of the expression of MDR1 transporters on the surface of OVASC-1 cells in tumorspheres. A-B) Unstained OVASC-1 cells and cells labeled with fluorescent IgG1 isotype were used as controls. C) OVASC-1 cells from tumorspheres were labeled with fluorescent anti-MDR1 primary antibody and analyzed by flow cytometry. X-mean denotes the fold difference in expression of the transporter on the surface of OVASC-1 cells stained with the anti-MDR1 antibody in comparison to the IgG isotype control indicating the transporter density.

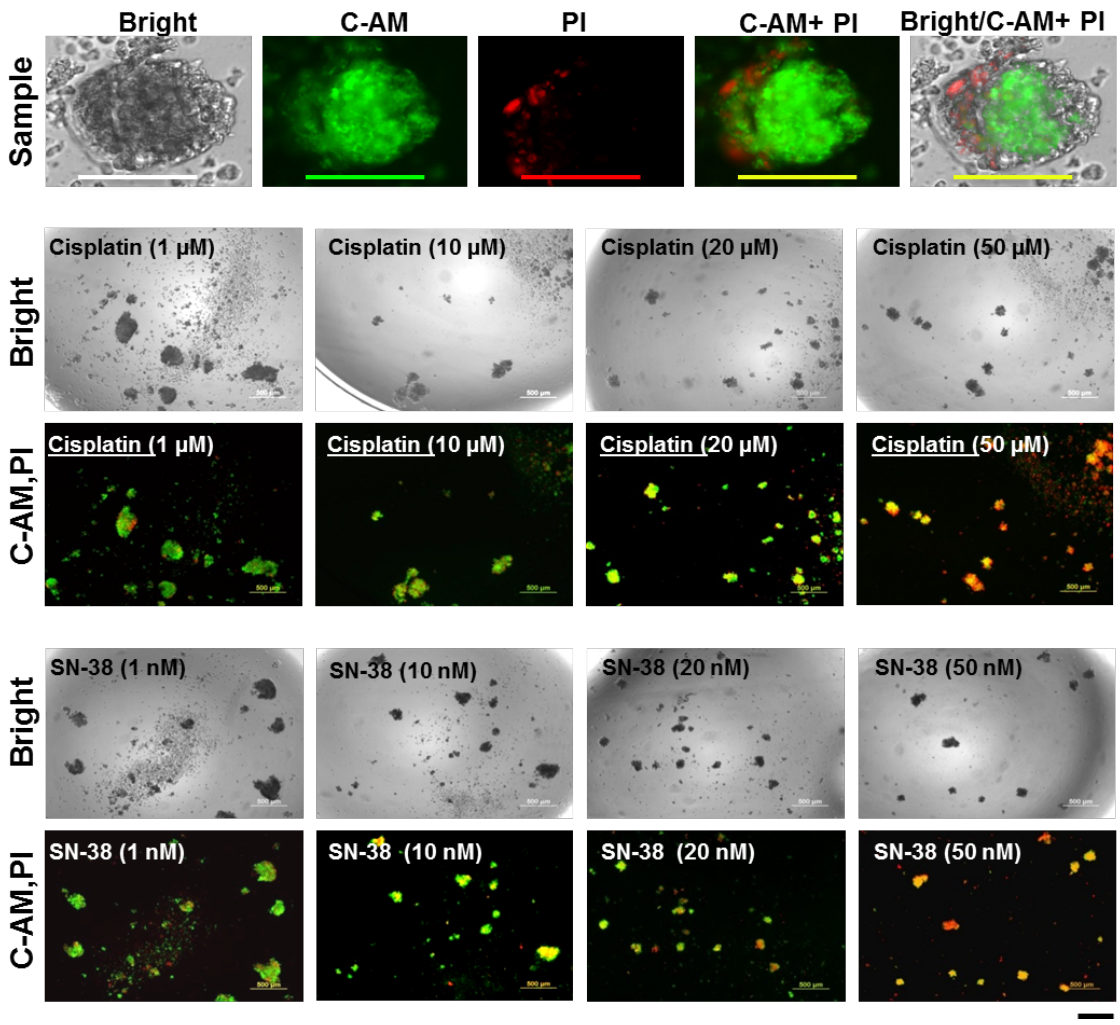

Figure 4.10: Evaluation of the OVASC-1 tumorspheres sensitivity to SN-38 and cisplatin. Tumorspheres were stained with the fluorophores calcein-AM (CAM) and propidium iodide (PI) to visualize live (green) and dead (red) cells, respectively. Scale bar= 500 µm. This figure shows that the tumorspheres consisted of mostly live cells when exposed to SN-38 at less than 50 nM and cisplatin at less than 50 µM.

4.2.3 Evaluation of the functionality of the genetically engineered ASCs

An ASC clone that stably expressed shCE2 and nanoluciferase genes (ASC-shCE2:nLuc) was genetically engineered to allow for simultaneous disease therapy and in vivo imaging (Figure 4.11A). To examine whether functional shCE2 was in fact secreted outside of the ASCs, two experiments were performed. First, the activity of the carboxylesterase enzyme secreted into the culture media was examined by removing the media in which the ASC-shCE2:nLuc cells were grown and through treatment with FDA (CE2 substrate and nonfluorescent). The kinetics of FDA conversion into its fluorescently active byproduct fluorescein was then measured. The results of this experiment show that the fluorescence of media continuously increased over time, revealing the activity of shCE2. Relative to the fluorescent intensity of the culture media never put in contact with cells, an almost 8 fold (81.88/10.74) increase in the rate of FDA conversion was observed for the media in which ASC- shCE2:nLuc cells were grown (Figure 4.11B). In contrast, the culture media of the ASC-hCE2:nLuc cells (non-secretory CE2) did not show any significant changes in fluorescent intensity, indicating inefficiency in FDA conversion. We also examined the capacity for the secreted shCE2 in the culture media to convert irinotecan into SN38. For this purpose, we removed the culture media in which ASC-shCE2:nLuc cells were grown and then treated it with irinotecan. The culture media was then analyzed by LC/MS to identify corresponding irinotecan and SN-38 ion fragments. The results of this experiment show that shCE2 secreted from ASC-shCE2:nLuc cells converted a portion of the irinotecan prodrug into SN-38 (Figure 4.11C - 4.11D). The two experiments validated that the ASC-shCE2:nLuc cells secrete an active form of shCE2 into culture

media with the ability to convert irinotecan into SN-38. We also examined the activity of the nanoluciferase in ASC-shCE2:nLuc cells by incubating them with enzyme substrate furimazine. A clone of ASC- shCE2:nLuc cells with the highest expression of both shCE2 and nanoluciferase genes was isolated (Figure 4.12). We then performed an experiment to assess whether the isolated ASC-shCE2:nLuc clone in combination with irinotecan could generate sufficiently high concentrations of SN-38 lethal to OVASC-1 cells. For this purpose, we first determined the maximum concentration of irinotecan that can be used in cell culture media without being toxic to ASCs or OVASC-1 cells. The results of this experiment show that irinotecan at a 1 μM concentration was not toxic to either group of cells (Figure 4.13A- 4.13B). Then, ASC- shCE2:nLuc and OVASC-1 cells were cocultured and treated with irinotecan (1 μM). The results of this experiment show a significant reduction in the viability of the OVASC-1 cells cocultured with ASC- shCE2:nLuc cells and treated with irinotecan (1 μM) (Figure. 4.13C).

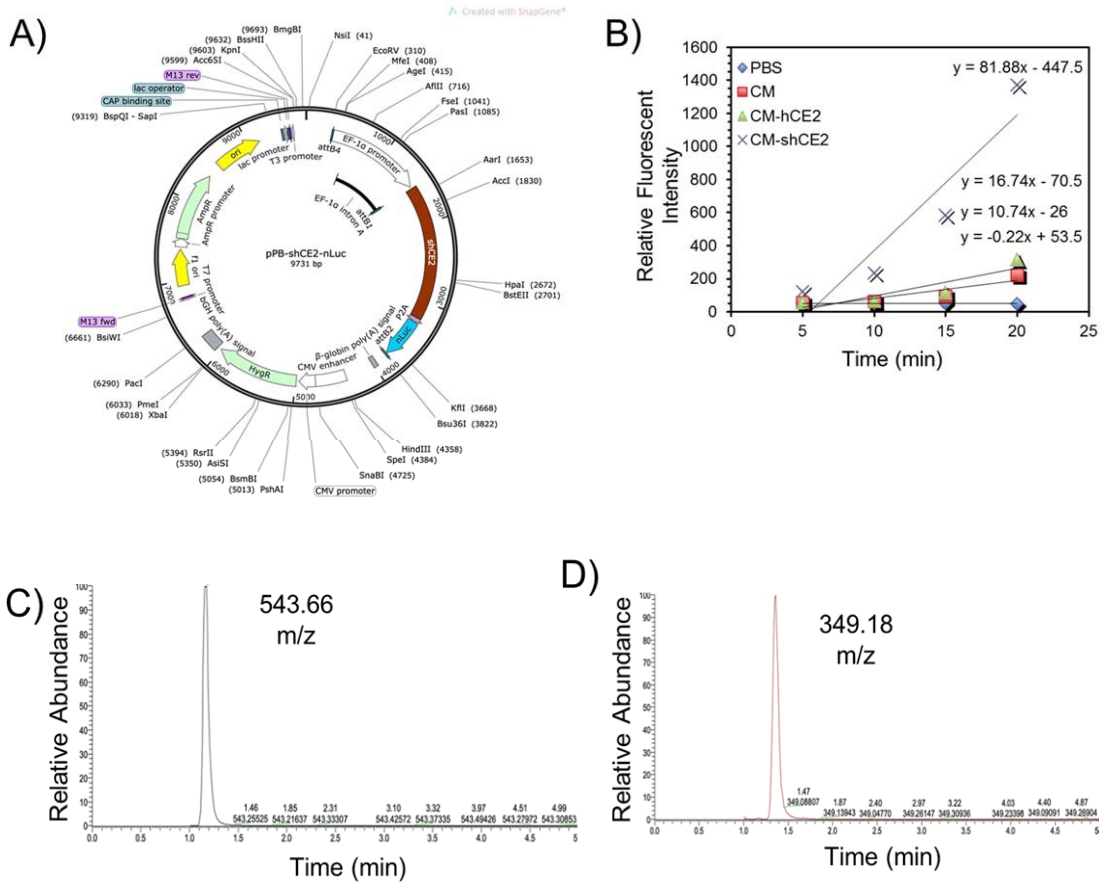

Figure 4.11: Genetic engineering and evaluation of the functionality of the genetically engineered ASC- shCE2:nLuc cells. A) The map of the plasmid DNA encoding shCE2 in fusion with nLuc. B) Measurement of the kinetics of FDA conversion over time. The ASC-shCE2:nLuc cells that secreted CE2 into the media could effectively convert FDA into its fluorescent byproduct (Y-axis). CM stands for culture media and PBS is phosphate buffer saline. CM-shCE2 stands for culture media from the ASC- shCE2:nLuc cells (secretory), whereas CM-hCE2 stands for culture media from the ASC-hCE2:nLuc cells (non-secretory). C) The mass spectroscopy chromatogram with major fragment ion of 543.66 m/z corresponding to irinotecan. D) The mass spectroscopy chromatogram with major fragment ion of 349.18 m/z corresponding to SN-38.

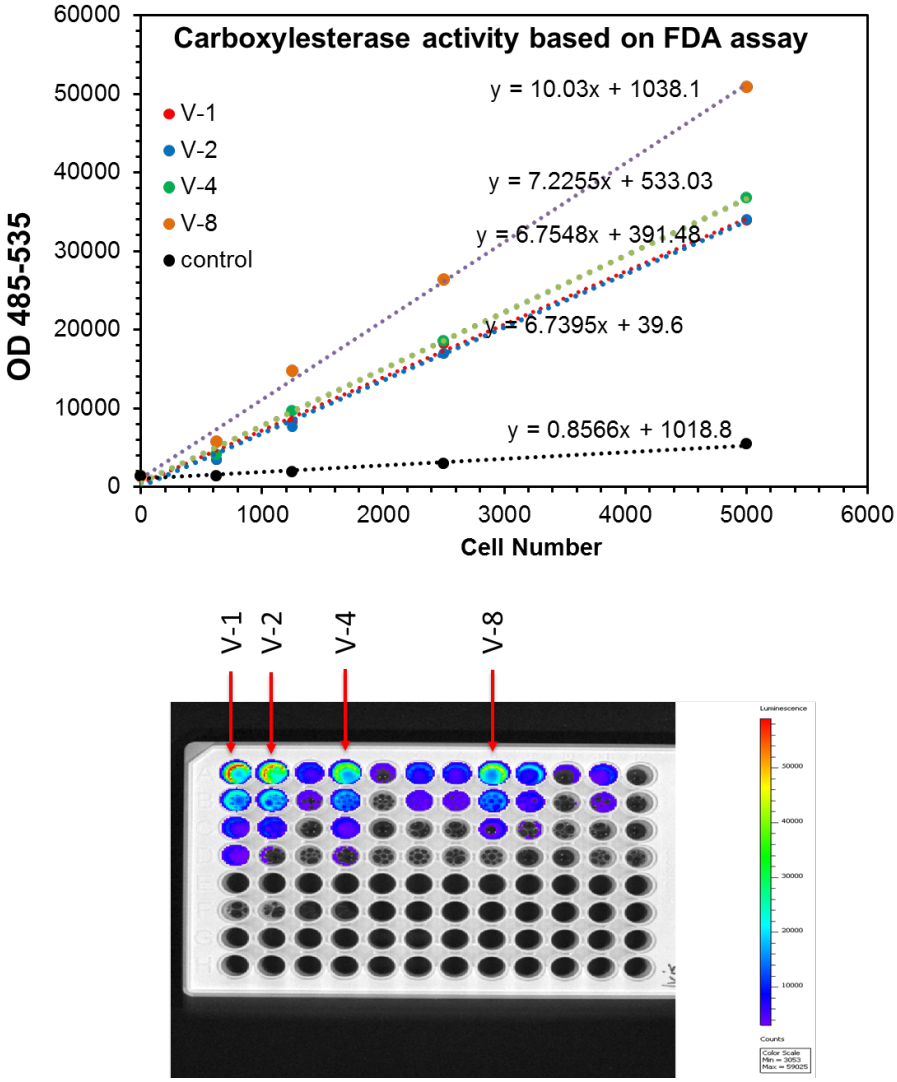

Figure 4.12: Selection of a clone of ASC-shCE2:nLuc cells that have high expression of both carboxylesterase and nanoluciferase genes. Top panel) FDA conversion assay that shows clone V8 had the highest carboxylesterase activity. Lower panel) nanoluciferase expression assay which shows clone V8 had significant luciferase expression levels (third highest). The clone V8, which expressed both genes at acceptable levels and suitable for the studies, was selected.

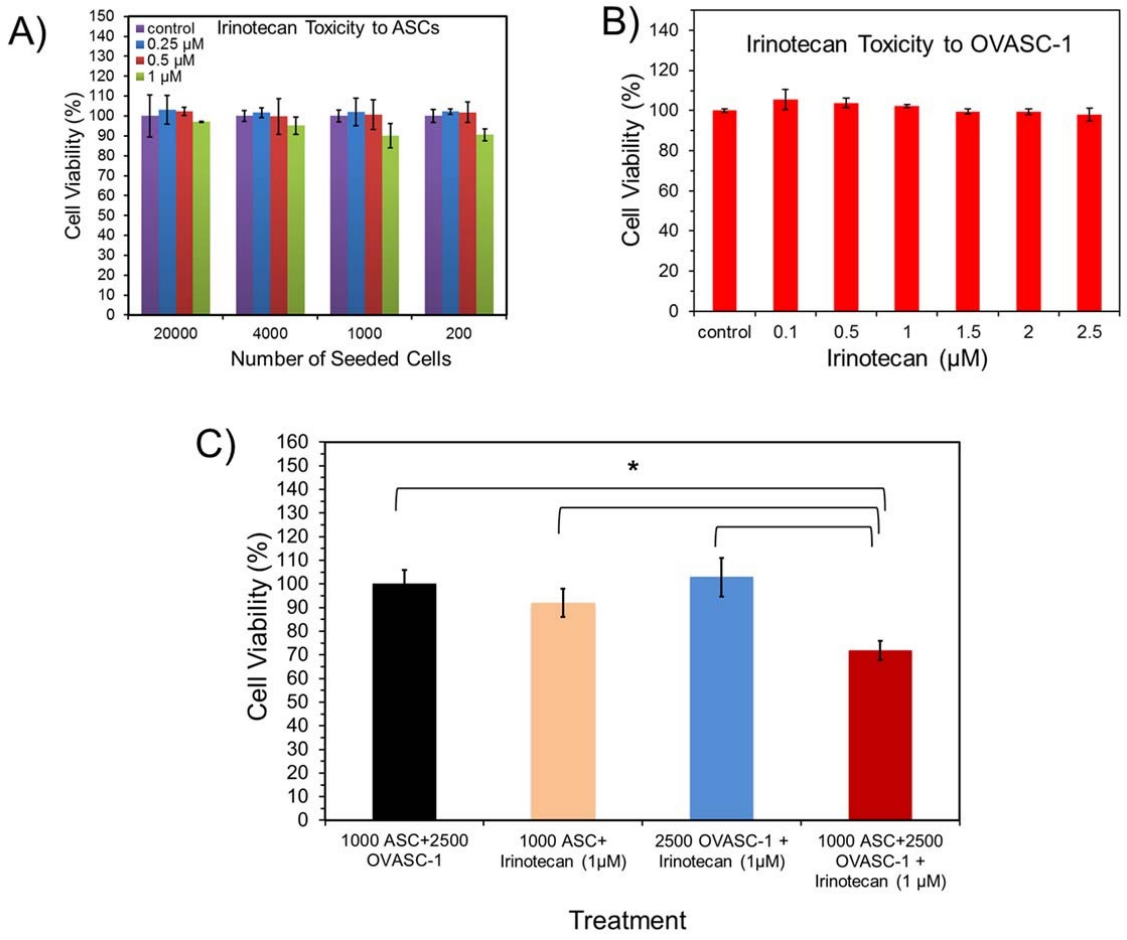

Figure 4.13: Evaluation of the effect of CPT-11 and shCE2/CPT-11 combination on ASC and OVASC-1 cell viability: A) Evaluation of the viability of OVASC-1 cells treated with different concentrations of irinotecan. Irinotecan was not toxic to OVASC-1 cell up to 2.5 µM. B) Evaluation of the viability of ASCs seeded at different numbers and treated with different concentrations of irinotecan. Irinotecan at 1µM concentration was not toxic to ASCs when at least 1000 cells were seeded. C) Evaluation of the cytotoxicity of the ASC-shCE2:nLuc cells in combination with CPT-11 to OVASC-1 cells. The absorbance of the 1000 ASCs co-cultured with 2500 OVASC-1 cells (without irinotecan) was considered as 100% viable. (*ANOVA followed by a Post hoc Tukey test, $p<0.05$)

4.2.4 Evaluation of the tumor tropism of the engineered ASCs by BLI, MRI and histopathology

To study the tropism of the ASC-shCE2:nLuc cells, we first injected the cells into the peritoneal cavity of a nude mouse (without tumors) and tracked the cells by BLI. The intention was to study the fate of the ASC- shCE2:nLuc cells in mouse peritoneal cavity. The results of the experiment show that most of the ASCs disappeared from the field of view and were not detectable after two weeks. However, long-term imaging tests detected bioluminescence signals from two locations within the mouse body after seven weeks (Figure 4.14A- Figure 4.14B). To investigate further, the mouse was euthanized, and the luminescent area removed, stained and studied under a microscope. The histopathology results show that the luminescent area included an aggregate of ASCs in mesentery without evidence of malignancy (Figure 4.14C).

We then performed experiments to assess the tumor tropism of the engineered ASC-shCE2:nLuc cells. For this purpose, OVASC-1 cells that stably expressed the firefly luciferase gene (OVASC-fLuc) were geneti- cally engineered. OVASC-fLuc cells were then injected IP and were left to grow for three weeks to provide ample time for the tumors to establish and metastasize (Figure 4.14D).

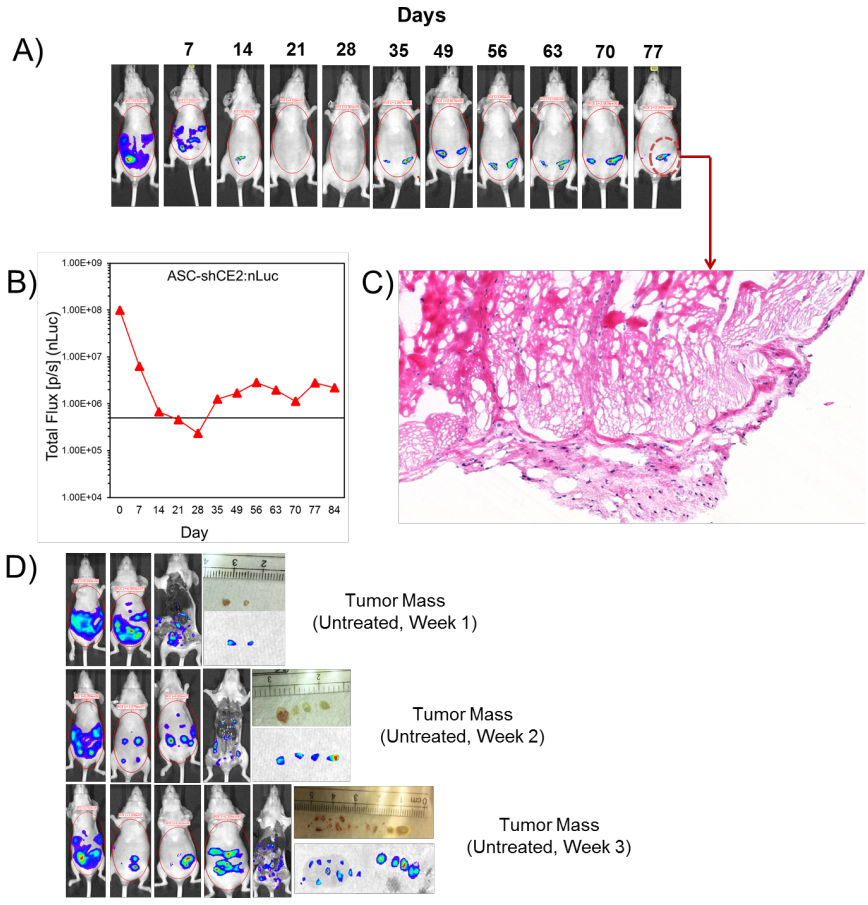

Figure 4.14: Evaluation of the fate of the injected ASCs over the period of 12 weeks. A) Bioluminescent imaging of the live mouse that was injected intraperitoneally with ASC-shCE2:nLuc cells. B) The bioluminescent signal quantification over the 12 weeks period. C) Tissue section slide of the bioluminescent area showing the presence of no malignancy. D) The growth of tumor mass inside mouse peritoneal cavity over the course of three weeks. Mice were studied by BLI and then dissected to remove the tumors. The size of the tumors measured and number of tumors were counted.

Three weeks after tumor establishment, the ASC-shCE2:nLuc cells were injected IP and their distribution and migration was tracked by BLI. Since firefly luciferase and nanoluciferase substrates do not cross-react, they could be imaged without interference. The BLI data show that the ASC-shCE2:nLuc cells colocalized with OVASC-fLuc cells as soon as three days post injection (Figure 4.15A). On day 11, the mouse was euthanized, the tumors removed and imaged in the presence of furimazine (nLuc substrate). The results of this experiment showed the existence of nLuc enzyme within the dissected tumors indicating the presence of ASC-shCE2:nLuc cells (Figure 4.15A). We then prepared a suspension of single cells from the extracted tumors and studied them for CD90 biomarker expression. CD90 is a typical biomarker expressed on the surface of ASCs [223], but not on OVASC-1 cells (Figure. 4.16). The results of this experiment showed that approximately 5% of the analyzed cells were CD90+ (Figure. 4.15B). Using cell sorting, we separated the CD90+ cells and transferred them into a well followed by addition of furimazine. The results of this experiment showed that the CD90+ cells had nLuc expression whereas the $CD90^{-}$ cells did not. To examine the localization of the ASC-shCE2:nLuc cells within tumors at a higher resolution and to determine potential applications of this approach in clinical settings, we treated the ASC-shCE2:nLuc cells with SPIONs at a non-toxic concentration to form ASC-shCE2:nLuc-SP cells (Figure. 4.17). Since the cells were loaded with SPIONs, they could be detected by T2*- weighted MRI sequence. The MRI data revealed the areas within the peritoneal cavity in which ASC-shCE2:nLuc-SP cells were localized (Figure. 4.15C). Using the MR images as a guide, a cluster of tumors with blackened surfaces were detected under the liver after tissue dissection (Figure 4.15D).

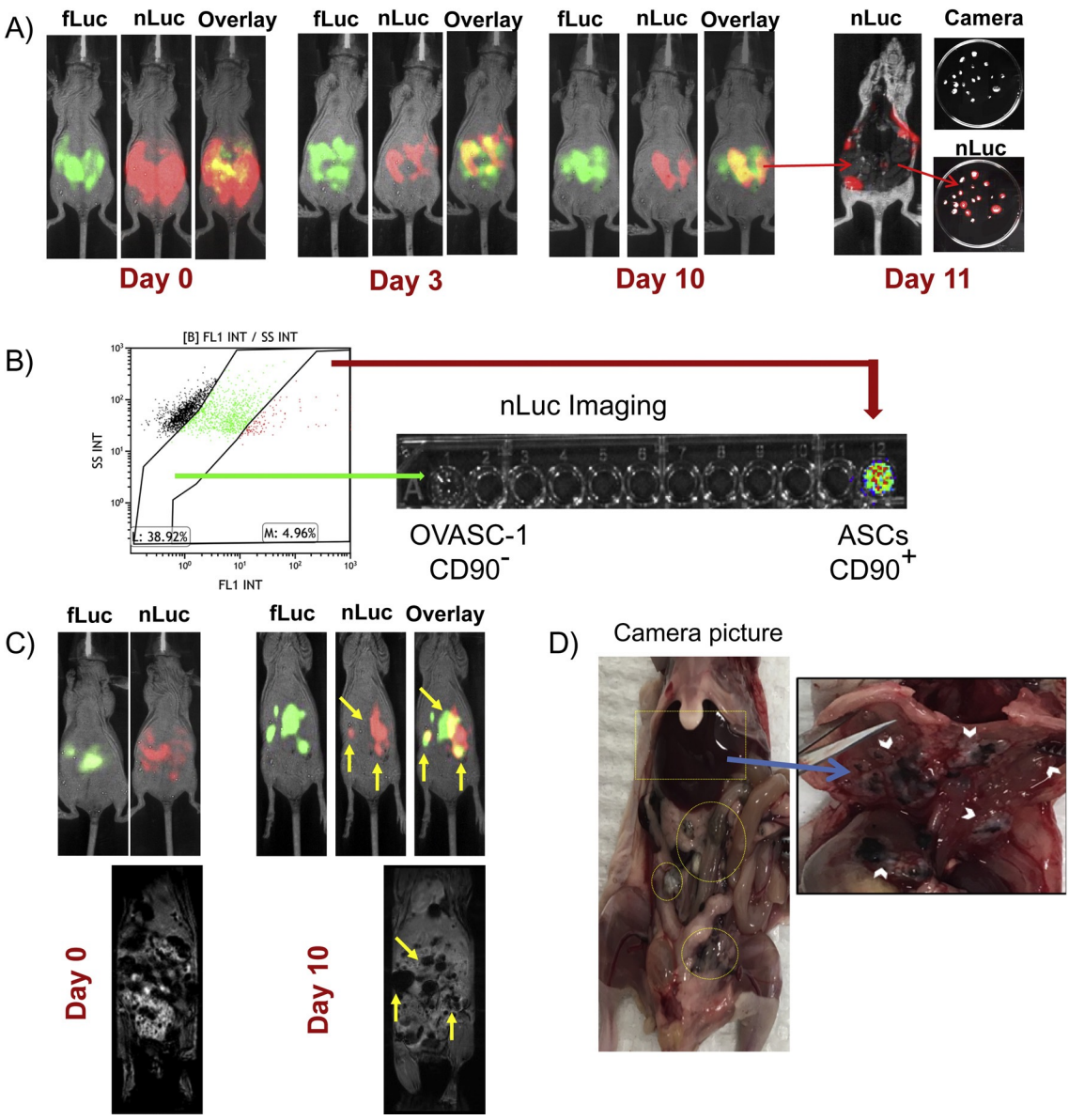

Figure 4.15: Evaluation of the tumor tropism of ASC-shCE2:nLuc cells. A) BLI of nude mice with intraperitoneal OVASC-fLuc tumors (green) and ASC-shCE2:nLuc cells (red) over ten days. The co-localization of ASCs with OVASC-1 cells (yellow) could be observed as soon as three days. The excised tumors on day 11 showed expression of nLuc. B) Flow cytometry analysis of single cell suspension of extracted tumors labeled with anti-CD90 primary antibody. The CD90+ and CD90$^-$cells were then sorted into separate wells and incubated with furimazine and imaged for bioluminescence. C) BLI of the mouse with the intraperitoneal OVASC-1-fLuc tumors and the corresponding T2*-weighted MRI sequence of ASC-shCE2:nLuc-SP cells on days zero and ten. The tumors that were detectable by BLI could be marked by MRI with more accuracy. D) Camera picture of the dissected mouse abdomen with blackened tumor surfaces. The blackened tumors suggest presence of SPION nanoparticles.

A)

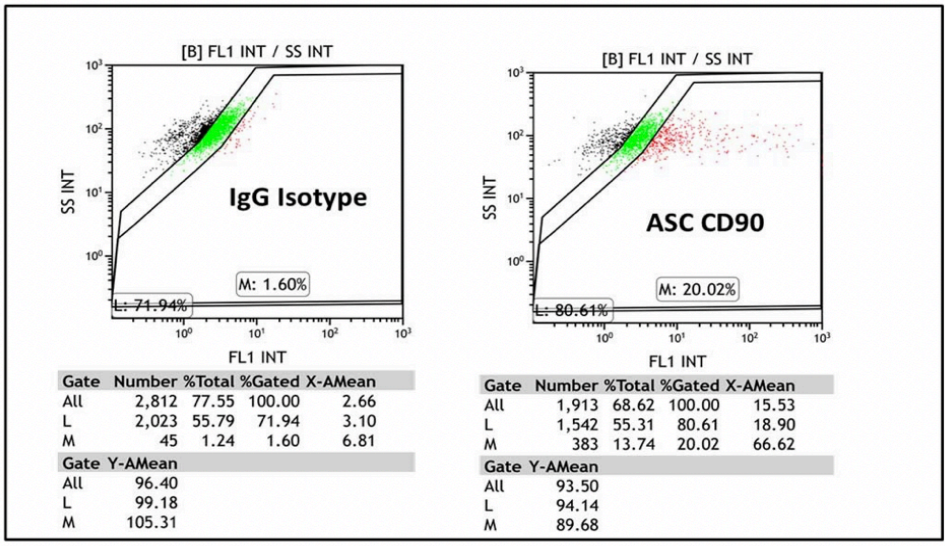

B)

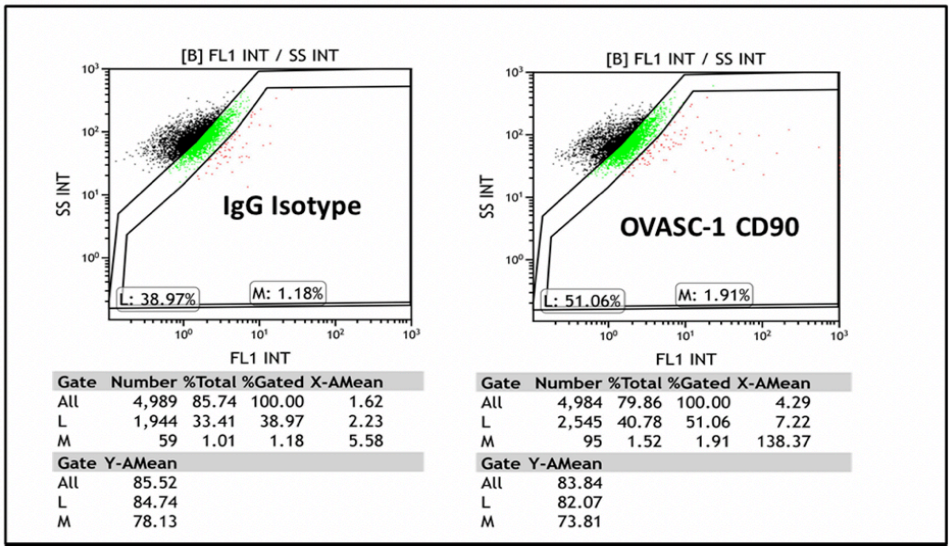

Figure 4.16: Evaluation of the expression of CD90 biomarker on the surfaces of ASC-shCE2:nLuc and OVASC-1 cells by flow cytometry. A) ASC-shCE2:nLuc cells labeled with fluorescent IgG1 isotype or anti-CD90 primary antibodies. B) OVASC-1 cells labeled with fluorescent IgG1 or anti-CD90 primary antibodies.

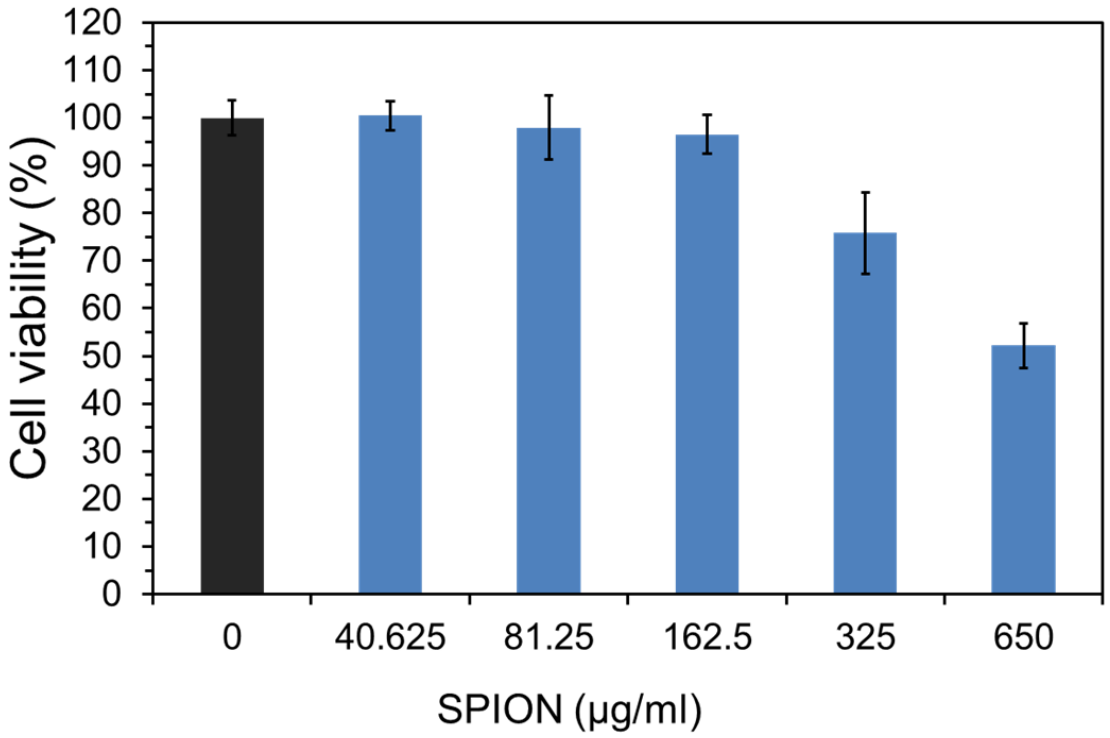

Figure 4.17: Evaluation of the toxicity of FluidMAG-D SPIONs to ASC-shCE2:nLuc cells. Cells were incubated with FluidMAG-D for 24 hours at different concentrations and the viability of the ASCs was measured by WST-1 cell toxicity assay. This figure shows that FluidMAG-D SPIONs are not toxic to ASCs at concentrations equal to or less than 162.5 µg/ml.

Furthermore, the presence of SPION nanoparticles in the ASCs made it possible to identify the exact locations of the ASCs within the tumors by iron-staining and immuno/histochemistry. The histochemistry of the dissected tumors shows that the ASC-shCE2:nLuc-SP cells were localized in both tumor stroma and necrotic regions (Figure. 4.18A– 4.18B). The staining of the tumor tissue sections with CD90 antibody confirmed the presence of ASCs inside the tumor tissues (Figure. 4.18A– 4.18B). A higher magnification of the H&E stained tumor tissue section clearly showed presence of iron in cells with vacuolated cytoplasm consistent with adipocytes (Figure 4.18C).

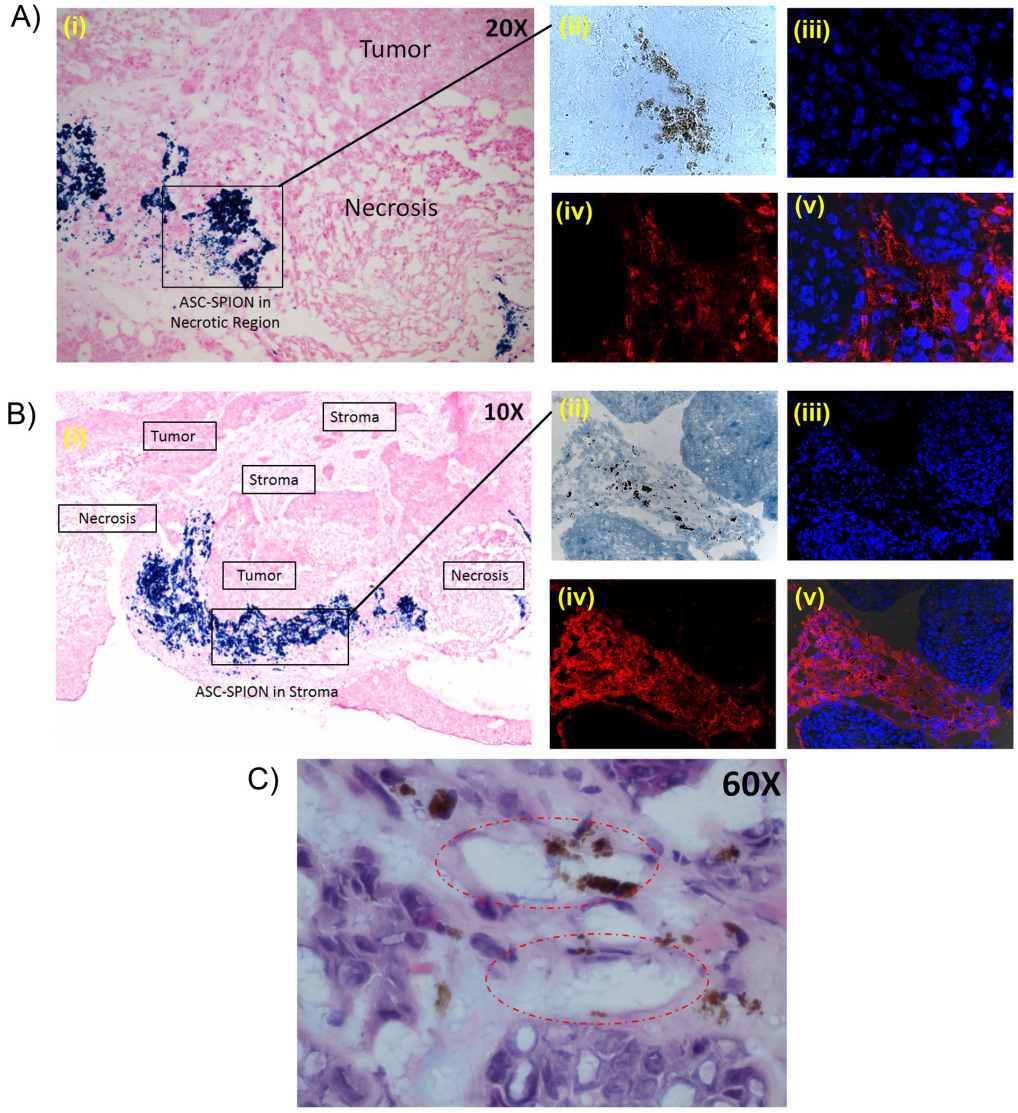

Figure 4.18. Haemotoxylin and Eosin (H&E) staining, Prussian blue staining and CD90 labeling of sectioned tumor tissues. A-B) The tumor tissue sections under the microscope (10× and 20× magnification) showing localization of the ASC-shCE2:nLuc-SP cells in necrotic and stroma regions (i). The immunohistochemistry of the tumor tissue section and visualization under the fluorescent microscope (40× magnification); tumor tissue section under transmitted light showing presence of SPIONs in tumor tissues (ii), stained cell nucleus by DAPI showing the locations of cells in the field of view (iii), CD90+ cells stained by Texas Red in the same field of view (iv), and DAPI/Texas Red overlays showing the presence of numerous CD90+ cells among the CD90$^-$ cells (v). C) 60× magnification of tumor tissue section stained by H&E and Prussian Blue. The circled region shows the SPION-loaded ASCs with vacuolated cytoplasm within the tumor tissue.

4.2.5 Evaluation of ovarian cancer progression, response to therapy and prevention of relapse

To determine the efficacy of the engineered ASCs in treating metastatic drug-resistant ovarian cancer, the suicide gene expressing ASC-shCE2:nLuc cells were used in combination with CPT-11. OVASC-1-fluc cells were injected into the peritoneal cavity of nude mice to establish tumors. After three weeks, the change in tumor mass inside mice peritoneal cavity was measured by BLI to confirm the establishment of tumors and advanced disease. The mice were then divided into five groups (G1 to G5) of five and given treatments as delineated in Table 4.2. The analysis of images of mice in G1 illustrated a steady-state enhancement in the bioluminescence signal, denoting an increase in tumor mass over time (Figure 4.19A– 4.19B). The animals in this group were either euthanized (∼7 weeks after tumor implantation) due to significant weight loss or died due to disease progression into vital organs (Table 4.2, Figure 4.19C).

Table 4.2: Stratification of mice into five treatment groups and evaluation of response to therapy, toxicity, and recurrence. CR: complete response meaning no evidence of the tumor mass. PR: partial response meaning a decrease in tumor volume (≥25%). NR: no response meaning no significant decrease in tumor mass. Recurrence: increase in tumor mass after a complete or partial response. * Drug-related observable toxicity during treatment: More than 10% weight loss in a week or more than 20% weight loss over any time period; diarrhea, bulky ascites, distended abdomen, or lethargy.

Group	Treatment	Mice/ group	CR	PR	NR	Treatment -Related Toxicity*	Recurrence
G1	Vehicle control	5	0	0	5	0	N/A
G2	Cisplatin+ Paclitaxel 5 + 15 (mg/kg)	5	0	0	5	0	N/A
G3	CPT-11 40 (mg/kg)	5	1	3	1	0	3
G4	CPT-11 80 (mg/kg)	5	3	2	0	3	2
G5	ASC-shCE2:nLuc + CPT-11 40 (mg/kg)	5	4	1	0	0	1

* Drug-related observable toxicity during treatment: > 10% weight loss in a week or > 20% weight loss over any time period; diarrhea, bulky ascites, distended abdomen, or lethargy.

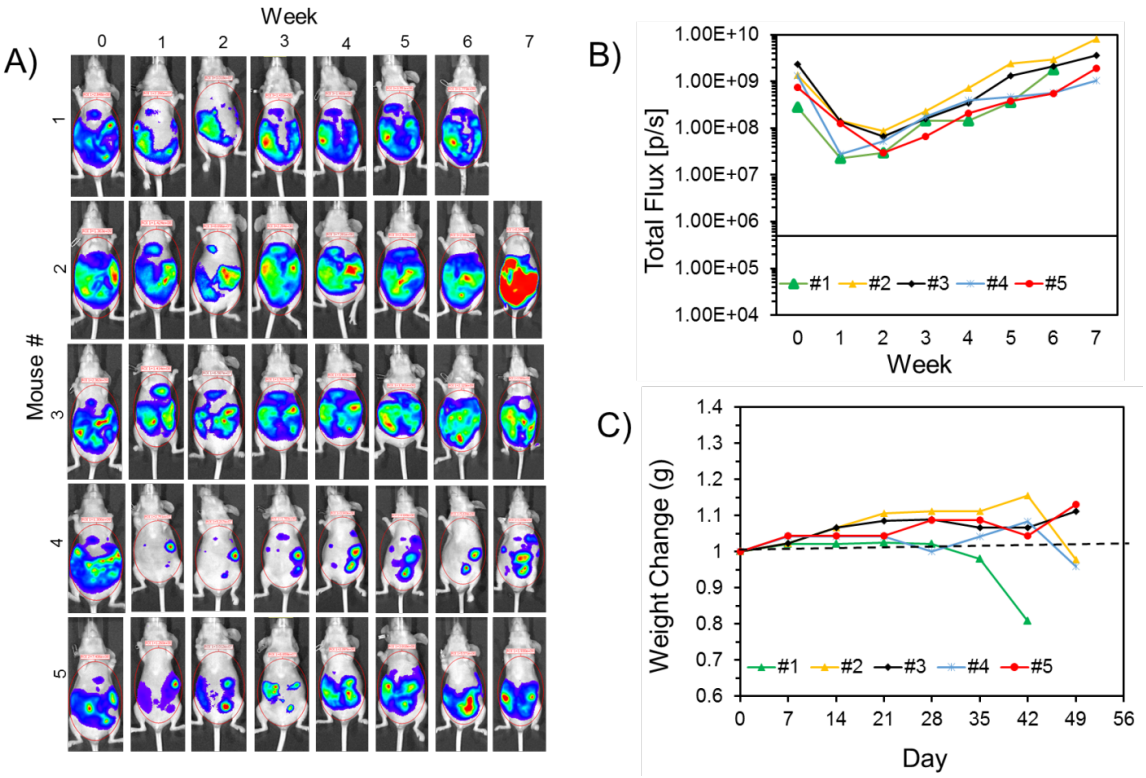

Figure 4.19: BLI and weight of nude mice with intraperitoneal tumors and the quantification of the bioluminescent signal over the period of seven weeks. A) BLI of nude mice with intraperitoneal tumors (firefly luciferase imaging). B) The quantification of the bioluminescent signal over the period of seven weeks. The line at 5×10^5 (p/s) shows the background bioluminescence of mice body without any tumors. C) Change in mice weight over the period of seven weeks. The weights of the mice before the treatment are normalized and considered as 1.

Mice in G2 received standard-of-care cisplatin/PTX using a regimen based on previously published reports [31, 224]. The mice in this group did not respond to the standard-of-care therapy, as tumor masses did not significantly decrease over the treatment period. The mice in this group were euthanized due to disease progression and the development of bulky ascites after ∼8 weeks (Table 4.2, Figure. 4.20A– 4.20B, Figure 4.21).

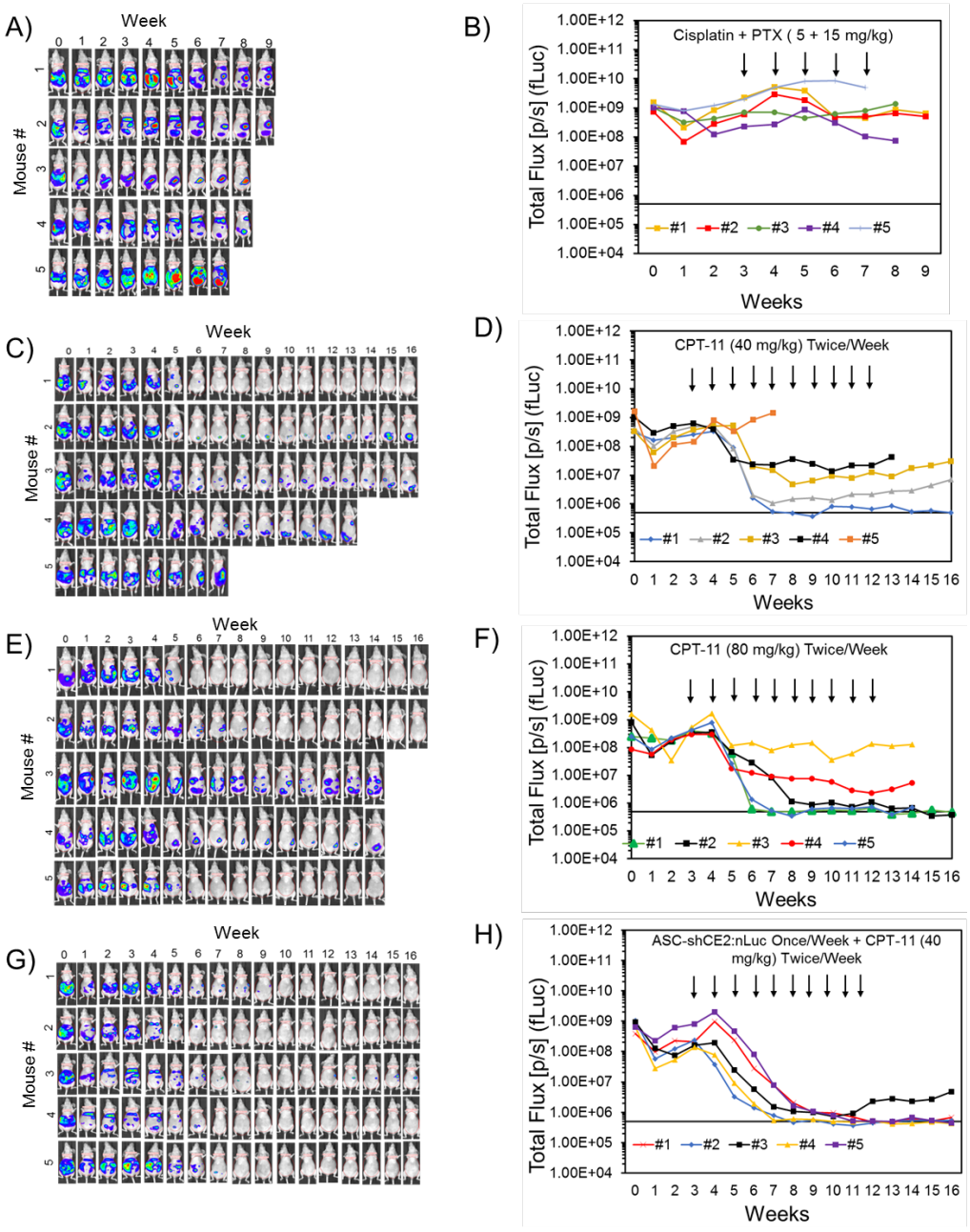

Figure 4.20: Evaluation of therapy response and cancer relapse by BLI (firefly luciferase imaging). A-B) BLI of nude mice with intraperitoneal tumors and quantitative analysis of signal in mice treated with the standard-of-care regimen of cisplatin+PTX. C-D) BLI of nude mice with intraperitoneal tumors and quantitative analysis of the signal in mice treated with CPT-11 (40 mg/kg). E-F) BLI of nude mice with intraperitoneal tumors and quantitative analysis of the signal in mice treated with CPT-11 (80 mg/kg). G-H) BLI of nude mice with intraperitoneal tumors and quantitative analysis of the signal in mice treated with ASC-shCE2:nLuc cells and CPT-11 (40 mg/kg).

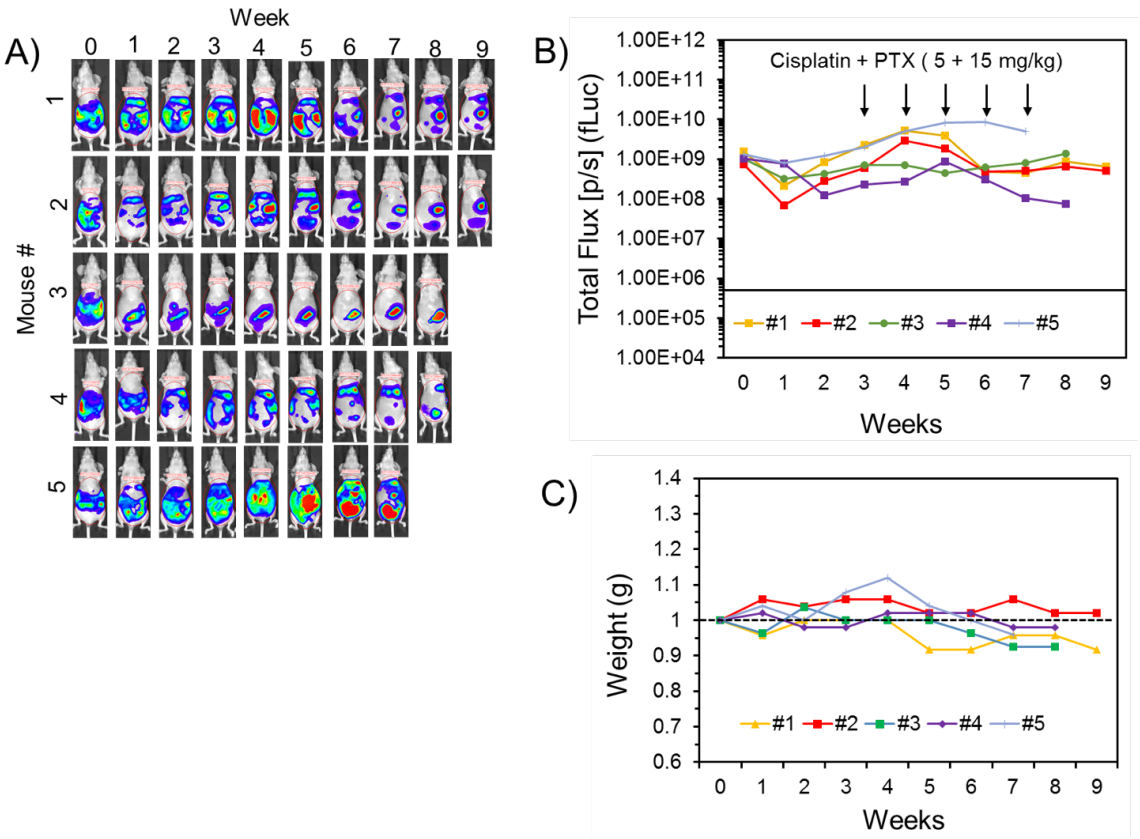

Figure 4.21: A) BLI and weight of nude mice with intraperitoneal tumors and quantification of the bioluminescent signal over the treatment period with cisplatin and PTX. Arrows denote the points at which the mice received treatment. The line at 5 $\times 10^5$ (p/s) shows the background bioluminescence of mice body without any tumors. C) Change in mice weight over the period of nine weeks. The weights of the mice before the treatment are normalized and considered as 1.

Mice in G3 received a therapeutic dose of irinotecan (40 mg/kg) because it is close to the equivalent dose used in humans and following previously published preclinical studies of mice [225-227]. One mouse in this group showed a complete response without any relapse, whereas one mouse showed no response at all. The three remaining mice in this group showed a partial response. All mice that responded to therapy remained healthy and did not show any gastrointestinal (GI)-related toxicity as evidenced by the absence of weight loss, diarrhea and loss of appetite during the treatment period. Post treatment, mice were euthanized when they showed signs of disease progression into vital organs, including significant weight loss and/or the formation of bulky ascites and interference with normal functions (Table 4.2, Figure 4.20C – 4.20D, Figure 4.22). An analysis of ABCG2 transporters on the surfaces of OVASC-1 cells extracted from nonresponsive tumors in this group showed a significant upregulation of the said transporter (Figure 4.23).

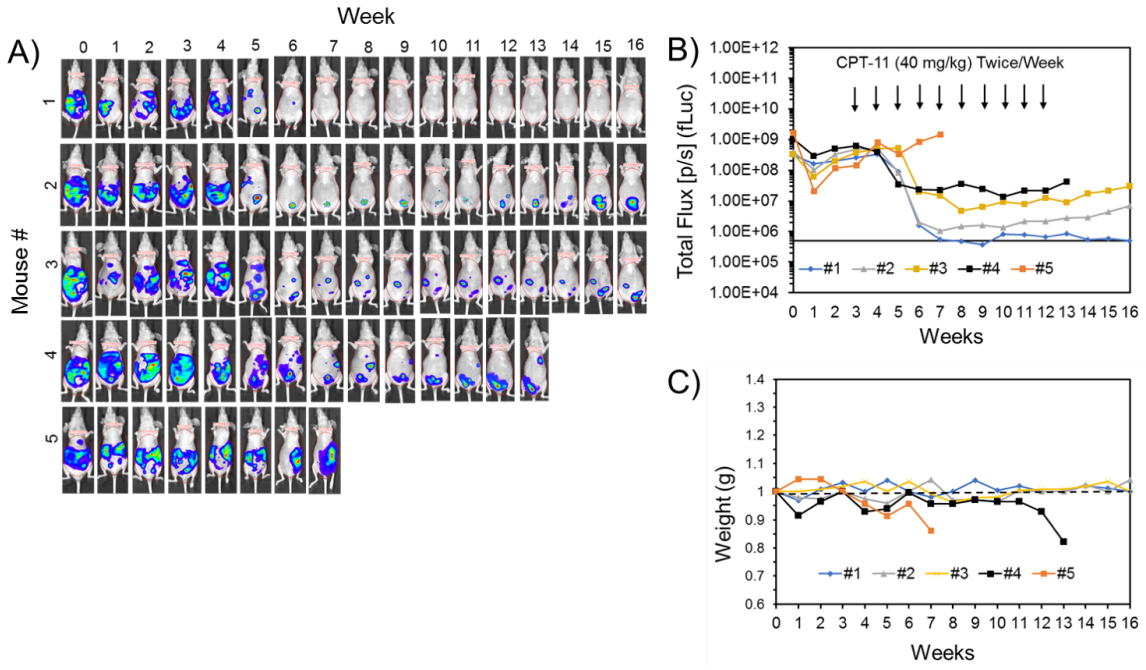

Figure 4.22: BLI and weight of nude mice with intraperitoneal tumors and quantification of the bioluminescent signal over the treatment period with CPT-11 (40 mg/kg). A) BLI of nude mice with intraperitoneal tumors (firefly luciferase imaging). B) The quantification of the bioluminescent signal over the treatment period with CPT-11 (40 mg/kg). Arrows denote the points at which the mice received treatment. The line at 5 $\times 10^5$ (p/s) shows the background bioluminescence of mice body without any tumors. C) Change in mice weight over the treatment period. The weights of the mice before the treatment are normalized and considered as 1.

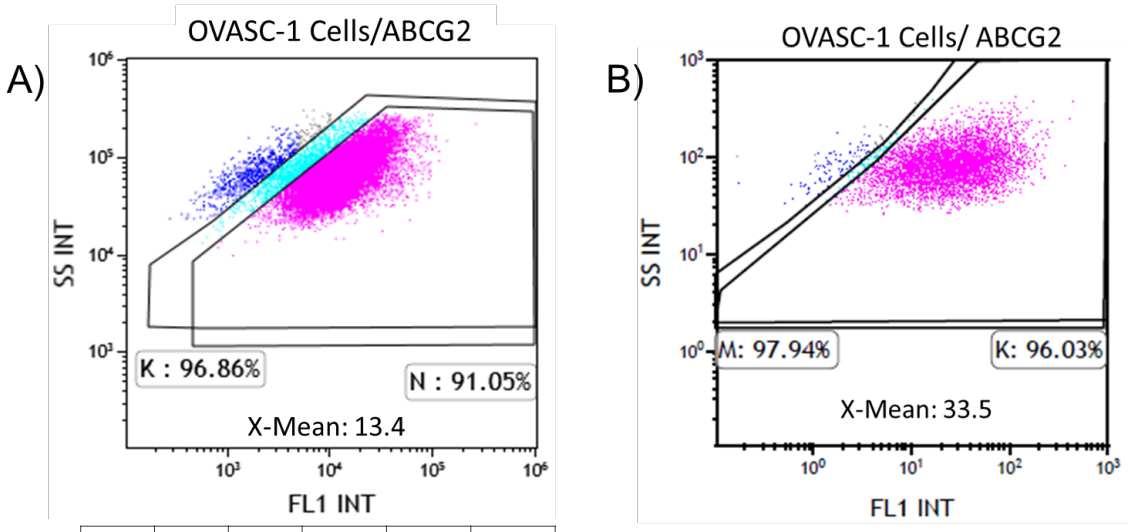

Region	Number	%Total	%Gated	X-Mean	Y-Mean
ALL	25000	85.44	100	13.4	69.3
K	24219	82.77	96.86	13.8	68.7
N	22737	77.71	91.05	14.3	67.2

Gate	Number	%Total	%Gated	X-Mean	Y-Mean
All	5,837	76.69	100	33.5	88.48
M	5,717	75.11	97.94	34.15	88.29
K	5,605	73.64	96.03	34.74	88

Figure 4.23: Evaluation of the expression of ABCG2 transporters on the surface of OVASC-1 cells. A) OVASC-1 cells grown in cell culture (in vitro) were labeled with fluorescent anti-ABCG2 primary antibody and analyzed by flow cytometry. X-mean denotes the fold difference in expression of the transporter on the surface of OVASC-1 cells stained with the anti-AGCG2 antibody in comparison to the IgG isotype control indicating the transporter density. B) OVASC-1 cells were harvested from the tumor of the non-responsive mouse that was treated with CPT-11 (40 mg/kg). Cells were propagated in vitro, labeled with fluorescent anti-ABCG2 primary antibody, and then analyzed by flow cytometry. X-mean denotes the fold difference in expression of the transporter on the surface of OVASC-1 cells stained with the anti-AGCG2 antibody in comparison to the IgG isotype control indicating the transporter density.

Mice in G4 received irinotecan (80 mg/kg) where three mice in this group showed a complete response and two exhibited a partial response. The two mice that partially responded and the one mouse with the complete response experienced significant weight variations, frequent diarrhea, low levels of activity, and a loss of appetite during the treatment period, suggesting the manifestation of GI-related toxicity. Mice in this group were euthanized either due to significant and rapid weight loss or formation of bulky ascites (Table 4.2, Figure 4.20E - 4.20F, Figure 4.24).

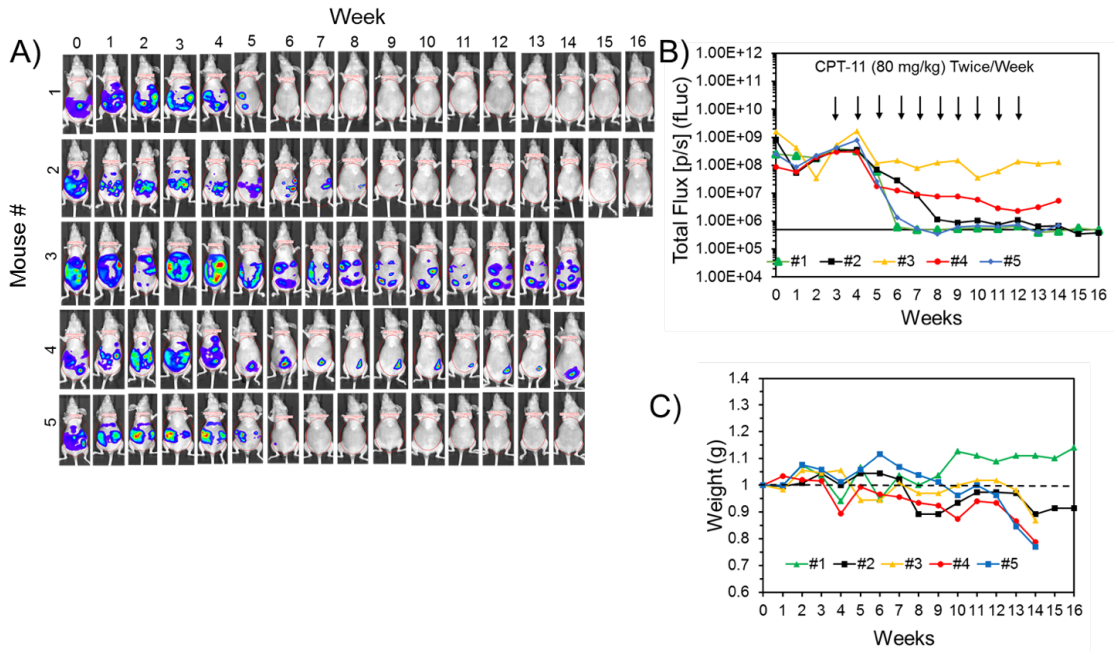

Figure 4.24: BLI and weight of nude mice with intraperitoneal tumors and quantification of bioluminescent signal over the treatment period with CPT-11 (80 mg/kg). A) BLI of nude mice with intraperitoneal tumors (firefly luciferase imaging). B) The quantification of bioluminescent signal over the treatment period with CPT-11 (80 mg/kg). Arrows denote the points at which the mice received treatment. The line at 5×10^5 (p/s) shows the background bioluminescence of mice body without any tumors. C) Change in mice weight over the treatment period. The weights of the mice before the treatment are normalized and considered as 1.

Mice in G5 were treated with ASC-shCE2:nLuc cells and irinotecan (40 mg/kg). The biolumi- nescent intensities of OVASC-1-fLuc tumors (firefly luciferase) and ASC-shCE2:nLuc cells (nanoluciferase) were measured and data related to each mouse analyzed. A quantitative analysis of bioluminescence levels of ASC-shCE2:nLuc cells measured before and after irinotecan injection shows that the ASC cells responded to the prodrug as evidenced by a significant change in signal intensity (Figure 4.25). Four mice in this group showed a complete response to therapy, remained healthy during the treatment period and did not show any signs of GI-related toxicity. Furthermore, we did not detect any bioluminescent signals even four weeks after the last day of therapy. One mouse in this group showed a > 90% response to therapy but the residual tumor was still detectable on the last day of therapy and relapsed when the therapy stopped (Table 4.2, Figure 4.20G - 4.20H, Figure 4.26). The relapsed tumor in this mouse was found to be the result of metastasis to regions outside of the peritoneal cavity.

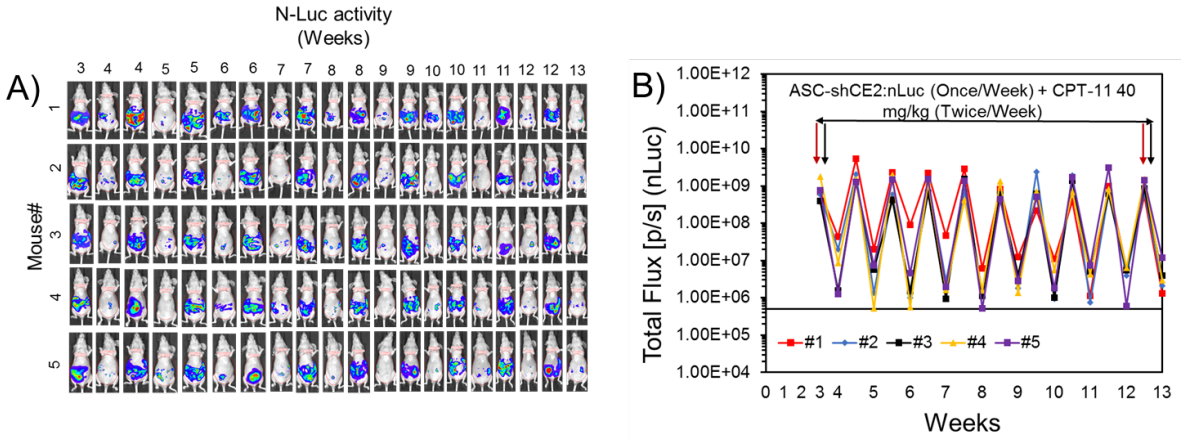

Figure 4.25: BLI of nude mice injected with ASC-shCE2:nLuc cells and CPT-11 (40 mg/kg) and quantification of nanoluciferase signal from the ASC-shCE2:nLuc cells. A) BLI of nude mice injected with ASC-shCE2:nLuc cells once a week for ten weeks and CPT-11 (40 mg/kg) twice a week for ten weeks. B) The quantification of bioluminescent signal (nanoluciferase) from the ASC-shCE2:nLuc cells over the treatment period with CPT-11 (40 mg/kg). Red arrow denotes the point at which the mice received cells and black arrow denotes the point at which the mice received CPT-11. The line at 5×10^5 (p/s) shows the background bioluminescence of mice body without any tumors. The significant drop in bioluminescent signal intensity indicates the death of ASC-shCE2:nLuc cells after CPT-11 injection.

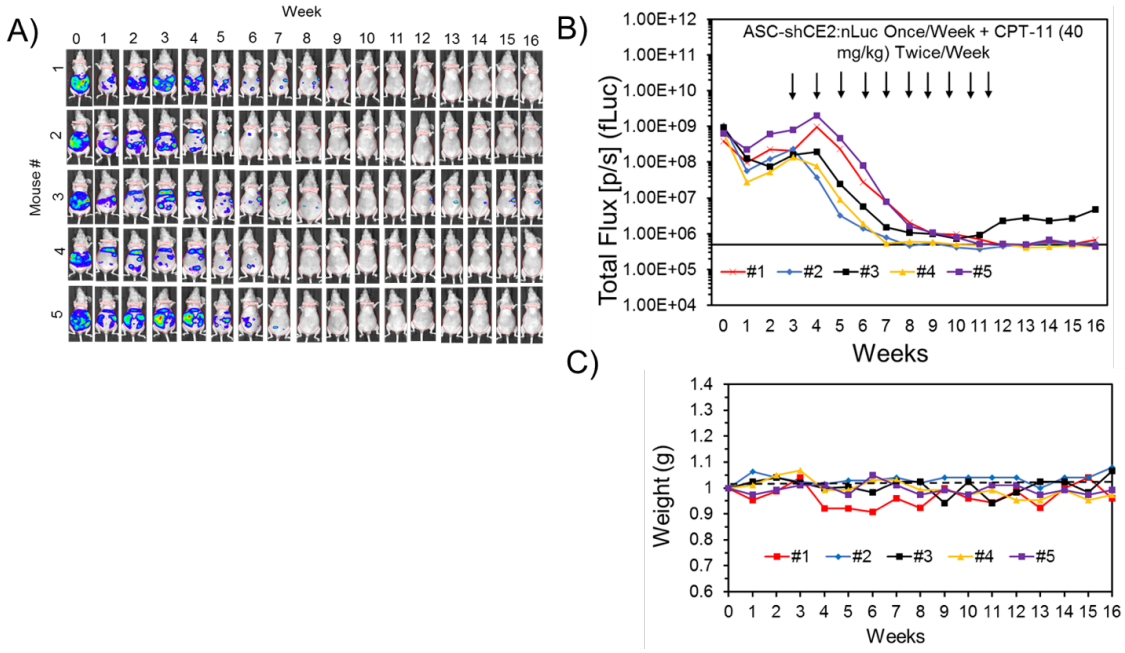

Figure 4.26: The quantification of the bioluminescent signal and change in mice weight over the treatment period with shCE2/CPT-11 (40 mg/kg). A) BLI of nude mice with intraperitoneal tumors (firefly luciferase imaging). B) The quantification of the bioluminescent signal over the treatment period with CPT-11 (40 mg/kg). Arrows denote the points at which the mice received treatment. The line at 5×10^5 (p/s) shows the background bioluminescence of mice body without any tumors. C) Change in mice weight over the treatment period. The weights of the mice before the treatment are normalized and considered as 1.

The statistical analysis of bioluminescent signal intensity levels among groups (ANOVA, Post hoc Tukey test, *$p < .05$) in conjunction with the Kaplan-Meier Survival Estimator show that the treatment of mice bearing drug-resistant intraperitoneal tumors with cisplatin+PTX neither reduced the tumor mass ($p = 0.78$) nor provided a survival benefit (0% survival rate) (Figure 4.27A- 4.27B, Table 4.3). Data analysis also shows that relative to cisplatin+PTX treated group, the treatment of mice with irinotecan 40 mg/kg ($p = .027$) and irinotecan 80 mg/kg ($p = .0005$) significantly reduced tumor masses and increased survival rates by 20% and 40%, respectively (Figure 4.27A- 4.27B, Table 4.3).

The observed 80% death in G3 (irinotecan 40 mg/kg) occurring after treatment was due to disease progression, the formation of bulky ascites and interference with normal vital organs' functions. In contrast, the observed 60% death in G4 (irinotecan 80 mg/kg) occurring during the treatment period, was mainly due to toxicity to the GI tract. Overall, the treatment of mice with ASC-shCE2:nLuc plus irinotecan (40 mg/kg) was found to be the most effective in reducing the tumor burden ($p = 0.000043$), delivering complete responses and increasing survival rates in 80% of the mice without any observable treatment-related toxicity (Figure 4.27A- 4.27B, Table 4.3).

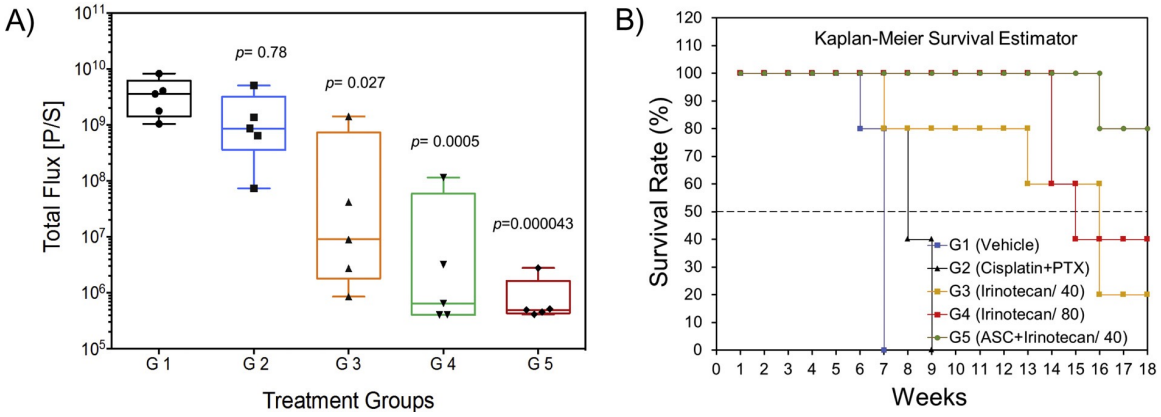

Figure 4.27. Evaluation of response to therapy and survival rate in mice groups: A) Evaluation of the responses to therapy from the bioluminescence signal intensity (total flux) of the tumor burden observed immediately after the last treatment point. (*ANOVA, followed by Post hoc Tukey test). In this figure, the statistical significance (p value) is shown for G2 when compared to G1. G3, G4 and G5 are compared to G2 with the corresponding p values. B) Evaluation of survival benefit by Kaplan-Meier survival estimator. The survival rates for G1 to G5 were 0%, 0%, 20%, 40% and 80%, respectively. For details of the data analysis for this test please see Table 4.3.

Table 4.3: Kaplan-Meier survival estimator data highlighting the increase in survival time and percent survival among the groups.

	Mean				Survival
			95% Confidence Interval		
Treatment	Estimate	Std. Error	Lower Bound	Upper Bound	Percent
Control, untreated	6.800	.200	6.408	7.192	0%
Cisplatin + PTX (5 + 15 mg/kg)	8.200	.374	7.467	8.933	0%
CPT-11 (40 mg/kg)	14.000	1.720	10.628	17.372	20%
CPT-11 (80 mg/kg)	15.800	.820	14.193	17.407	40%
ASC + CPT-11 (40 mg/kg)	17.600	.358	16.899	18.301	80%

4.2.6 Evaluation of tissue toxicity by histopathology and hematology

The monitoring of weight over the treatment period shows that mice in G2, G3 and G5 tolerated the therapy as evidenced by negligible negative impacts on weight changes (Figure. 4.19 – 4.27). However, the mice in G4 treated with irinotecan (80 mg/kg) exhibited significant weight variations, a loss of appetite, lethargy and frequent diarrhea. To investigate whether any toxicity occurred at the cellular level, we applied histopathological methods to major peritoneal organs. An analysis of tissue slides did not reveal any notable toxicity to the peritoneal organs of mice in any group (Figure. 4.28). Furthermore, we analyzed mice blood (hematology) because neutropenia is one of the hematological toxicities (rare) reported in patients treated with irinotecan. The results show that mice in all groups tolerated the therapy and that there was no significant change to any of the blood factors (Table 4.4).

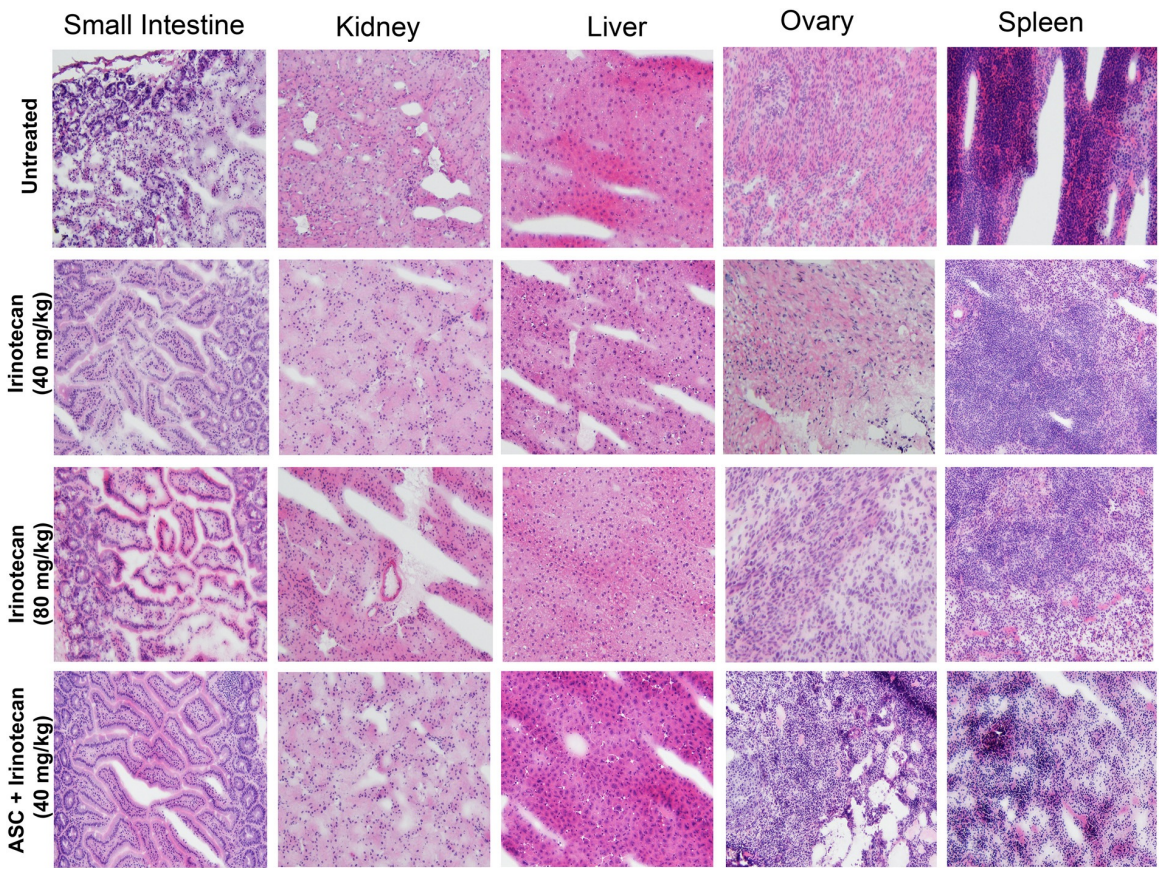

Figure 4.28: Hematoxylin and eosin (H& E) staining of dissected mouse peritoneal organs. Photomicrography was conducted by using a Leica microscope with a 20× objective. Mice in different treatment groups showed no morphologic changes in major intraperitoneal organs reviewed as compared to control mice.

Table 4.4: Analysis of blood factors in mice groups 1 to 5. No significant hematological toxicity was observed in mice of any group.

Test	Vehicle control	CPT-11 40 mg/kg	CPT-11 80 mg/kg	ASC-shCE2 + CPT-11 (40 mg/kg)	Normal range	Units
WBC	2.37	5.82	3.2	5.29	0.80 - 10.60	10^3/µL
NEU	0.42	1.17	0.52	1.59	0.23 - 3.60	10^3/µL
LYM	1.80	3.51	2.03	2.47	0.60 - 8.90	10^3/µL
MONO	0.12	0.95	0.31	0.57	0.04 - 1.40	10^3/µL
EOS	0.03	0.13	0.29	**0.52**	0.00 - 0.51	10^3/µL
BAS	0.01	0.06	0.05	0.01	0.00 - 0.12	10^3/µL
RBC	7.73	8.22	7.79	7.81	6.50 - 11.50	10^6/µL
HGB	15.5	14.7	14.6	14.8	11.00 - 16.50	g/dL
HCT	42.8	43.8	43	43.7	35.00 - 55.00	%
MCV	**55.3**	53.3	55.2	**55.65**	41.00 - 55.00	fL
MCH	19.3	17.9	18.7	18.65	13.00 - 18.00	pg
MCHC	35.1	33.5	33.9	33.7	30.00 - 36.00	g/dL
RDW %	12.05	13.7	14.1	12.85	12.00 - 19.00	%
PLT	**356**	1347	778	533	400 - 1600	10^3/µL
MPV	6.15	5.4	7.3	5.9	4.00 - 6.2	fL

4.3 Discussion

As a first step toward achieving our objectives, we obtained OVASC- 1 cells from a patient with recurrent ovarian cancer and used them as a drug-resistant model in this study. To validate the resistance of this model to chemotherapeutics and to identify an effective enzyme/prodrug system for its treatment, we treated OVASC-1 cells with cisplatin, 5-FU, SN-38 and 6-MP. The results of cell viability and clonogenic assays showed that OVASC-1 cells were highly resistant to cisplatin and even more so than A2780-Cis as well as to the prodrug metabolites. The only drug that could kill the OVASC-1 cells within a low nanomolar range was SN-38. Based on this outcome and given that the potency of prodrug metabolites plays an important role in the anticancer efficacy of enzyme/prodrug systems, we selected CE2/ irinotecan as the most suitable one for the subsequent in vivo studies. To identify factors contributing to OVASC-1 cell resistance to chemotherapy, we measured percentages of ALDH+ cells and CICs (CSCs) as these two cell populations have been shown to be key players in imparting drug resistance. Interestingly, the LDA showed that almost 5% of the cell population exhibited stem-like characteristics with the ability to self-renew and generate new colonies. Although published data with established cell lines show that usually < 2% of cancer cell populations are CSCs [228], it was curious to observe that approximately 5% of the OVASC-1 cells had stem-like characteristics. From our data and similar observations by other groups [229, 230], it appears that donor's (patient) treatment with chemotherapeutics may have led to enrichment in CSC populations. While cancer cells develop resistance against anticancer drugs through a variety of different mechanisms [231], overall it appears that the presence of high percentages of ALDH+ cells, CSCs, and

MDR-1/ ABCG2 positive cells are among the main factors contributing to OVASC-1 cell drug resistance. As a next step, we characterized OVASC-1 cells as tumorspheres because almost all ovarian cancer patients have ascites at recurrence with leaked cancer cells into the peritoneal cavity and existing as spheroids (tumorspheres). The significance of tumorspheres lies in their exhibiting cancer stem-like phenotypes and the capacity for distal meta- static spread [232]. Our OVASC-1 tumorsphere characterization studies show that they are enriched with CSCs with significantly high expressions of ABCG2 transporters. Since ABCG2 transporters are responsible for resistance to SN-38 [29, 30], we examined whether the selection of SN-38 as the most effective prodrug metabolite used in this study was also effective against tumorspheres. We observed that SN-38 can era- dicate OVASC-1 tumorspheres as long as they are exposed to at least 100 nM of the drug. While this is exciting, achieving this drug concentration within tumors may be difficult through systemic chemotherapy, as many patients may not be able tolerate the associated cytotoxicity to normal tissues. To address this dilemma, we hypothesized that by using MSCs that express shCE2 enzyme and in combina- tion with irinotecan, high concentrations of SN-38 can be targeted and delivered to tumors killing OVASC-1 drug-resistant cells but without toxicity to normal tissues. It is noteworthy that SN-38 is approximately 1000 fold more potent than its prodrug irinotecan [143]. MSCs are known to be recruited to sites of wound healing and growing tumors (wounds that do not heal) due to their repair functions [233-235]. The migration and extravasation of mesenchymal stem cells into a tumor tissue involves an active process driven by tumor-secreted cytokines [236]. This characteristic of MSCs is currently being exploited in both preclinical and clinical studies to develop more effective and less toxic treatments for different types of cancer [237-239] (clinicaltrials.gov,

NCT02530047 and NCT02015819). To test the hypothesis, we genetically engineered a clone of ASCs that stably expressed both shCE2 and nanoluciferase genes (ASC-shCE2:nLuc). The expression and functionality of both enzymes were confirmed via an enzyme activity assay, LC/MS and a cell toxicity assay. We then examined whether the genetically engineered ASCs could migrate toward ovarian peritoneal tumors after IP injection. The live cell tracking study shows that in the absence of intraperitoneal tumors, ASCs tend to migrate toward mesentery (ASC niche) after IP injection. This observation is consistent with past reports on the fate of MSCs after intraperitoneal administration [240]. However, in the presence of intraperitoneal tumors the ASCs colocalized with cancer cells as soon as three days post injection. SPION-loaded ASCs also afforded us the opportunity to locate ASCs within the peritoneal cavity by MRI at a higher resolution. From the MRI images we identified hot spots otherwise hidden from human eyes. Using MRI results as a guide, we dissected the mouse abdomen and detected several tumors hidden under the liver. Interestingly, the presence of SPION-loaded ASCs in tumors made it possible for us to detect them easily owing to their blackened surfaces. This suggests that engineered SPION-loaded ASCs can be used by surgeons to accurately mark sites of metastasis by MRI and to then perform more successful debulking surgery procedures given the tumors' darkened surfaces. Most importantly, the immune/ histochemistry of tumor tissues showed a localization of ASCs in both tumor stroma and necrotic regions, providing a unique opportunity to deliver therapeutics to not only the tumor stroma in which the tumor supporting cells such as fibroblasts and tumor-associated macrophages reside, but also to necrotic and hypoxic regions in which the CSCs reside [241, 242].

Our in vivo data show that the treatment of OVASC-1 tumors with cisplatin and PTX did not result in a statistically significant therapy response. Since the OVASC-1 cells were isolated from a patient with recurrent drug-resistant disease, this response rate was expected. In contrast, mice treated with 40 mg/kg of irinotecan showed a significant response to therapy although the survival benefit was marginal (20%). This survival rate is in agreement with clinical outcomes of ovarian cancer therapy using irinotecan, which has survival benefits of 10% to 30% [212]. These results also indicate that a 40 mg/kg drug concentration is sufficient in killing mostly the drug-sensitive cell populations and with negligible drug-related toxicity during the treatment period. However, this drug dose was inadequate in killing the drug- resistant cell population, as 4/5 mice exhibited a partial response followed by cancer relapse. An analysis of ABCG2 transporter expression in nonresponsive mice in this group showed a significant upregulation of this transporter. This result is consistent with published data de- noting ABCG2 as a major source of cancer resistance to therapy with irinotecan /SN-38 [29, 30, 213]. As a next step, we doubled the drug dose to 80 mg/kg to push the limits close to the maximum tolerating dose to examine the possibility of obtaining a superior therapy response [243].

While we observed a more significant response to therapy (3 mice were cured), unfortunately one of the cured mice died and two others with partial responses also showed severe signs of drug-related toxicity such as frequent diarrhea and significant body weight loss. Although treatment with higher concentrations of irinotecan cured more mice of the disease, it also led to higher rates of treatment-related mortality. To limit toxicity to the tumors and to preserve healthy tissues, we treated another group of mice with ASC-shCE2:nLuc cells in combination with the safe irinotecan dose (i.e., 40 mg/kg). The dosing

regimen was scheduled such that the first drug dose was administered 72 h after ASC injection. This was adopted to leave ample time for the ASCs to migrate to tumors, colocalize with cancer cells and secrete high concentrations of CE2. In addition, rather than providing a bolus dose, the irinotecan was injected in two separate smaller doses to minimize drug-related toxicity. Based on our preliminary studies we also found that leaving 48 h of lag time in between the first and second dose of irinotecan is more effective than daily administration. The outcomes of this therapeutic protocol show that mice in this group responded fully to the therapy without any signs of toxicity. In fact, 4/5 mice in this group remained cancer free for at least six weeks post treatment and did not show any signs of cancer relapse or toxicity to normal tissues. Overall, the data show that shCE2-expressing ASCs applied in combination with irinotecan can kill drug-resistant OVASC-1 tumors more effectively than applying irinotecan alone or cisplatin+PTX. Regarding the safety of this approach, hematology and histopathology results show that the toxic effects of therapy were limited to tumor tissues, as we could not detect any negative impacts on blood factors (e.g., neutropenia and leukopenia) or on major intraperitoneal organs. In the clinic, major forms of nonhematological toxicity that interrupt cancer therapy with irinotecan are GI-related and echo what we observed in G4 (e.g., diarrhea, vomiting, edema, etc.) [212]. Overall, our toxicity data in combination with efficacy outcomes reveal a very promising non-surgical approach to overcoming drug resistance in recurrent metastatic ovarian cancer.

4.4 Conclusions

Two ongoing clinical trials on the use of stem cells for the targeted therapy of ovarian cancer are currently underway (NCT02068794 and NCT02530047) setting the stage for future stem cell-mediated therapeutics. Our data show that SN-38 is more effective as a prodrug metabolite than 5-FU and 6-MP. Therefore, CE2/irinotecan was used as the most effective enzyme/prodrug system for killing drug-sensitive and resistant ovarian cancer cells. As the data presented in this work showed a complete tumor response and imparted survival benefits in 80% of the subjects, stem cell-mediated suicide gene therapy delivered through the shCE2/irinotecan system appears to constitute an effective nonsurgical means of treating recurrent ovarian cancer with intraperitoneal metastasis. The developed stem cell-mediated tumor-selective approach has the potential to be used for the treatment of other cancers of peritoneal cavity, such as those of the liver, pancreas, stomach, kidneys and colon.

Chapter 5

General Conclusions

Late diagnosis of ovarian cancer can lead to peritoneal metastasis and significantly reduces the efficacy of cancer treatment and increase the chance of cancer relapse. One of the major causes of inadequate response to treatment is the creation of drug-resistant CSCs. Developing therapeutic methods that can target these cells can improve the outcomes of treatments. In this project, Ascites-derived malignant cells (OVASC-1) obtained from a patient, were found to have CSCs with unlimited renewal capacity in suspension culture. We formed tumorspheres under in vitro condition to test different anticancer drugs on CSCs and found that the combination of MMAE, and SN-38 can either significantly diminish or completely eradicate CSC spheroids with effective doses as low as 10 nM. Importantly, no evidence of recurrence (repopulation of spheroids) was observed in MMAE and SN-38 treated group even after 30 days of post-treatment. Testing our combination therapy method in a xenograft model of ovarian cancer showed the efficacy of the method. These results with the two chemotherapeutic drugs show their ability to kill highly drug-resistant CSC-rich tumors in the ovarian cancer patients.

In ovarian cancer patients who are not suitable candidates for debulking surgery, we developed a different treatment method by using an enzyme prodrug system. As a model, we used OVASC-1 cancer cells that show significant resistance to chemotherapy. To treat OVASC-1 peritoneal tumors, adipose-derived stem cells (ASCs) that have tumor-tropic properties were first genetically modified to express secretory human carboxylesterase (shCE-2) enzyme and then injected into the mice peritoneal cavity. Subsequently, CPT-11 was administered to be converted into its cytotoxic form (i.e., SN-38) by the secreted hCE-2 from the ASCs.

Our results showed ASCs tropism toward the tumor site. Complete response and a

lower chance of relapse was observed in the shCE-2/CPT-11 treated group. There was no sign of toxicity in histopathology and hematology studies. Our findings suggest that Carboxylesterase/CPT-11 system is an effective treatment against metastatic and highly drug-resistant ovarian cancer tumor cells.

This research showed that low-dose localized therapy with MMAE and SN-38 after debulking surgery or the stem cell-mediated suicide gene therapy by the shCE2/CPT-11 system in patients that cannot go through debulking surgery could be considered as effective new approaches for ovarian cancer therapy. These methods can also be evaluated for other types of cancer with intraperitoneal metastasis.

References

1. Stewart, C., C. Ralyea, and S. Lockwood, *Ovarian Cancer: An Integrated Review.* Semin Oncol Nurs, 2019. **35**(2): p. 151-156.
2. Alberts, D.S., et al., *Improved therapeutic index of carboplatin plus cyclophosphamide versus cisplatin plus cyclophosphamide: final report by the Southwest Oncology Group of a phase III randomized trial in stages III and IV ovarian cancer.* J Clin Oncol, 1992. **10**(5): p. 706-17.
3. Hennessy, B.T., R.L. Coleman, and M. Markman, *Ovarian cancer.* Lancet, 2009. **374**(9698): p. 1371-82.
4. Young, R.C., et al., *Adjuvant therapy in stage I and stage II epithelial ovarian cancer. Results of two prospective randomized trials.* N Engl J Med, 1990. **322**(15): p. 1021-7.
5. Dyall, S., S.A. Gayther, and D. Dafou, *Cancer stem cells and epithelial ovarian cancer.* J Oncol, 2010. **2010**: p. 105269.
6. Ochiai, K., *[Strategy for the ovarian cancer treatment].* Gan To Kagaku Ryoho, 1993. **20**(16): p. 2454-60.
7. Ozols, R.F., *Chemotherapy for ovarian cancer.* Semin Oncol, 1999. **26**(6 Suppl 18): p. 34-40.
8. Shah, M.M. and C.N. Landen, *Ovarian cancer stem cells: are they real and why are they important?* Gynecol Oncol, 2014. **132**(2): p. 483-9.
9. Burgos-Ojeda, D., B.R. Rueda, and R.J. Buckanovich, *Ovarian cancer stem cell markers: prognostic and therapeutic implications.* Cancer Lett, 2012. **322**(1): p. 1-7.
10. Wright, A.A., et al., *Use and Effectiveness of Intraperitoneal Chemotherapy for Treatment of Ovarian Cancer.* J Clin Oncol, 2015. **33**(26): p. 2841-7.
11. Armstrong, D.K., et al., *Intraperitoneal cisplatin and paclitaxel in ovarian cancer.* N Engl J Med, 2006. **354**(1): p. 34-43.
12. Shah, V., et al., *Targeted nanomedicine for suppression of CD44 and simultaneous cell death induction in ovarian cancer: an optimal delivery of siRNA and anticancer drug.* Clin Cancer Res, 2013. **19**(22): p. 6193-204.
13. Savla, R., et al., *Tumor-targeted responsive nanoparticle-based systems for magnetic resonance imaging and therapy.* Pharm Res, 2014. **31**(12): p. 3487-502.
14. Sarkar, S., et al., *Chemoprevention gene therapy (CGT) of pancreatic cancer using perillyl alcohol and a novel chimeric serotype cancer terminator virus.* Curr Mol Med, 2014. **14**(1): p. 125-40.
15. Webb, J., *Effects of more than one inhibitor. In: Webb JL (ed) Enzyme and metabolic inhibitors.* Academic Press, 1963. **1**: p. 487-512.
16. Nouri, F.S., X. Wang, and A. Hatefi, *Genetically engineered theranostic mesenchymal stem cells for the evaluation of the anticancer efficacy of enzyme/prodrug systems.* J Control Release, 2015. **200**: p. 179-87.
17. Burleson, K.M., et al., *Disaggregation and invasion of ovarian carcinoma ascites spheroids.* J Transl Med, 2006. **4**: p. 6.

18. Desoize, B. and J. Jardillier, *Multicellular resistance: a paradigm for clinical resistance?* Crit Rev Oncol Hematol, 2000. **36**(2-3): p. 193-207.
19. Pettit, G.R., et al., *Antineoplastic agents 337. Synthesis of dolastatin 10 structural modifications.* Anticancer Drug Des, 1995. **10**(7): p. 529-44.
20. Doronina, S.O., et al., *Development of potent monoclonal antibody auristatin conjugates for cancer therapy.* Nat Biotechnol, 2003. **21**(7): p. 778-84.
21. Malekshah, O.M., et al., *Enzyme/Prodrug Systems for Cancer Gene Therapy.* Curr Pharmacol Rep, 2016. **2**(6): p. 299-308.
22. Baldwin, E.L. and N. Osheroff, *Etoposide, topoisomerase II and cancer.* Curr Med Chem Anticancer Agents, 2005. **5**(4): p. 363-72.
23. Dasari, S. and P.B. Tchounwou, *Cisplatin in cancer therapy: molecular mechanisms of action.* Eur J Pharmacol, 2014. **740**: p. 364-78.
24. Parker, W.B., et al., *Metabolism and metabolic actions of 6-methylpurine and 2-fluoroadenine in human cells.* Biochem Pharmacol, 1998. **55**(10): p. 1673-81.
25. Karjoo, Z., X. Chen, and A. Hatefi, *Progress and problems with the use of suicide genes for targeted cancer therapy.* Adv Drug Deliv Rev, 2016. **99**(Pt A): p. 113-128.
26. Longley, D.B., D.P. Harkin, and P.G. Johnston, *5-fluorouracil: mechanisms of action and clinical strategies.* Nat Rev Cancer, 2003. **3**(5): p. 330-8.
27. Chen, R., et al., *CD30 Downregulation, MMAE Resistance, and MDR1 Upregulation Are All Associated with Resistance to Brentuximab Vedotin.* Mol Cancer Ther, 2015. **14**(6): p. 1376-84.
28. Tagen, M., et al., *P-glycoprotein, but not multidrug resistance protein 4, plays a role in the systemic clearance of irinotecan and SN-38 in mice.* Drug Metab Lett, 2010. **4**(4): p. 195-201.
29. Tuy, H.D., et al., *ABCG2 expression in colorectal adenocarcinomas may predict resistance to irinotecan.* Oncol Lett, 2016. **12**(4): p. 2752-2760.
30. Jandu, H., et al., *Molecular characterization of irinotecan (SN-38) resistant human breast cancer cell lines.* BMC Cancer, 2016. **16**: p. 34.
31. Helland, O., et al., *First in-mouse development and application of a surgically relevant xenograft model of ovarian carcinoma.* PLoS One, 2014. **9**(3): p. e89527.
32. Campos, M.P. and G.E. Konecny, *The target invites a foe: antibody-drug conjugates in gynecologic oncology.* Curr Opin Obstet Gynecol, 2018. **30**(1): p. 44-50.
33. Senter, P.D. and E.L. Sievers, *The discovery and development of brentuximab vedotin for use in relapsed Hodgkin lymphoma and systemic anaplastic large cell lymphoma.* Nat Biotechnol, 2012. **30**(7): p. 631-7.
34. van de Donk, N.W. and E. Dhimolea, *Brentuximab vedotin.* MAbs, 2012. **4**(4): p. 458-65.
35. Forbes, N.S., *Engineering the perfect (bacterial) cancer therapy.* Nat Rev Cancer, 2010. **10**(11): p. 785-94.
36. Cattaneo, R., et al., *Reprogrammed viruses as cancer therapeutics: targeted, armed and shielded.* Nature reviews. Microbiology, 2008. **6**(7): p. 529-540.
37. Mohit, E. and S. Rafati, *Biological delivery approaches for gene therapy: strategies to potentiate efficacy and enhance specificity.* Mol Immunol, 2013. **56**(4): p. 599-611.

38. Yi, Y., M.J. Noh, and K.H. Lee, *Current advances in retroviral gene therapy.* Curr Gene Ther, 2011. **11**(3): p. 218-28.
39. Dass, C.R. and P.F. Choong, *Non-viral methods for gene transfer towards osteosarcoma therapy.* J Drug Target, 2007. **15**(3): p. 184-9.
40. Braybrooke, J.P., et al., *Phase I study of MetXia-P450 gene therapy and oral cyclophosphamide for patients with advanced breast cancer or melanoma.* Clin Cancer Res, 2005. **11**(4): p. 1512-20.
41. Wold, W.S. and K. Toth, *Adenovirus vectors for gene therapy, vaccination and cancer gene therapy.* Curr Gene Ther, 2013. **13**(6): p. 421-33.
42. Kim, K.H., et al., *A phase I clinical trial of Ad5.SSTR/TK.RGD, a novel infectivity-enhanced bicistronic adenovirus, in patients with recurrent gynecologic cancer.* Clin Cancer Res, 2012. **18**(12): p. 3440-51.
43. Majhen, D., et al., *Adenovirus-based vaccines for fighting infectious diseases and cancer: progress in the field.* Hum Gene Ther, 2014. **25**(4): p. 301-17.
44. Santiago-Ortiz, J.L. and D.V. Schaffer, *Adeno-associated virus (AAV) vectors in cancer gene therapy.* J Control Release, 2016. **240**: p. 287-301.
45. Mingozzi, F. and K.A. High, *Immune responses to AAV vectors: overcoming barriers to successful gene therapy.* Blood, 2013. **122**(1): p. 23-36.
46. Munch, R.C., et al., *Displaying high-affinity ligands on adeno-associated viral vectors enables tumor cell-specific and safe gene transfer.* Mol Ther, 2013. **21**(1): p. 109-18.
47. Voges, J., et al., *Imaging-guided convection-enhanced delivery and gene therapy of glioblastoma.* Ann Neurol, 2003. **54**(4): p. 479-87.
48. Kang, Y., et al., *Tumor-directed gene therapy in mice using a composite nonviral gene delivery system consisting of the piggyBac transposon and polyethylenimine.* BMC Cancer, 2009. **9**: p. 126.
49. Cortez, M.A., et al., *The Synthesis of Cyclic Poly(ethylene imine) and Exact Linear Analogues: An Evaluation of Gene Delivery Comparing Polymer Architectures.* J Am Chem Soc, 2015. **137**(20): p. 6541-9.
50. Canine, B.F., Y. Wang, and A. Hatefi, *Biosynthesis and characterization of a novel genetically engineered polymer for targeted gene transfer to cancer cells.* J Control Release, 2009. **138**(3): p. 188-96.
51. Wang, Y., B.F. Canine, and A. Hatefi, *HSV-TK/GCV cancer suicide gene therapy by a designed recombinant multifunctional vector.* Nanomedicine, 2011. **7**(2): p. 193-200.
52. Nouri, F.S., et al., *A recombinant biopolymeric platform for reliable evaluation of the activity of pH-responsive amphiphile fusogenic peptides.* Biomacromolecules, 2013. **14**(6): p. 2033-40.
53. Hoffman, R.M. and M. Zhao, *Methods for the development of tumor-targeting bacteria.* Expert Opin Drug Discov, 2014. **9**(7): p. 741-50.
54. MacDiarmid, J.A. and H. Brahmbhatt, *Minicells: versatile vectors for targeted drug or si/shRNA cancer therapy.* Curr Opin Biotechnol, 2011. **22**(6): p. 909-16.
55. Tsuji, S., et al., *Preclinical evaluation of VAX-IP, a novel bacterial minicell-based biopharmaceutical for nonmuscle invasive bladder cancer.* Mol Ther Oncolytics, 2016. **3**: p. 16004.

56. Aboody, K.S., et al., *Neural stem cell-mediated enzyme/prodrug therapy for glioma: preclinical studies.* Sci Transl Med, 2013. **5**(184): p. 184ra59.
57. Kan, O., et al., *Direct retroviral delivery of human cytochrome P450 2B6 for gene-directed enzyme prodrug therapy of cancer.* Cancer Gene Ther, 2001. **8**(7): p. 473-82.
58. Nouri, F.S., D. Banerjee, and A. Hatefi, *Practical Issues with the Use of Stem Cells for Cancer Gene Therapy.* Stem Cell Rev, 2015. **11**(5): p. 688-98.
59. Caruso, M., et al., *Regression of established macroscopic liver metastases after in situ transduction of a suicide gene.* Proc Natl Acad Sci U S A, 1993. **90**(15): p. 7024-8.
60. Floeth, F.W., et al., *Local inflammation and devascularization--in vivo mechanisms of the "bystander effect" in VPC-mediated HSV-Tk/GCV gene therapy for human malignant glioma.* Cancer Gene Ther, 2001. **8**(11): p. 843-51.
61. Nemunaitis, J., et al., *A phase I study of telomerase-specific replication competent oncolytic adenovirus (telomelysin) for various solid tumors.* Mol Ther, 2010. **18**(2): p. 429-34.
62. Chen, X., et al., *Cancer-specific promoters for expression-targeted gene therapy: ran, brms1 and mcm5.* J Gene Med, 2016. **18**(7): p. 89-101.
63. Chen, X.G. and W.T. Godbey, *The potential of the human osteopontin promoter and single-nucleotide polymorphisms for targeted cancer gene therapy.* Curr Gene Ther, 2015. **15**(1): p. 82-92.
64. Hine, C.M., A. Seluanov, and V. Gorbunova, *Rad51 promoter-targeted gene therapy is effective for in vivo visualization and treatment of cancer.* Mol Ther, 2012. **20**(2): p. 347-55.
65. Davis, J.J., et al., *Oncolysis and suppression of tumor growth by a GFP-expressing oncolytic adenovirus controlled by an hTERT and CMV hybrid promoter.* Cancer Gene Ther, 2006. **13**(7): p. 720-3.
66. Greco, O., et al., *Mechanisms of cytotoxicity induced by horseradish peroxidase/indole-3-acetic acid gene therapy.* J Cell Biochem, 2002. **87**(2): p. 221-32.
67. Schlabach, M.R., et al., *Synthetic design of strong promoters.* Proc Natl Acad Sci U S A, 2010. **107**(6): p. 2538-43.
68. Chen, H., G.P. Beardsley, and D.M. Coen, *Mechanism of ganciclovir-induced chain termination revealed by resistant viral polymerase mutants with reduced exonuclease activity.* Proc Natl Acad Sci U S A, 2014. **111**(49): p. 17462-7.
69. Nasu, Y., et al., *Suicide gene therapy with adenoviral delivery of HSV-tK gene for patients with local recurrence of prostate cancer after hormonal therapy.* Mol Ther, 2007. **15**(4): p. 834-40.
70. Aguilar, L.K., et al., *Gene-mediated cytotoxic immunotherapy as adjuvant to surgery or chemoradiation for pancreatic adenocarcinoma.* Cancer Immunol Immunother, 2015. **64**(6): p. 727-36.
71. Sangro, B., et al., *A phase I clinical trial of thymidine kinase-based gene therapy in advanced hepatocellular carcinoma.* Cancer Gene Ther, 2010. **17**(12): p. 837-43.
72. Traversari, C., et al., *The potential immunogenicity of the TK suicide gene does not prevent full clinical benefit associated with the use of TK-transduced donor*

lymphocytes in HSCT for hematologic malignancies. Blood, 2007. **109**(11): p. 4708-15.
73. Wu, L., et al., *Connexin32mediated antitumor effects of suicide gene therapy against hepatocellular carcinoma: In vitro and in vivo anticancer activity.* Mol Med Rep, 2016. **13**(4): p. 3213-9.
74. Adachi, M., et al., *Expression of MRP4 confers resistance to ganciclovir and compromises bystander cell killing.* J Biol Chem, 2002. **277**(41): p. 38998-9004.
75. Kokoris, M.S. and M.E. Black, *Characterization of herpes simplex virus type 1 thymidine kinase mutants engineered for improved ganciclovir or acyclovir activity.* Protein Sci, 2002. **11**(9): p. 2267-72.
76. Malekshah, O.M., et al., *PXR and NF-kappaB correlate with the inducing effects of IL-1beta and TNF-alpha on ABCG2 expression in breast cancer cell lines.* Eur J Pharm Sci, 2012. **47**(2): p. 474-80.
77. Hu, W. and W. Liu, *Side populations of glioblastoma cells are less sensitive to HSV-TK/GCV suicide gene therapy system than the non-side population.* In Vitro Cell Dev Biol Anim, 2010. **46**(6): p. 497-501.
78. Black, M.E., et al., *Creation of drug-specific herpes simplex virus type 1 thymidine kinase mutants for gene therapy.* Proc Natl Acad Sci U S A, 1996. **93**(8): p. 3525-9.
79. Preuss, E., et al., *Cancer suicide gene therapy with TK.007: superior killing efficiency and bystander effect.* J Mol Med (Berl), 2011. **89**(11): p. 1113-24.
80. Park, S.Y., et al., *Combination gene therapy using multidrug resistance (MDR1) gene shRNA and herpes simplex virus-thymidine kinase.* Cancer Lett, 2008. **261**(2): p. 205-14.
81. Xiong, T., et al., *Monitoring of bystander effect of herpes simplex virus thymidine kinase/acyclovir system using fluorescence resonance energy transfer technique.* J Biomed Nanotechnol, 2012. **8**(1): p. 74-9.
82. Shirakawa, T., et al., *Long-term outcome of phase I/II clinical trial of Ad-OC-TK/VAL gene therapy for hormone-refractory metastatic prostate cancer.* Hum Gene Ther, 2007. **18**(12): p. 1225-32.
83. Chiocca, E.A., et al., *Phase IB study of gene-mediated cytotoxic immunotherapy adjuvant to up-front surgery and intensive timing radiation for malignant glioma.* J Clin Oncol, 2011. **29**(27): p. 3611-9.
84. Huber, B.E., et al., *In vivo antitumor activity of 5-fluorocytosine on human colorectal carcinoma cells genetically modified to express cytosine deaminase.* Cancer Res, 1993. **53**(19): p. 4619-26.
85. Kerr, I.G., et al., *Effect of intravenous dose and schedule on cerebrospinal fluid pharmacokinetics of 5-fluorouracil in the monkey.* Cancer Res, 1984. **44**(11): p. 4929-32.
86. Fischer, U., et al., *Mechanisms of thymidine kinase/ganciclovir and cytosine deaminase/ 5-fluorocytosine suicide gene therapy-induced cell death in glioma cells.* Oncogene, 2005. **24**(7): p. 1231-43.
87. Deng, L.Y., et al., *Antitumor activity of mutant bacterial cytosine deaminase gene for colon cancer.* World J Gastroenterol, 2011. **17**(24): p. 2958-64.

88. Kaliberov, S.A., et al., *Mutation of Escherichia coli cytosine deaminase significantly enhances molecular chemotherapy of human glioma.* Gene Ther, 2007. **14**(14): p. 1111-9.
89. Kaliberova, L.N., et al., *Molecular chemotherapy of pancreatic cancer using novel mutant bacterial cytosine deaminase gene.* Mol Cancer Ther, 2008. **7**(9): p. 2845-54.
90. Nagy, B., et al., *Combined effect of cisplatin and 5-fluorouracil with irradiation on tumor cells in vitro.* Anticancer Res, 2002. **22**(1a): p. 135-8.
91. Shirakawa, T., et al., *Cytotoxicity of adenoviral-mediated cytosine deaminase plus 5-fluorocytosine gene therapy is superior to thymidine kinase plus acyclovir in a human renal cell carcinoma model.* J Urol, 1999. **162**(3 Pt 1): p. 949-54.
92. Trinh, Q.T., et al., *Enzyme/prodrug gene therapy: comparison of cytosine deaminase/5-fluorocytosine versus thymidine kinase/ganciclovir enzyme/prodrug systems in a human colorectal carcinoma cell line.* Cancer Res, 1995. **55**(21): p. 4808-12.
93. Johnson, A.J., et al., *Comparative analysis of enzyme and pathway engineering strategies for 5FC-mediated suicide gene therapy applications.* Cancer Gene Ther, 2011. **18**(8): p. 533-42.
94. Wang, F., et al., *Increased sensitivity of glioma cells to 5-fluorocytosine following photo-chemical internalization enhanced nonviral transfection of the cytosine deaminase suicide gene.* J Neurooncol, 2014. **118**(1): p. 29-37.
95. Miyagi, T., et al., *Gene therapy for prostate cancer using the cytosine deaminase/uracil phosphoribosyltransferase suicide system.* J Gene Med, 2003. **5**(1): p. 30-7.
96. Richard, C., et al., *Sensitivity of 5-fluorouracil-resistant cancer cells to adenovirus suicide gene therapy.* Cancer Gene Ther, 2007. **14**(1): p. 57-65.
97. Leveille, S., et al., *Enhancing VSV oncolytic activity with an improved cytosine deaminase suicide gene strategy.* Cancer Gene Ther, 2011. **18**(6): p. 435-43.
98. Ortiz de Montellano, P.R., *Cytochrome P450-activated prodrugs.* Future Med Chem, 2013. **5**(2): p. 213-28.
99. Roy, P. and D.J. Waxman, *Activation of oxazaphosphorines by cytochrome P450: application to gene-directed enzyme prodrug therapy for cancer.* Toxicol In Vitro, 2006. **20**(2): p. 176-86.
100. Chen, C.S., Y. Jounaidi, and D.J. Waxman, *Enantioselective metabolism and cytotoxicity of R-ifosfamide and S-ifosfamide by tumor cell-expressed cytochromes P450.* Drug Metab Dispos, 2005. **33**(9): p. 1261-7.
101. Giraud, B., et al., *Oxazaphosphorines: new therapeutic strategies for an old class of drugs.* Expert Opin Drug Metab Toxicol, 2010. **6**(8): p. 919-38.
102. Ross, A.D., et al., *Effect of propylthiouracil treatment on NADPH-cytochrome P450 reductase levels, oxygen consumption and hydroxyl radical formation in liver microsomes from rats fed ethanol or acetone chronically.* Biochem Pharmacol, 1995. **49**(7): p. 979-89.
103. Tychopoulos, M., et al., *A virus-directed enzyme prodrug therapy (VDEPT) strategy for lung cancer using a CYP2B6/NADPH-cytochrome P450 reductase fusion protein.* Cancer Gene Ther, 2005. **12**(5): p. 497-508.

104. Rodriguez-Antona, C., et al., *Cytochrome P450 expression in human hepatocytes and hepatoma cell lines: molecular mechanisms that determine lower expression in cultured cells.* Xenobiotica, 2002. **32**(6): p. 505-20.
105. Kumar, S., *Engineering cytochrome P450 biocatalysts for biotechnology, medicine and bioremediation.* Expert Opin Drug Metab Toxicol, 2010. **6**(2): p. 115-31.
106. Williams, E.M., et al., *Nitroreductase gene-directed enzyme prodrug therapy: insights and advances toward clinical utility.* Biochem J, 2015. **471**(2): p. 131-53.
107. Sharma, K., K. Sengupta, and H. Chakrapani, *Nitroreductase-activated nitric oxide (NO) prodrugs.* Bioorg Med Chem Lett, 2013. **23**(21): p. 5964-7.
108. Vass, S.O., et al., *E. coli NfsA: an alternative nitroreductase for prodrug activation gene therapy in combination with CB1954.* Br J Cancer, 2009. **100**(12): p. 1903-11.
109. Prosser, G.A., et al., *Discovery and evaluation of Escherichia coli nitroreductases that activate the anti-cancer prodrug CB1954.* Biochem Pharmacol, 2010. **79**(5): p. 678-87.
110. Swe, P.M., et al., *Targeted mutagenesis of the Vibrio fischeri flavin reductase FRase I to improve activation of the anticancer prodrug CB1954.* Biochem Pharmacol, 2012. **84**(6): p. 775-83.
111. Green, L.K., et al., *Pseudomonas aeruginosa NfsB and nitro-CBI-DEI--a promising enzyme/prodrug combination for gene directed enzyme prodrug therapy.* Mol Cancer, 2013. **12**: p. 58.
112. Prosser, G.A., et al., *Creation and screening of a multi-family bacterial oxidoreductase library to discover novel nitroreductases that efficiently activate the bioreductive prodrugs CB1954 and PR-104A.* Biochem Pharmacol, 2013. **85**(8): p. 1091-103.
113. Patel, P., et al., *A phase I/II clinical trial in localized prostate cancer of an adenovirus expressing nitroreductase with CB1954 [correction of CB1984].* Mol Ther, 2009. **17**(7): p. 1292-9.
114. Mitchell, D.J. and R.F. Minchin, *E. coli nitroreductase/CB1954 gene-directed enzyme prodrug therapy: role of arylamine N-acetlytransferase 2.* Cancer Gene Ther, 2008. **15**(11): p. 758-64.
115. Kestell, P., et al., *Pharmacokinetics and metabolism of the nitrogen mustard bioreductive drug 5.* Cancer Chemother Pharmacol, 2000. **46**(5): p. 365-74.
116. Davies, L.C., et al., *Novel fluorinated prodrugs for activation by carboxypeptidase G2 showing good in vivo antitumor activity in gene-directed enzyme prodrug therapy.* J Med Chem, 2005. **48**(16): p. 5321-8.
117. Francis, R.J., et al., *A phase I trial of antibody directed enzyme prodrug therapy (ADEPT) in patients with advanced colorectal carcinoma or other CEA producing tumours.* Br J Cancer, 2002. **87**(6): p. 600-7.
118. Spooner, R.A., et al., *A novel vascular endothelial growth factor-directed therapy that selectively activates cytotoxic prodrugs.* Br J Cancer, 2003. **88**(10): p. 1622-30.
119. Martin, J., et al., *Antibody-directed enzyme prodrug therapy: pharmacokinetics and plasma levels of prodrug and drug in a phase I clinical trial.* Cancer Chemother Pharmacol, 1997. **40**(3): p. 189-201.

120. Mayer, A., et al., *A phase I study of single administration of antibody-directed enzyme prodrug therapy with the recombinant anti-carcinoembryonic antigen antibody-enzyme fusion protein MFECP1 and a bis-iodo phenol mustard prodrug.* Clin Cancer Res, 2006. **12**(21): p. 6509-16.
121. Silamkoti, A.V., et al., *Synthesis and biological activity of 2-fluoro adenine and 6-methyl purine nucleoside analogs as prodrugs for suicide gene therapy of cancer.* Nucleosides Nucleotides Nucleic Acids, 2005. **24**(5-7): p. 881-5.
122. Sorscher, E.J., et al., *In vivo antitumor activity of intratumoral fludarabine phosphate in refractory tumors expressing E. coli purine nucleoside phosphorylase.* Cancer Chemother Pharmacol, 2012. **70**(2): p. 321-9.
123. Parker, W.B., et al., *Effect of expression of adenine phosphoribosyltransferase on the in vivo anti-tumor activity of prodrugs activated by E. coli purine nucleoside phosphorylase.* Cancer Gene Ther, 2011. **18**(6): p. 390-8.
124. Afshar, S., T. Asai, and S.L. Morrison, *Humanized ADEPT comprised of an engineered human purine nucleoside phosphorylase and a tumor targeting peptide for treatment of cancer.* Mol Cancer Ther, 2009. **8**(1): p. 185-93.
125. Rosenthal, E.L., et al., *Phase I dose-escalating trial of Escherichia coli purine nucleoside phosphorylase and fludarabine gene therapy for advanced solid tumors.* Ann Oncol, 2015. **26**(7): p. 1481-7.
126. Kim, D.S., S.E. Jeon, and K.C. Park, *Oxidation of indole-3-acetic acid by horseradish peroxidase induces apoptosis in G361 human melanoma cells.* Cell Signal, 2004. **16**(1): p. 81-8.
127. Huang, C., et al., *Apoptosis of pancreatic cancer BXPC-3 cells induced by indole-3-acetic acid in combination with horseradish peroxidase.* World J Gastroenterol, 2005. **11**(29): p. 4519-23.
128. Jeong, Y.M., et al., *Indole-3-acetic acid/horseradish peroxidase induces apoptosis in TCCSUP human urinary bladder carcinoma cells.* Pharmazie, 2010. **65**(2): p. 122-6.
129. Tupper, J., et al., *In vivo characterization of horseradish peroxidase with indole-3-acetic acid and 5-bromoindole-3-acetic acid for gene therapy of cancer.* Cancer Gene Ther, 2010. **17**(6): p. 420-8.
130. Dai, M., et al., *Tumor-targeted gene therapy using Adv-AFP-HRPC/IAA prodrug system suppresses growth of hepatoma xenografted in mice.* Cancer Gene Ther, 2012. **19**(2): p. 77-83.
131. Bonifert, G., et al., *Recombinant horseradish peroxidase variants for targeted cancer treatment.* Cancer Med, 2016. **5**(6): p. 1194-203.
132. Hosokawa, M., *Structure and catalytic properties of carboxylesterase isozymes involved in metabolic activation of prodrugs.* Molecules, 2008. **13**(2): p. 412-31.
133. Pommier, Y., *Topoisomerase I inhibitors: camptothecins and beyond.* Nat Rev Cancer, 2006. **6**(10): p. 789-802.
134. Vanhoefer, U., et al., *Irinotecan in the treatment of colorectal cancer: clinical overview.* J Clin Oncol, 2001. **19**(5): p. 1501-18.
135. Choi, S.A., et al., *Clinically applicable human adipose tissue-derived mesenchymal stem cells delivering therapeutic genes to brainstem gliomas.* Cancer Gene Ther, 2015. **22**(6): p. 302-11.

136. Kojima, A., N.R. Hackett, and R.G. Crystal, *Reversal of CPT-11 resistance of lung cancer cells by adenovirus-mediated gene transfer of the human carboxylesterase cDNA.* Cancer Res, 1998. **58**(19): p. 4368-74.
137. Yano, H., et al., *Overexpression of carboxylesterase-2 results in enhanced efficacy of topoisomerase I inhibitor, irinotecan (CPT-11), for multiple myeloma.* Cancer Sci, 2008. **99**(11): p. 2309-14.
138. Matzow, T., et al., *Hypoxia-targeted over-expression of carboxylesterase as a means of increasing tumour sensitivity to irinotecan (CPT-11).* J Gene Med, 2007. **9**(4): p. 244-52.
139. Humerickhouse, R., et al., *Characterization of CPT-11 hydrolysis by human liver carboxylesterase isoforms hCE-1 and hCE-2.* Cancer Res, 2000. **60**(5): p. 1189-92.
140. Sanghani, S.P., et al., *Hydrolysis of irinotecan and its oxidative metabolites, 7-ethyl-10-[4-N-(5-aminopentanoic acid)-1-piperidino] carbonyloxycamptothecin and 7-ethyl-10-[4-(1-piperidino)-1-amino]-carbonyloxycamptothecin, by human carboxylesterases CES1A1, CES2, and a newly expressed carboxylesterase isoenzyme, CES3.* Drug Metab Dispos, 2004. **32**(5): p. 505-11.
141. Oosterhoff, D., et al., *Secreted and tumour targeted human carboxylesterase for activation of irinotecan.* Br J Cancer, 2002. **87**(6): p. 659-64.
142. Capello, M., et al., *Carboxylesterase 2 as a Determinant of Response to Irinotecan and Neoadjuvant FOLFIRINOX Therapy in Pancreatic Ductal Adenocarcinoma.* J Natl Cancer Inst, 2015. **107**(8).
143. Danks, M.K., et al., *Comparison of activation of CPT-11 by rabbit and human carboxylesterases for use in enzyme/prodrug therapy.* Clin Cancer Res, 1999. **5**(4): p. 917-24.
144. Wierdl, M., et al., *An improved human carboxylesterase for enzyme/prodrug therapy with CPT-11.* Cancer Gene Ther, 2008. **15**(3): p. 183-92.
145. Vangara, K.K., et al., *SN-38-cyclodextrin complexation and its influence on the solubility, stability, and in vitro anticancer activity against ovarian cancer.* AAPS PharmSciTech, 2014. **15**(2): p. 472-82.
146. Seo, G.M., et al., *A self-contained enzyme activating prodrug cytotherapy for preclinical melanoma.* Mol Biol Rep, 2012. **39**(1): p. 157-65.
147. Metz, M.Z., et al., *Neural stem cell-mediated delivery of irinotecan-activating carboxylesterases to glioma: implications for clinical use.* Stem Cells Transl Med, 2013. **2**(12): p. 983-92.
148. Yi, Y., M. Jong Noh, and K. Hee Lee, *Current Advances in Retroviral Gene Therapy.* Current Gene Therapy, 2011. **11**(3): p. 218-228.
149. Wold, W.S.M. and K. Toth, *Adenovirus Vectors for Gene Therapy, Vaccination and Cancer Gene Therapy.* Current gene therapy, 2013. **13**(6): p. 421-433.
150. Santiago-Ortiz, J.L. and D.V. Schaffer, *Adeno-associated virus (AAV) vectors in cancer gene therapy.* Journal of Controlled Release, 2016.
151. Braybrooke, J.P., et al., *Phase I Study of MetXia-P450 Gene Therapy and Oral Cyclophosphamide for Patients with Advanced Breast Cancer or Melanoma.* Clinical Cancer Research, 2005. **11**(4): p. 1512-1520.
152. Kim, K.H., et al., *A Phase I Clinical Trial of Ad5.SSTR/TK.RGD, a Novel Infectivity-Enhanced Bicistronic Adenovirus, in Patients with Recurrent*

Gynecologic Cancer. Clinical cancer research : an official journal of the American Association for Cancer Research, 2012. **18**(12): p. 3440-3451.
153. Dass, C.R. and P.F.M. Choong, *Non-viral methods for gene transfer towards osteosarcoma therapy.* Journal of Drug Targeting, 2007. **15**(3): p. 184-189.
154. Fang, Y.L., X.G. Chen, and T.G. W, *Gene delivery in tissue engineering and regenerative medicine.* J Biomed Mater Res B Appl Biomater, 2015. **103**(8): p. 1679-99.
155. Majhen, D., et al., *Adenovirus-Based Vaccines for Fighting Infectious Diseases and Cancer: Progress in the Field.* Human Gene Therapy, 2014. **25**(4): p. 301-317.
156. Yamamoto, M. and D.T. Curiel, *Current Issues and Future Directions of Oncolytic Adenoviruses.* Molecular Therapy, 2009. **18**(2): p. 243-250.
157. Sarkar, S., et al., *Chemoprevention gene therapy (CGT): novel combinatorial approach for preventing and treating pancreatic cancer.* Curr Mol Med, 2013. **13**(7): p. 1140-59.
158. Kojima, Y., et al., *Oncolytic Gene Therapy Combined with Double Suicide Genes for Human Bile Duct Cancer in Nude Mouse Models.* Journal of Surgical Research, 2009. **157**(1): p. e63-e70.
159. Freytag, S.O., K.N. Barton, and Y. Zhang, *Efficacy of oncolytic adenovirus expressing suicide genes and interleukin-12 in preclinical model of prostate cancer.* Gene therapy, 2013. **20**(12): p. 10.1038/gt.2013.40.
160. Sarkar, S., et al., *Novel therapy of prostate cancer employing a combination of viral-based immunotherapy and a small molecule BH3 mimetic.* Oncoimmunology, 2016. **5**(3): p. e1078059.
161. Waehler, R., S.J. Russell, and D.T. Curiel, *Engineering targeted viral vectors for gene therapy.* Nat Rev Genet, 2007. **8**(8): p. 573-587.
162. Kim, J.W., et al., *A Genetically Modified Adenoviral Vector with a Phage Display-Derived Peptide Incorporated into Fiber Fibritin Chimera Prolongs Survival in Experimental Glioma.* Human Gene Therapy, 2015. **26**(9): p. 635-646.
163. Yamamoto, Y., et al., *A targeting ligand enhances infectivity and cytotoxicity of an oncolytic adenovirus in human pancreatic cancer tissues.* J Control Release, 2014. **192**: p. 284-93.
164. Sarkar, S., et al., *Chemoprevention Gene Therapy (CGT) of Pancreatic Cancer Using Perillyl Alcohol and a Novel Chimeric Serotype Cancer Terminator Virus.* Current Molecular Medicine, 2014. **14**(1): p. 125-140.
165. Sarkar, S., et al., *Reversing Translational Suppression and Induction of Toxicity in Pancreatic Cancer Cells Using a Chemoprevention Gene Therapy Approach.* Molecular Pharmacology, 2015. **87**(2): p. 286-295.
166. Wickham, T.J., et al., *Increased in vitro and in vivo gene transfer by adenovirus vectors containing chimeric fiber proteins.* Journal of Virology, 1997. **71**(11): p. 8221-8229.
167. Münch, R.C., et al., *Displaying High-affinity Ligands on Adeno-associated Viral Vectors Enables Tumor Cell-specific and Safe Gene Transfer.* Molecular Therapy, 2013. **21**(1): p. 109-118.

168. Nomani, A., et al., *Intracellular gene delivery is dependent on the type of non-viral carrier and defined by the cell surface glycosaminoglycans.* Journal of Controlled Release, 2014. **187**: p. 59-65.
169. Ziraksaz, Z., et al., *Cell-surface glycosaminoglycans inhibit intranuclear uptake but promote post-nuclear processes of polyamidoamine dendrimer-pDNA transfection.* European Journal of Pharmaceutical Sciences, 2013. **48**(1-2): p. 55-63.
170. Voges, J., et al., *Imaging-guided convection-enhanced delivery and gene therapy of glioblastoma.* Annals of Neurology, 2003. **54**(4): p. 479-487.
171. Kang, Y., et al., *Tumor-directed gene therapy in mice using a composite nonviral gene delivery system consisting of the piggyBac transposon and polyethylenimine.* BMC Cancer, 2009. **9**: p. 126-126.
172. Moghimi, S.M., et al., *A two-stage poly(ethylenimine)-mediated cytotoxicity: implications for gene transfer/therapy.* Mol Ther, 2005. **11**(6): p. 990-995.
173. Cortez, M.A., et al., *The Synthesis of Cyclic Poly(ethylene imine) and Exact Linear Analogues: An Evaluation of Gene Delivery Comparing Polymer Architectures.* Journal of the American Chemical Society, 2015. **137**(20): p. 6541-6549.
174. Huang, B., et al., *The Synthesis of a c(RGDyK) Targeted SN38 Prodrug with an Indolequinone Structure for Bioreductive Drug Release.* Organic letters, 2010. **12**(7): p. 1384-1387.
175. Wen, Y., et al., *A Biodegradable Low Molecular Weight Polyethylenimine Derivative as Low Toxicity and Efficient Gene Vector.* Bioconjugate Chemistry, 2009. **20**(2): p. 322-332.
176. Barenholz, Y., *Doxil - The first FDA-approved nano-drug: Lessons learned.* Journal of Controlled Release, 2012. **160**(2): p. 117-134.
177. Zhou, Y., et al., *Receptor-Mediated, Tumor-Targeted Gene Delivery Using Folate-Terminated Polyrotaxanes.* Molecular Pharmaceutics, 2012. **9**(5): p. 1067-1076.
178. Canine, B.F., et al., *Development of targeted recombinant polymers that can deliver siRNA to the cytoplasm and plasmid DNA to the cell nucleus.* Journal of Controlled Release, 2011. **151**(1): p. 95-101.
179. Canine, B.F., Y.H. Wang, and A. Hatefi, *Biosynthesis and characterization of a novel genetically engineered polymer for targeted gene transfer to cancer cells.* Journal of Controlled Release, 2009. **138**(3): p. 188-196.
180. Karjoo, Z., et al., *Systematic engineering of uniform, highly efficient, targeted and shielded viral-mimetic nanoparticles.* Small, 2013. **9**(16): p. 2774-83.
181. Nouri, F.S., et al., *Reducing the Visibility of the Vector/DNA Nanocomplexes to the Immune System by Elastin-Like Peptides.* Pharm Res, 2015. **32**(9): p. 3018-28.
182. Hoffman, R.M. and M. Zhao, *Methods for the development of tumor-targeting bacteria.* Expert Opinion on Drug Discovery, 2014. **9**(7): p. 741-750.
183. Baban, C.K., et al., *Bacteria as vectors for gene therapy of cancer.* Bioeng Bugs, 2010. **1**(6): p. 385-94.
184. Giacalone, M.J., et al., *The use of bacterial minicells to transfer plasmid DNA to eukaryotic cells.* Cellular Microbiology, 2006. **8**(10): p. 1624-1633.

185. MacDiarmid, J.A., et al., *Sequential treatment of drug-resistant tumors with targeted minicells containing siRNA or a cytotoxic drug.* Nat Biotech, 2009. **27**(7): p. 643-651.
186. Brahmbhatt, H. and J. MacDiarmid, *Targeted gene delivery to non-phagocytic mammalian cells via bacterially derived intact minicells*. 2015, Google Patents.
187. Solomon, B.J., et al., *A First-Time-In-Human Phase I Clinical Trial of Bispecific Antibody-Targeted, Paclitaxel-Packaged Bacterial Minicells.* PLoS ONE, 2015. **10**(12): p. e0144559.
188. Aboody, K.S., et al., *Neural Stem Cells Mediated Enzyme/Prodrug Therapy for Glioma: Preclinical Studies.* Science Translational Medicine, 2013. **5**(184): p. 184ra59-184ra59.
189. On Kan, et al., *Direct retroviral delivery of human cytochrome P450 2B6 for gene-directed enzyme prodrug therapy of cancer.* Cancer Gene Ther, 2001. **8**(7): p. 473-82.
190. Klopp, A.H., et al., *Tumor Irradiation Increases the Recruitment of Circulating Mesenchymal Stem Cells into the Tumor Microenvironment.* Cancer Research, 2007. **67**(24): p. 11687-11695.
191. François, S., et al., *Local Irradiation Not Only Induces Homing of Human Mesenchymal Stem Cells at Exposed Sites but Promotes Their Widespread Engraftment to Multiple Organs: A Study of Their Quantitative Distribution After Irradiation Damage.* STEM CELLS, 2006. **24**(4): p. 1020-1029.
192. Seo, S.H., et al., *The effects of mesenchymal stem cells injected via different routes on modified IL-12-mediated antitumor activity.* Gene Ther, 2011. **18**(5): p. 488-95.
193. Yong, R.L., et al., *Human bone marrow-derived mesenchymal stem cells for intravascular delivery of oncolytic adenovirus Delta24-RGD to human gliomas.* Cancer Res, 2009. **69**(23): p. 8932-40.
194. Gao, Z., et al., *Mesenchymal stem cells: a potential targeted-delivery vehicle for anti-cancer drug, loaded nanoparticles.* Nanomedicine, 2013. **9**(2): p. 174-84.
195. Jain, S., et al., *RGD-anchored magnetic liposomes for monocytes/neutrophils-mediated brain targeting.* International Journal of Pharmaceutics, 2003. **261**(1-2): p. 43-55.
196. Batrakova, E.V., H.E. Gendelman, and A.V. Kabanov, *Cell-Mediated Drugs Delivery.* Expert opinion on drug delivery, 2011. **8**(4): p. 415-433.
197. Li, W. and A.P. Xiang, *Safeguarding clinical translation of pluripotent stem cells with suicide genes.* Organogenesis, 2013. **9**(1): p. 34-39.
198. Wu, T.L. and D. Zhou, *Viral delivery for gene therapy against cell movement in cancer.* Adv Drug Deliv Rev, 2011. **63**(8): p. 671-7.
199. Lachelt, U. and E. Wagner, *Nucleic Acid Therapeutics Using Polyplexes: A Journey of 50 Years (and Beyond).* Chem Rev, 2015. **115**(19): p. 11043-78.
200. Karjoo, Z., X. Chen, and A. Hatefi, *Progress and problems with the use of suicide genes for targeted cancer therapy.* Advanced Drug Delivery Reviews, 2015. **99, Part A**: p. 113-128.
201. Chen, X., et al., *Cancer-specific Promoters for Expression-targeted Gene Therapy: ran, brms1, and mcm5.* J Gene Med, 2016.

202. Greco, O., Dachs, G. U., Tozer, G. M. and Kanthou, C, *Mechanisms of cytotoxicity induced by horseradish peroxidase/indole-3-acetic acid gene therapy.* J. Cell. Biochem, 2002. **87**: p. 221–232.
203. Schlabach, M.R., et al., *Synthetic design of strong promoters.* Proceedings of the National Academy of Sciences, 2010. **107**(6): p. 2538-2543.
204. Marth, C., D. Reimer, and A.G. Zeimet, *Front-line therapy of advanced epithelial ovarian cancer: standard treatment.* Ann Oncol, 2017. **28**(suppl_8): p. viii36-viii39.
205. Miyoshi, Y., et al., *Salvage chemotherapy for ovarian carcinoma recurring during or after consolidation chemotherapy with paclitaxel.* Anticancer Res, 2011. **31**(12): p. 4613-7.
206. Bookman, M.A., et al., *Topotecan for the treatment of advanced epithelial ovarian cancer: an open-label phase II study in patients treated after prior chemotherapy that contained cisplatin or carboplatin and paclitaxel.* J Clin Oncol, 1998. **16**(10): p. 3345-52.
207. Bodurka, D.C., et al., *Phase II trial of irinotecan in patients with metastatic epithelial ovarian cancer or peritoneal cancer.* J Clin Oncol, 2003. **21**(2): p. 291-7.
208. Gordon, A.N., et al., *Phase II study of liposomal doxorubicin in platinum- and paclitaxel-refractory epithelial ovarian cancer.* J Clin Oncol, 2000. **18**(17): p. 3093-100.
209. Rose, P.G., et al., *Prolonged oral etoposide as second-line therapy for platinum-resistant and platinum-sensitive ovarian carcinoma: a Gynecologic Oncology Group study.* J Clin Oncol, 1998. **16**(2): p. 405-10.
210. Markman, M., et al., *Phase 2 trial of single-agent gemcitabine in platinum-paclitaxel refractory ovarian cancer.* Gynecol Oncol, 2003. **90**(3): p. 593-6.
211. Markman, M., et al., *Ifosfamide and mesna in previously treated advanced epithelial ovarian cancer: activity in platinum-resistant disease.* J Clin Oncol, 1992. **10**(2): p. 243-8.
212. Matsumoto, K., et al., *The safety and efficacy of the weekly dosing of irinotecan for platinum- and taxanes-resistant epithelial ovarian cancer.* Gynecol Oncol, 2006. **100**(2): p. 412-6.
213. Sarkar, S., et al., *A novel chemotherapeutic protocol for peritoneal metastasis and inhibition of relapse in drug resistant ovarian cancer.* Cancer Med, 2018. **7**(8): p. 3630-3641.
214. Ponte, A.L., et al., *The in vitro migration capacity of human bone marrow mesenchymal stem cells: comparison of chemokine and growth factor chemotactic activities.* Stem Cells, 2007. **25**(7): p. 1737-45.
215. Kidd, S., et al., *Direct evidence of mesenchymal stem cell tropism for tumor and wounding microenvironments using in vivo bioluminescent imaging.* Stem Cells, 2009. **27**(10): p. 2614-23.
216. Ayen, A., et al., *Recent Progress in Gene Therapy for Ovarian Cancer.* Int J Mol Sci, 2018. **19**(7).
217. Hu, Y. and G.K. Smyth, *ELDA: extreme limiting dilution analysis for comparing depleted and enriched populations in stem cell and other assays.* J Immunol Methods, 2009. **347**(1-2): p. 70-8.

218. Januchowski, R., et al., *Inhibition of ALDH1A1 activity decreases expression of drug transporters and reduces chemotherapy resistance in ovarian cancer cell lines.* The International Journal of Biochemistry & Cell Biology, 2016. **78**: p. 248-259.
219. Di Nicolantonio, F., et al., *Cancer cell adaptation to chemotherapy.* BMC Cancer, 2005. **5**: p. 78.
220. Dou, J., et al., *Using ABCG2-molecule-expressing side population cells to identify cancer stem-like cells in a human ovarian cell line.* Cell Biol Int, 2011. **35**(3): p. 227-34.
221. Wang, W.J., et al., *Ursolic acid inhibits proliferation and reverses drug resistance of ovarian cancer stem cells by downregulating ABCG2 through suppressing the expression of hypoxia-inducible factor-1alpha in vitro.* Oncol Rep, 2016. **36**(1): p. 428-40.
222. Ip, C.K., et al., *Stemness and chemoresistance in epithelial ovarian carcinoma cells under shear stress.* Sci Rep, 2016. **6**: p. 26788.
223. Mildmay-White, A. and W. Khan, *Cell Surface Markers on Adipose-Derived Stem Cells: A Systematic Review.* Curr Stem Cell Res Ther, 2017. **12**(6): p. 484-492.
224. Aston, W.J., et al., *A systematic investigation of the maximum tolerated dose of cytotoxic chemotherapy with and without supportive care in mice.* BMC Cancer, 2017. **17**(1): p. 684.
225. Gutova, M., et al., *Neural stem cell-mediated CE/CPT-11 enzyme/prodrug therapy in transgenic mouse model of intracerebellar medulloblastoma.* Gene Ther, 2013. **20**(2): p. 143-50.
226. Choi, M.K., et al., *Phase I study of intraperitoneal irinotecan in patients with gastric adenocarcinoma with peritoneal seeding.* Cancer Chemother Pharmacol, 2011. **67**(1): p. 5-11.
227. Yi, B.R., S.U. Kim, and K.C. Choi, *Co-treatment with therapeutic neural stem cells expressing carboxyl esterase and CPT-11 inhibit growth of primary and metastatic lung cancers in mice.* Oncotarget, 2014. **5**(24): p. 12835-48.
228. Enderling, H., L. Hlatky, and P. Hahnfeldt, *Cancer Stem Cells: A Minor Cancer Subpopulation that Redefines Global Cancer Features.* Front Oncol, 2013. **3**: p. 76.
229. Kakar, S.S., et al., *Withaferin a alone and in combination with cisplatin suppresses growth and metastasis of ovarian cancer by targeting putative cancer stem cells.* PLoS One, 2014. **9**(9): p. e107596.
230. Rich, J.N., *Cancer stem cells: understanding tumor hierarchy and heterogeneity.* Medicine, 2016. **95**(1 Suppl 1): p. S2-S7.
231. Ahmed, N., K. Abubaker, and J.K. Findlay, *Ovarian cancer stem cells: Molecular concepts and relevance as therapeutic targets.* Mol Aspects Med, 2014. **39**: p. 110-25.
232. Ahmed, N. and K.L. Stenvers, *Getting to know ovarian cancer ascites: opportunities for targeted therapy-based translational research.* Front Oncol, 2013. **3**: p. 256.
233. Dvorak, H.F., *Tumors: wounds that do not heal. Similarities between tumor stroma generation and wound healing.* N Engl J Med, 1986. **315**(26): p. 1650-9.

234. Gutova, M., et al., *Urokinase plasminogen activator and urokinase plasminogen activator receptor mediate human stem cell tropism to malignant solid tumors.* Stem Cells, 2008. **26**(6): p. 1406-13.
235. Shi, M., et al., *Regulation of CXCR4 expression in human mesenchymal stem cells by cytokine treatment: role in homing efficiency in NOD/SCID mice.* Haematologica, 2007. **92**(7): p. 897-904.
236. Teo, G.S., et al., *Mesenchymal stem cells transmigrate between and directly through tumor necrosis factor-alpha-activated endothelial cells via both leukocyte-like and novel mechanisms.* Stem Cells, 2012. **30**(11): p. 2472-86.
237. Altaner, C., et al., *Complete regression of glioblastoma by mesenchymal stem cells mediated prodrug gene therapy simulating clinical therapeutic scenario.* Int J Cancer, 2014. **134**(6): p. 1458-65.
238. Niess, H., et al., *Treatment of advanced gastrointestinal tumors with genetically modified autologous mesenchymal stromal cells (TREAT-ME1): study protocol of a phase I/II clinical trial.* BMC Cancer, 2015. **15**: p. 237.
239. Dembinski, J.L., et al., *Tumor stroma engraftment of gene-modified mesenchymal stem cells as anti-tumor therapy against ovarian cancer.* Cytotherapy, 2013. **15**(1): p. 20-32.
240. Bazhanov, N., et al., *Intraperitoneally infused human mesenchymal stem cells form aggregates with mouse immune cells and attach to peritoneal organs.* Stem cell research & therapy, 2016. **7**: p. 27-27.
241. Pistollato, F., et al., *Intratumoral hypoxic gradient drives stem cells distribution and MGMT expression in glioblastoma.* Stem Cells, 2010. **28**(5): p. 851-62.
242. Zhao, D., et al., *Neural stem cell tropism to glioma: critical role of tumor hypoxia.* Mol Cancer Res, 2008. **6**(12): p. 1819-29.
243. Jansen, W.J., et al., *Anti-tumor activity of CPT-11 in experimental human ovarian cancer and human soft-tissue sarcoma.* Int J Cancer, 1997. **73**(6): p. 891-6.